AN INVESTIGATION OF THE STEADY-STATE BURNING OF AMMONIUM PERCHLORATE COMPOSITE SOLID PROPELLANTS

Job S. Ebenezer, et al

Stevens Institute of Technology
Hoboken, New Jersey

June 1973

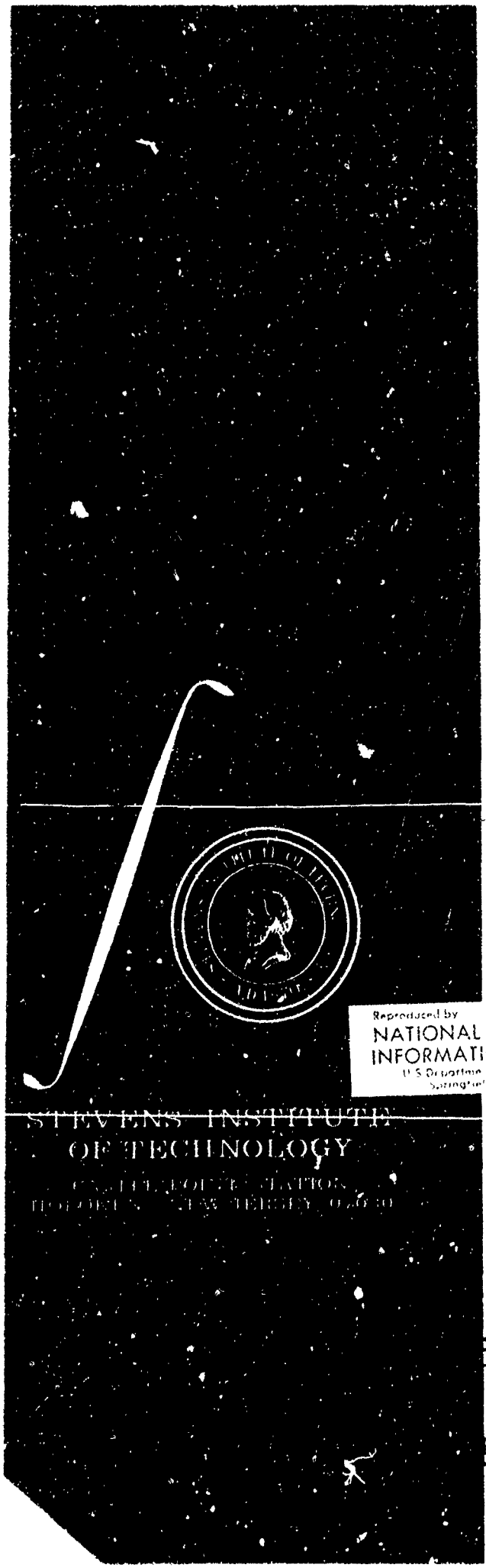

DEPARTMENT OF MECHANICAL ENGINEERING

AN INVESTIGATION OF THE STEADY-STATE BURNING OF AMMONIUM PERCHLORATE COMPOSITE SOLID PROPELLANTS

TECHNICAL REPORT ME-RT 73004

by

Job S. Ebenezer

Richard B. Cole

Robert F. McAlevy, III

June 1973

PREPARED FOR
DEPARTMENT OF THE NAVY
OFFICE OF NAVAL RESEARCH
POWER BRANCH
Contract No. 0014-67-A-0202-0035

143

UNCLASSIFIED

SECURITY CLASSIFICATION OF THIS PAGE (When Data Entered)

REPORT DOCUMENTATION PAGE		READ INSTRUCTIONS BEFORE COMPLETING FORM
1. REPORT NUMBER RT-73004	2. GOVT ACCESSION NO.	3. RECIPIENT'S CATALOG NUMBER
4. TITLE (and Subtitle) An Investigation of the Steady-State Burning of Ammonium Perchlorate Composite Solid Propellants		5. TYPE OF REPORT & PERIOD COVERED Technical Report 6. PERFORMING ORG. REPORT NUMBER
7. AUTHOR(s) Job Ebenezer, Richard B. Cole, Robert F. McAlevy, III		8. CONTRACT OR GRANT NUMBER(s) N00014-67-A-0202-0035
9. PERFORMING ORGANIZATION NAME AND ADDRESS Dept. of Mechanical Engineering Stevens Institute of Technology Hoboken, N.J. 07030		10. PROGRAM ELEMENT, PROJECT, TASK AREA & WORK UNIT NUMBERS NR 092-512/6-27-72(473)
11. CONTROLLING OFFICE NAME AND ADDRESS Office of Naval Research Department of the Navy Arlington, Va. 22217		12. REPORT DATE June 1973 13. NUMBER OF PAGES ~~146~~ 143
14. MONITORING AGENCY NAME & ADDRESS(if different from Controlling Office)		15. SECURITY CLASS. (of this report) Unclassified 15a. DECLASSIFICATION/DOWNGRADING SCHEDULE

16. DISTRIBUTION STATEMENT (of this Report)

Reproduction in whole or in part is permitted for any purpose of the United States Government.

17. DISTRIBUTION STATEMENT (of the abstract entered in Block 20, if different from Report)

18. SUPPLEMENTARY NOTES

19. KEY WORDS (Continue on reverse side if necessary and identify by block number)

Ammonium Perchlorate Propellants
Composite Propellants
Propellant Modelling
Solid Propellants
Steady-State Deflagration

20. ABSTRACT (Continue on reverse side if necessary and identify by block number)

A new, comprehensive steady-state model describing the burning of non-metalized, unimodal ammonium perchlorate (AP)-polymeric composite solid propellant has been developed and shown to yield better results than previous models.

Formulation of the model was guided by results of a critical review of previous comprehensive models. This new model incorporates a near-surface AP decomposition flame perturbed

DD FORM 1 JAN 73 1473 EDITION OF 1 NOV 65 IS OBSOLETE

UNCLASSIFIED

SECURITY CLASSIFICATION OF THIS PAGE (When Data Entered)

The contents of this report have been submitted in partial fulfillment of the requirements for the degree of Doctor of Philosophy from Stevens Institute of Technology, May 1973.

NOMENCLATURE

A	-	pre-exponential factors in Arrhenius expression
a	-	chemical-kinetic time parameter
a'	-	modified chemical-kinetic time parameter
B	-	pre-exponential factor in Arrhenius expression
b	-	diffusion-time parameter
b'	-	modified diffusion-time parameter
C_1	-	constant used in the MGDF model
C_2	-	constant used in the MGDF model
c_g	-	specific heat of gases
d_{ox}	-	diameter of oxidant particle
d_f	-	diameter of fuel particle
D	-	diffusion coefficient
E	-	activation energies
L	-	thickness of flame zones
$\dot{m}$	-	mass flow rates
$\dot{m}''$	-	mass fluxes
P	-	pressure
Q	-	heats of vaporization (heats of reaction of various flames in the MF model)
R	-	universal gas constant

r	-	burning rate
S	-	surface areas
T	-	absolute temperature
w	-	weight fraction of oxidant
ΔH	-	heats of reaction

Greek Symbols

α	-	constant related to "a"
α'	-	constant related to "a'"
β	-	constant related to "b"
β'	-	constant related to "b'"
λ_g	-	thermal conductivity of gases
μ	-	mass of fuel gas pocket
ρ	-	densities
τ	-	reaction times

Subscripts

1	-	condition at the end of the first-stage flame
2	-	condition at the end of the second-stage flame
AP	-	ammonium perchlorate
f	-	fuel

F - flame conditions

g - gas phase

p - propellant

o - initial condition in the solid phase

s - surface

ox - oxidant

st - stoichiometric

Abbreviations

AP - ammonium perchlorate

LP3 - polysulphide

P13 - polyester

PBAA- polybutadiene acrylic acid

PS - polystyrene

PMM - polymethylmethacrylate

GDFC- granular diffusion flame with collapsed AP decomposition flame

GDFD- granular diffusion flame with distended AP decomposition flame

HR - heterogeneous reaction model

MF - multiple flame model

ST - Stoichiometric

TABLE OF CONTENTS

CHAPTER II (continued)

CHAPTER II (continued)

LIST OF FIGURES

LIST OF FIGURES (continued)

LIST OF FIGURES (continued)

LIST OF FIGURES (continued)

LIST OF TABLES

CHAPTER I - INTRODUCTION

I.A GENERAL BACKGROUND

A composite solid propellant consists of finely divided oxidant and metal particles uniformly dispersed in a matrix of polymer binder. The most commonly used oxidant is ammonium perchlorate (AP) and some of the fuel binders used are polyurethane, polybutadiene-acrylic acid, polysulphide, polyester, etc. In the present investigation only non metalized propellants with AP particles of a single size (unimodal) were considered.

In the past few decades, a considerable number of experimental and theoretical investigations have been directed towards the study of the steady-state burning of composite propellants. The purpose of these investigations has been to predict or to allow willful modification of the performance of AP composite propellants in order to avoid the time consuming, repetitive, and costly experimental tests. In spite of these efforts, the present models are imperfect and are not capable of correctly representing the burning mechanism of composite solid propellants.

1.B BURNING MECHANISM OF A COMPOSITE PROPELLANT

The burning mechanism of a composite solid propellant is very complex due to the heterogeneous composition of the propellant. Several spatial dimensions, several phases, and several simultaneous and/or successive physical and chemical processes are involved.

During burning, gases evolve from the propellant surface and mix and react exothermally in the gas phase. The heat generated by the reactions is transferred to the surface and produces further vaporization of the surface material. Previous studies (1, 2, 3, 4) have indicated that the following physical and chemical processes are important in the burning of a composite solid propellant :

(i) heat conduction,

(ii) surface pyrolysis of the fuel (endothermic),

(iii) surface dissociative sublimation of AP into ammonia and perchloric acid (endothermic),

(iv) vapor diffusion,

(v) AP decomposition flame (exothermic reaction between ammonia and perchloric acid), and

(v) final flame (exothermic reaction between pyrolysed fuel and AP decomposition products).

Figure I-1 illustrates the burning mechanism schematically.

The linear rate at which the surface regresses macroscopically is a characteristic of the burning and is designated as the burning rate of the propellant (r). The desired end results of steady-state mechanistic models are the prediction of r and of the influences on r by pressure (P), oxidant particle size (d_{ox}), initial temperature (T_o) and weight fraction of oxidant (mixture ratio) (w).

I.C PURPOSE AND SCOPE OF THE PRESENT INVESTIGATION

I.C.1 Purpose

The purpose of the present investigation is to develop an improved steady-state-burning model for AP composite solid propellants. The need for such a model based on reasonable mechanistic grounds arises from the inadequacy of the existing models to describe the experimentally observed effects of all the important variables on the burning rate.

I.C.2 Scope

The presently reported work consists of :

a. review of prior experimental and theoretical investigations of the steady-state burning of AP-composite-solid propellants,

b. new experimental and theoretical investigations concerned

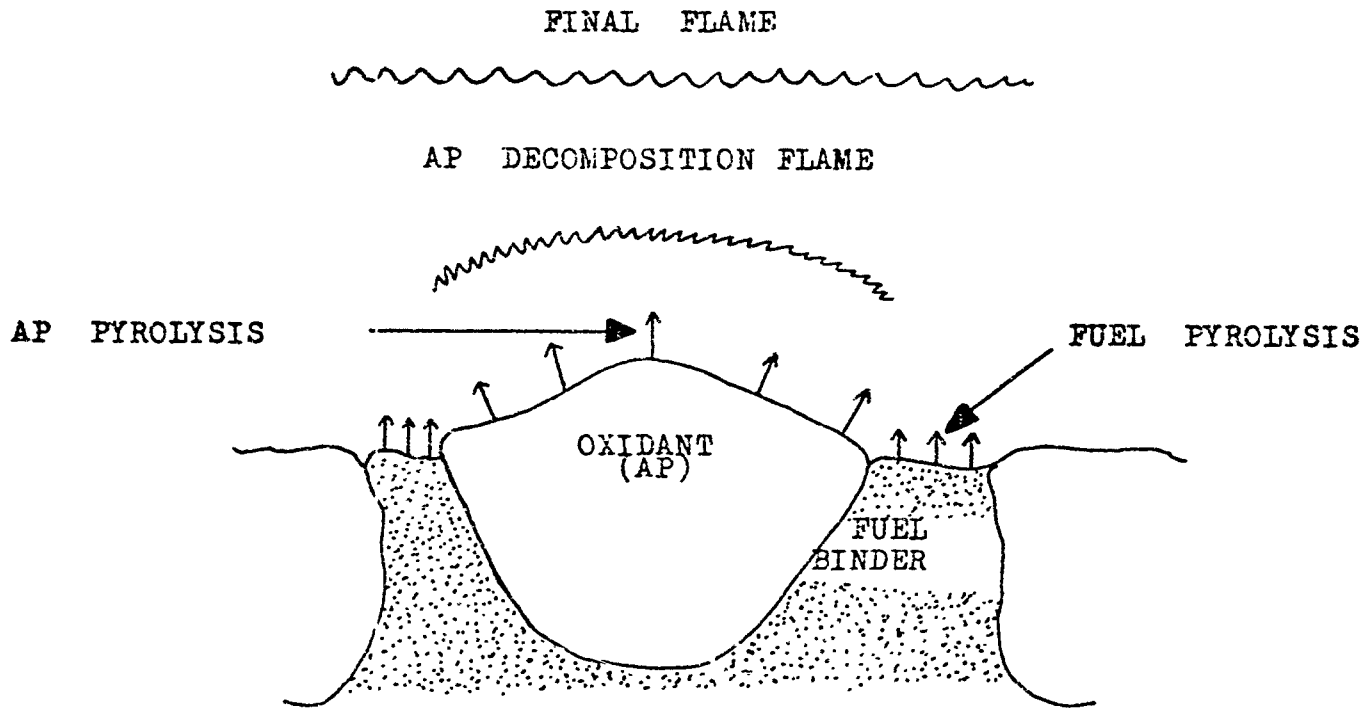

FIGURE I-1 : SCHEMATIC OF THE BURNING PROCESS OF A COMPOSITE SOLID PROPELLANT

with mixture-ratio influences on burning rates,

c. assessment of existing comprehensive models by means of numerical diagnostic tests, and finally,

d. formulation of a modified granular diffusion flame model, based on reasonable mechanistic grounds and testing of the model against experimental data.

CHAPTER II - REVIEW OF PRIOR INVESTIGATIONS

In the present chapter, prior experimental and theoretical investigations of the steady-state burning of AP composite solid propellants and their analogs are reviewed.

II.A EXPERIMENTAL INVESTIGATIONS

A great deal of effort has been devoted in the past to study burning rate behaviour of AP composite propellants with respect to pressure (P), oxidant particle size (d_{ox}), initial temperature (T_o), and mixture-ratio (w). Both actual propellants and their analogs have been used in these investigations.

II.A.1 Investigations with Propellants

A detailed review on this subject can be found in references 3 and 5. Hence, only a brief summary of the results are given below.

II.A.1.a Pressure

In general, r is found to increase as P increases. Based on the variations of r with P, three pressure domains have been defined as follows :

(i) low pressure domain (below 10 atm.),

(ii) moderate pressure domain (10 to 100 atm.), and

(iii) high pressure domain (above 100 atm.).

These demarcations are not rigid as they deform as other parameters are varied. These different domains are attributed to the domination of the overall burning process by different phenomena (e. g, chemical reaction and diffusional mixing at different pressures).

II. A. 1. b Oxidant Particle Size

Bastress (6) has done a systematic study of the influences of d_{ox} on r and found that, in general, r increased with decreasing d_{ox}. The influence of d_{ox} on r has also been found to be coupled with variations in other parameters, such as, oxidant weight fraction (3).

II. A. 1. c Initial Temperature

The burning rate usually increases as the initial temperature is increased. A considerable interest is shown at present in understanding the influence of initial temperature on the burning rate (7).

II. A. 1. d Mixture Ratio

A measure of the mixture ratio in this study is taken to be the weight fraction of oxidant (w). The influence of w on r has been virtually ignored by the previous investigators. Only very limited data is available with regard to the mixture ratio influences and no attempt has been made previously to interpret these data. Therefore, in the present investigation, the available data have been plotted as

r vs. w (none of the previous studies shows a plot of this type). Figures II-1, 2, and 3 show plots of r vs. w for various pressures, particle sizes, and different types of fuel.

The following observations can be made from these figures :

(i) The burning rate (r) increases monotonically with the mixture ratio (w) (all the w's considered are less than the stoichiometrically correct w, w_{st}).#

(ii) The mixture-ratio sensitivity of the burning rate, $\frac{\partial \ln r}{\partial w}$, varies with P, d_{ox}, w, and the type of fuel used.

(iii) r vs. w curves in figure II-1 and 2 suggest a tendency to attain a maximum r as w increases, though the available data are not extensive to ascertain this trend.

II.A.2 Investigations with Analogs

Analogs of AP propellants were used in the past to study burning-rate variations with changing P, d_{ox}, T_o, and w (4, 9, 10). The advantages cited for using analogs rather than true propellants are that the analogs are easy to fabricate and that they allow the composition to be varied at will, which is not possible with actual propellants.

---

w_{st} is defined here as that w which assumes the products of combustion to be H_2O, CO_2, SO_2, HCl, and N_2.

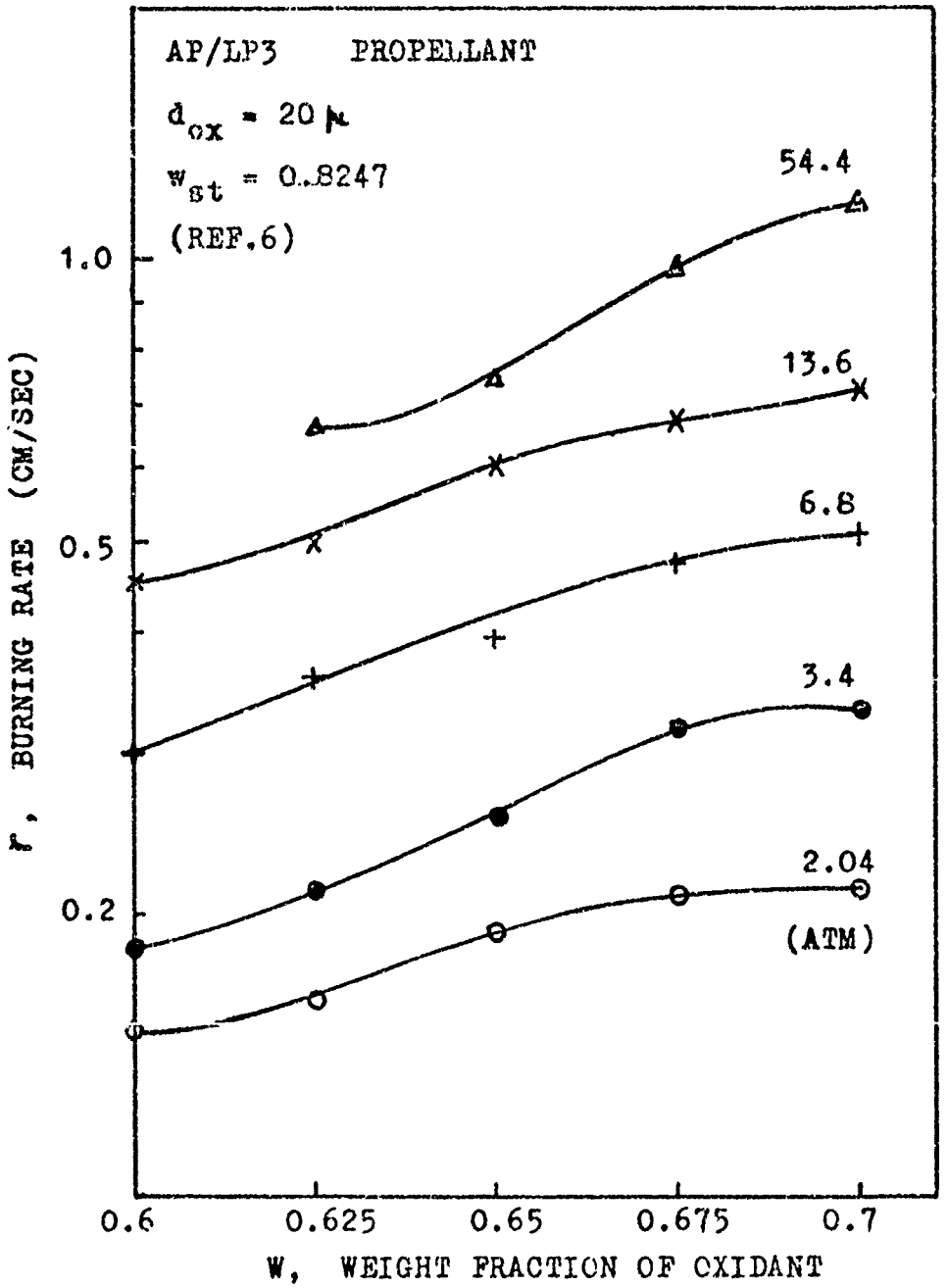

FIGURE II-1 DEPENDENCE OF BURNING RATE ON MIXTURE RATIO FOR AP/LP3 PROPELLANT AT VARIOUS PRESSURES

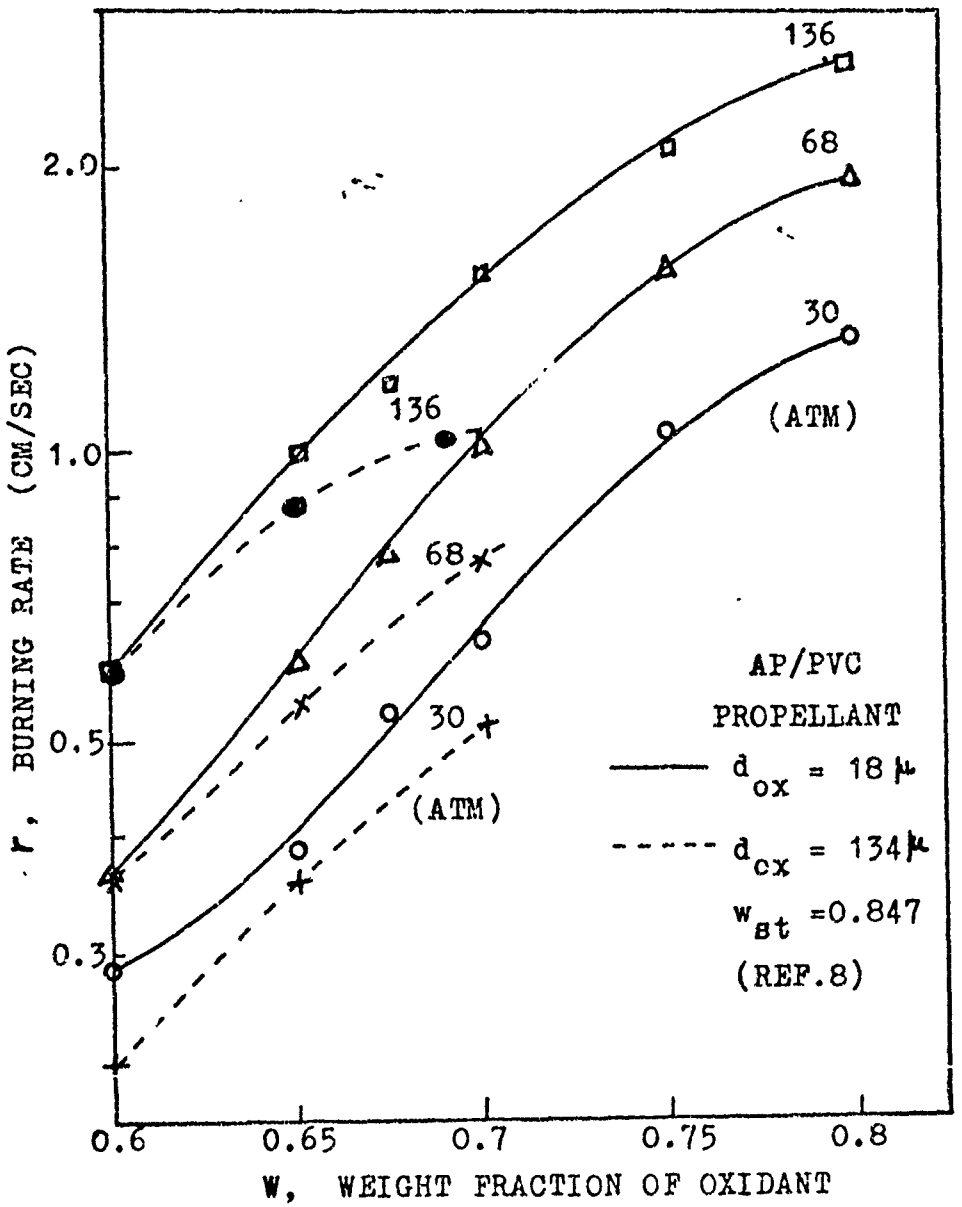

FIGURE II-2 DEPENDENCE OF BURNING RATE ON MIXTURE RATIO FOR AP/PVC PROPELLANT AT VARIOUS PRESSURES AND FOR DIFFERENT PARTICLE SIZES

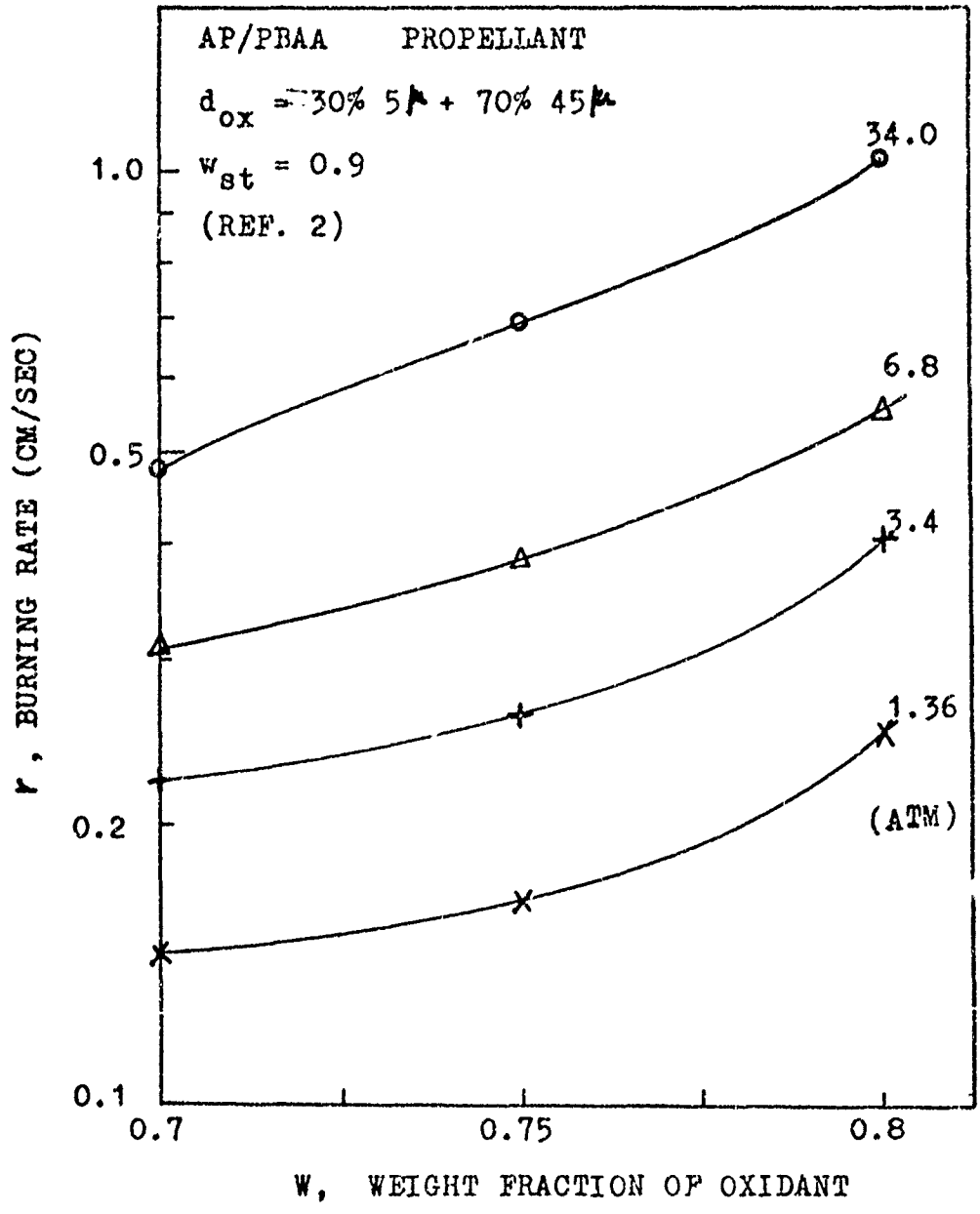

FIGURE II-3 DEPENDENCE OF BURNING RATE ON MIXTURE RATIO FOR AP/PBAA PROPELLANT AT VARIOUS PRESSURES

The three types of analogs used in the past are :

(i) Pressed-samples (4, 9),

(ii) Loose-granule burners (10), and

(iii) Porus-plug burners (10).

In the present study, additional loose-granule tests were used to investigate mixture-ratio influences.

II. A. 2.a Parametric Influences

The results obtained from analog studies show the same influences of pressure, oxidant particle size, and initial temperature on r as those shown by actual propellants (4, 9, 10). However, the analog studies provide additional information with regard to the mixture-ratio influences on r. Unlike propellants, analogs can be fabricated and tested over a wide range of mixture ratios. Figures II-4, 5, and 6 show r vs. w curves from previous studies (4, 10). These curves are useful in studying the influences of fuel, oxidant particle size and pressure on the trends of r vs. w curves (i.e. the shifts in the mixture ratio that correspond to maximum burning rate, $w_{r(max)}$.

Figure II-4 shows that for mixtures containing AP and polystyrene (PS), the mixture-ratio yielding maximum burning rate, $w_{r(max)}$, is on the fuel rich side of the stoichiometrically correct mixture ratio (w_{st}), whereas for mixtures containing AP and poly-

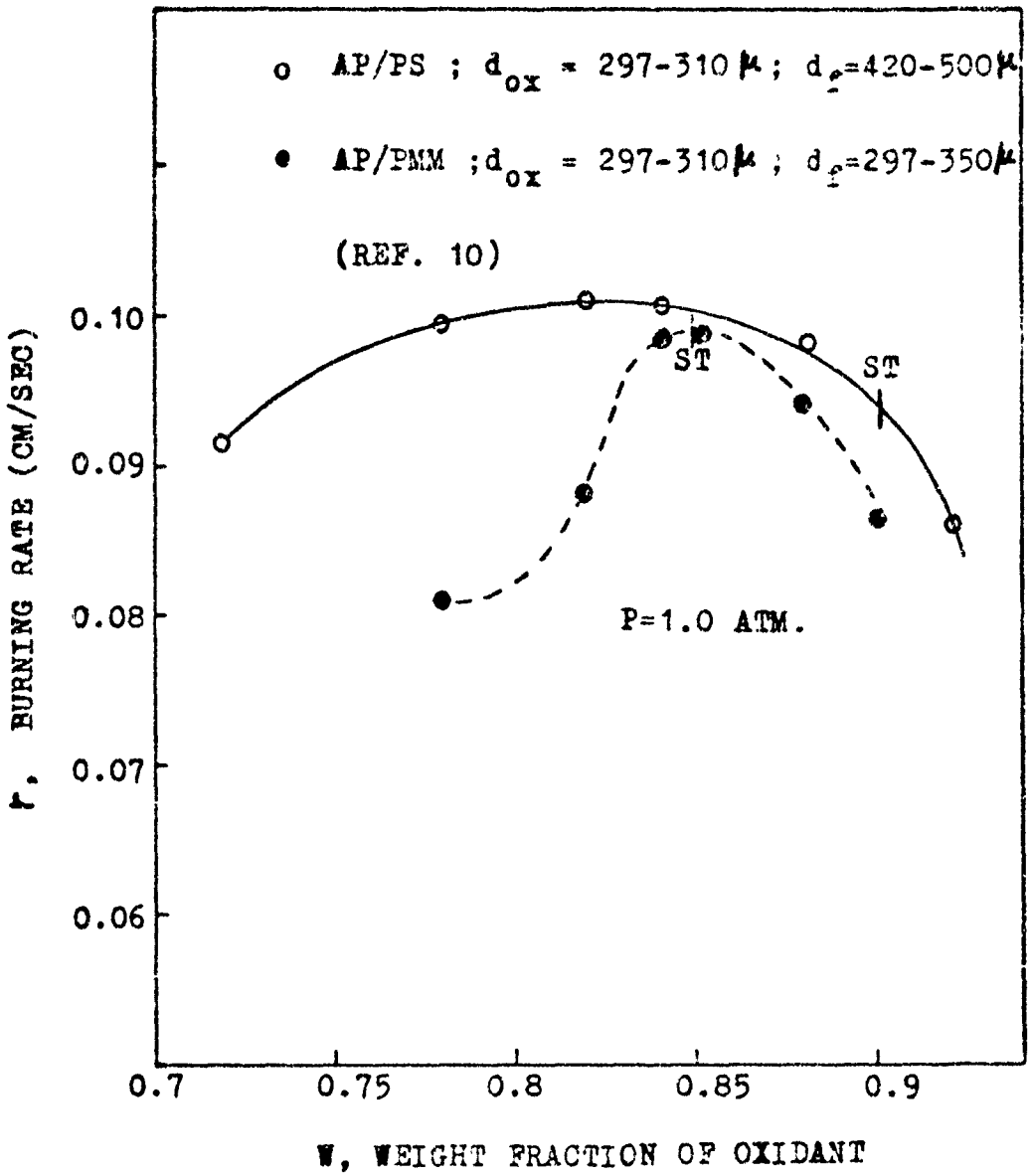

FIGURE II-4 : INFLUNCE OF FUEL ON THE POSITION OF MAXIMUM BURNING RATE (LOOSE-GRANULE BURNERS)

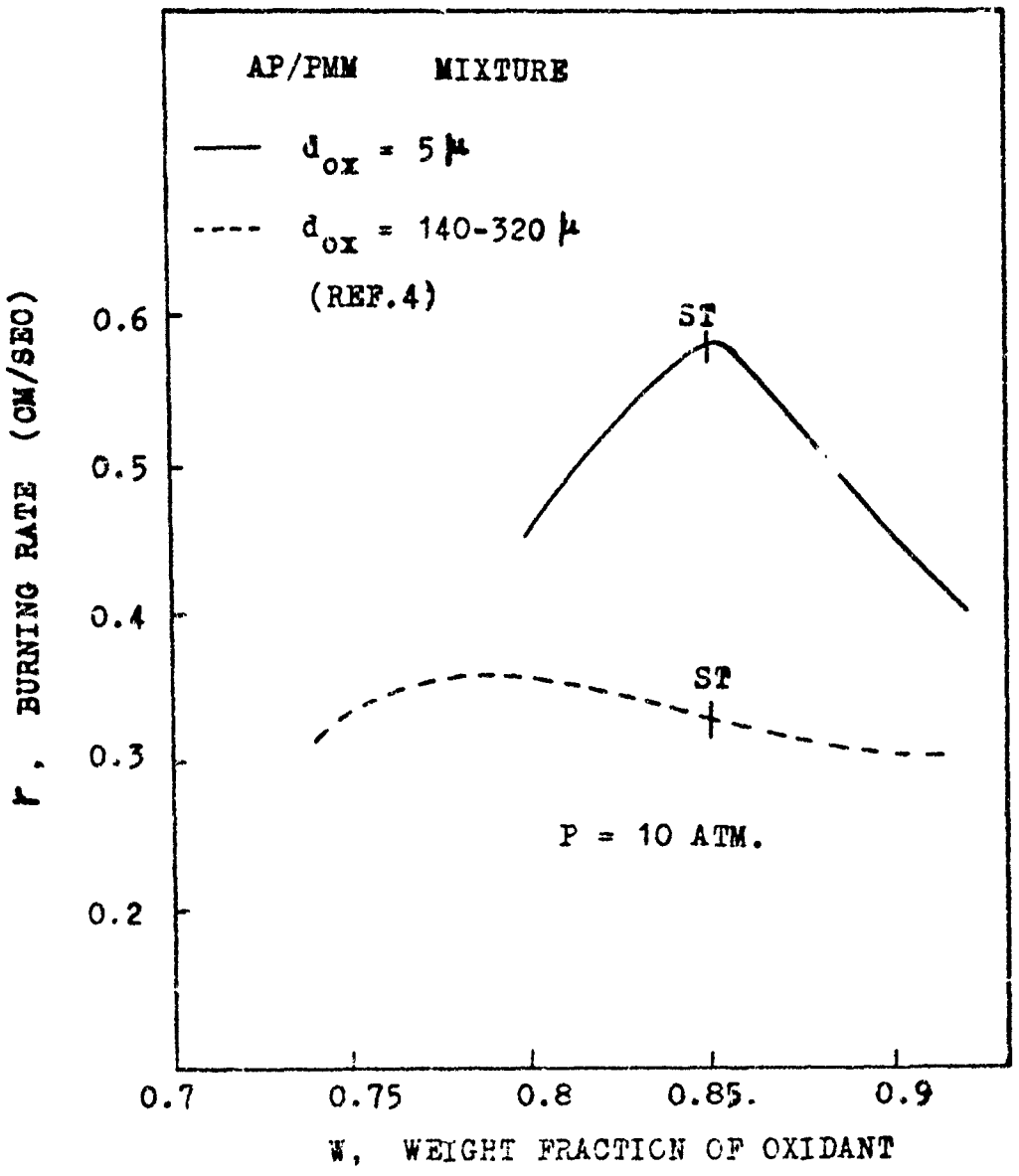

FIGURE II-5 : INFLUENCE OF THE OXIDANT PARTICLE SIZE ON THE POSITION OF MAXIMUM BURNING RATE (PRESSED-SAMPLES)

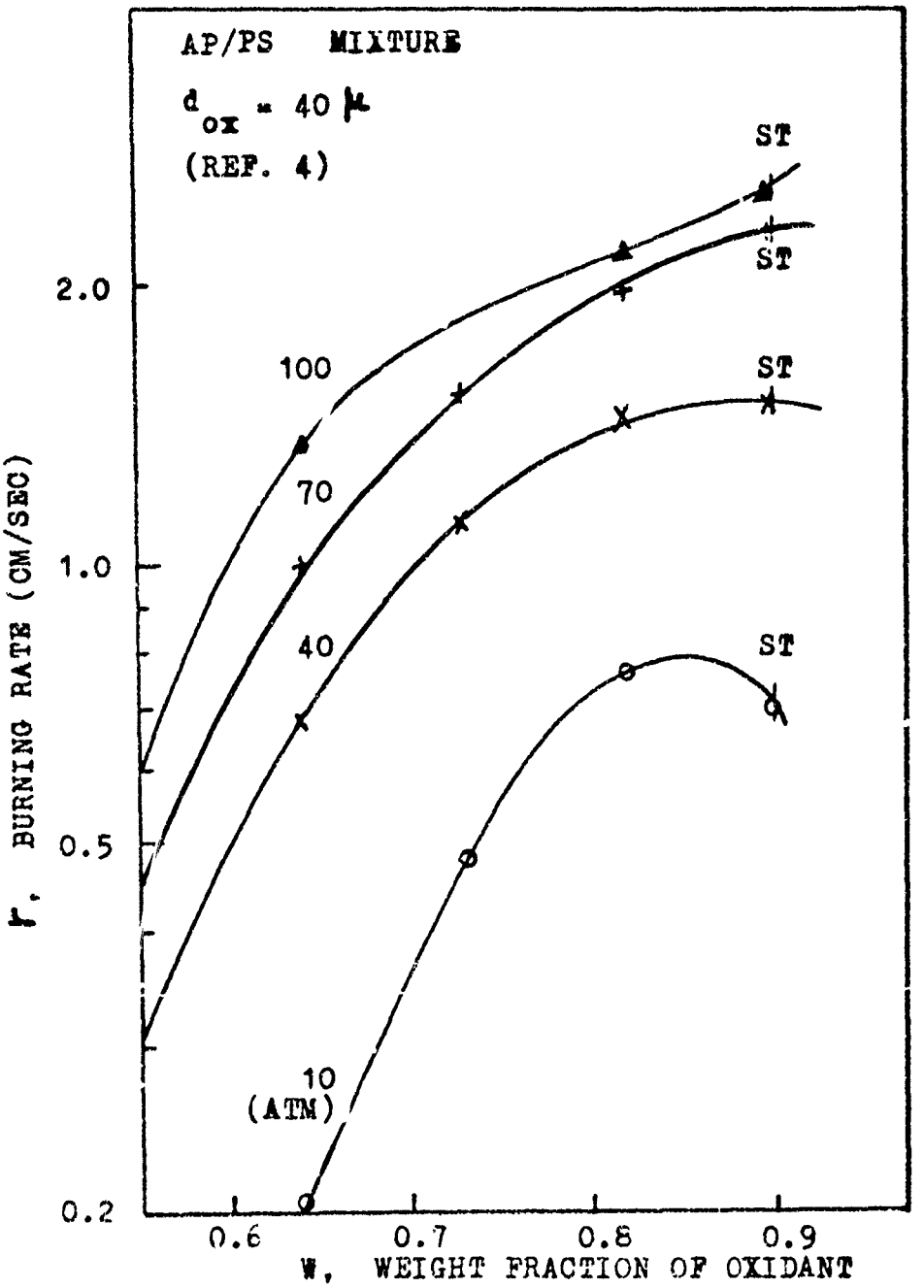

FIGURE II-6 : INFLUENCE OF PRESSURE ON THE POSITION OF MAXIMUM BURNING RATE (PRESSED-SAMPLES)

methylmethacrylate (PMM), $w_{r(max)}$ is near w_{st}. Hence, it is concluded that the type of fuel used in the propellant has an influence on the position of the maximum burning rate.

The influence of the oxidant particle size on the position of maximum burning rate is shown in Figure II-5. For a larger oxidant particle size, $w_{r(max)}$ is found to be on the fuel rich side, whereas for a smaller particle size, $w_{r(max)}$ is found to be near the stoichiometrically correct mixture ratio, w_{st}.

The influence of pressure on the position of maximum burning rate is shown in Figure II-6. At low pressures $w_{r(max)}$ is less than w_{st} and as the pressure is increased $w_{r(max)}$ shifts towards w_{st}.

The experimental data, shown in Figure II-6, were not taken beyond w_{st}, and hence the existence of the maximum burning rates with w variations at high pressures could not be conclusively confirmed. Part of the present investigation involves measuring regression rate for a wide range of variations in w at different pressures using loose-granule burners. The details and results of such measurements are given in Chapter III.

II. A. 3 Classification of Propellants

AP composite propellants have been classified by Steinz (2) into two categories: those that do and those that do not allow correlation

of r vs. P data by means of Summerfield's equation (1), viz.

$$\frac{1}{r} = \frac{a}{P} + \frac{b}{P^{1/3}} \qquad \ldots \text{ II-1}$$

where a - chemical-time parameter, and

b - diffusion-time parameter.

Both a and b are assumed to be independent of P.

The agreement (or lack of agreement) between the r vs. P data and Equation II-1 can be determined by plotting the data as $\frac{P}{r}$ vs. $P^{2/3}$ and checking whether such plots result in a straight line. This method of classification is illustrated in Figures II-7 and 8. Figure II-7 shows examples of propellants which do correlate via Equation II-1, and Figure II-8 shows an example of a propellant which does not follow Equation II-1. The corresponding r vs. P curves are shown in Figures II-9 and 10 respectively. It can be seen clearly from these figures that Summerfield's equation is a good representation for those propellants with burning rates (r) increasing monotonically with P and with the slope of r vs. P curves decreasing steadily.

In the present study, only those propellants for which data can be correlated with Equation II-1, are considered.

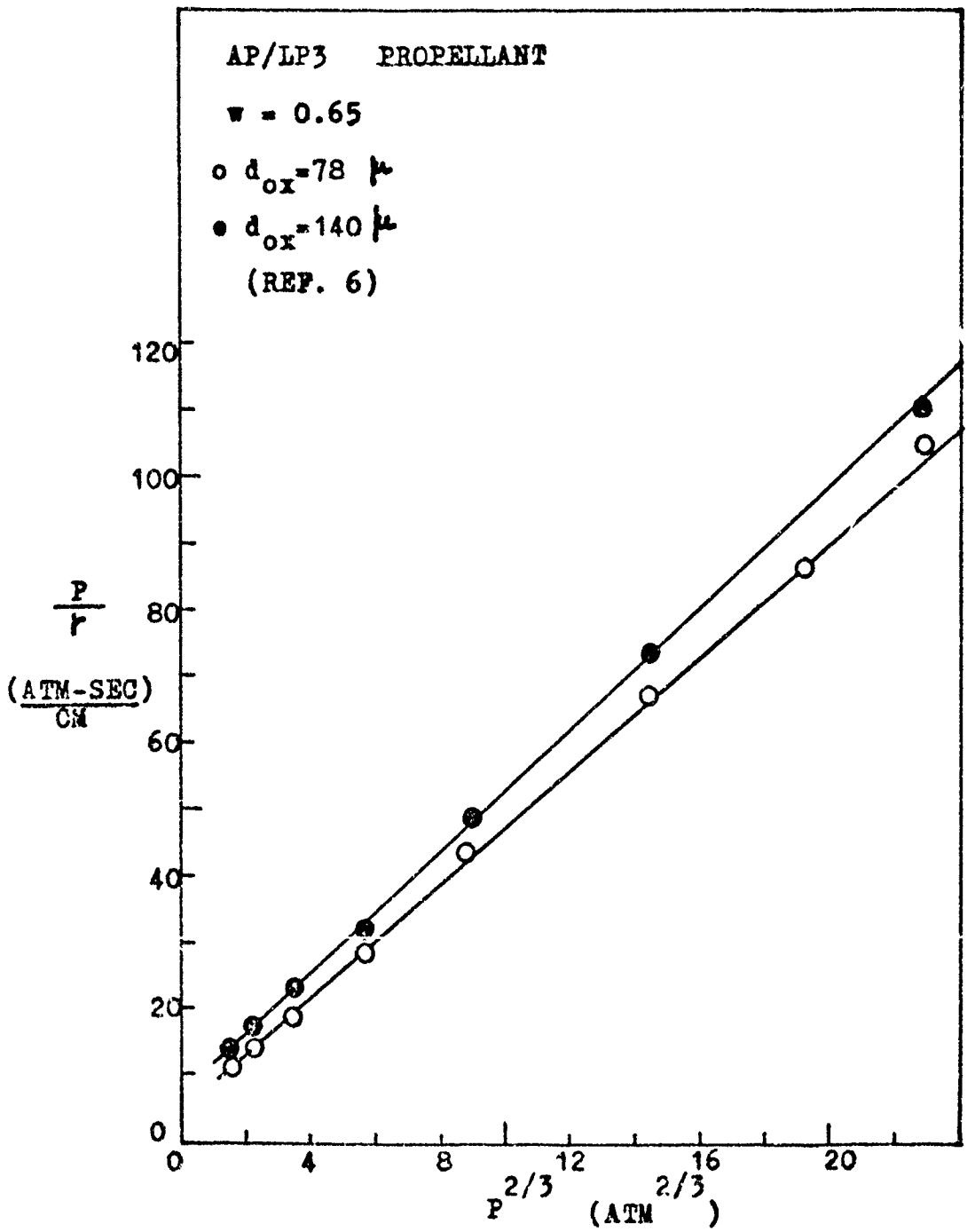

FIGURE II-7 BURNING RATE DATA CORRELATED WITH EQUATION II-1

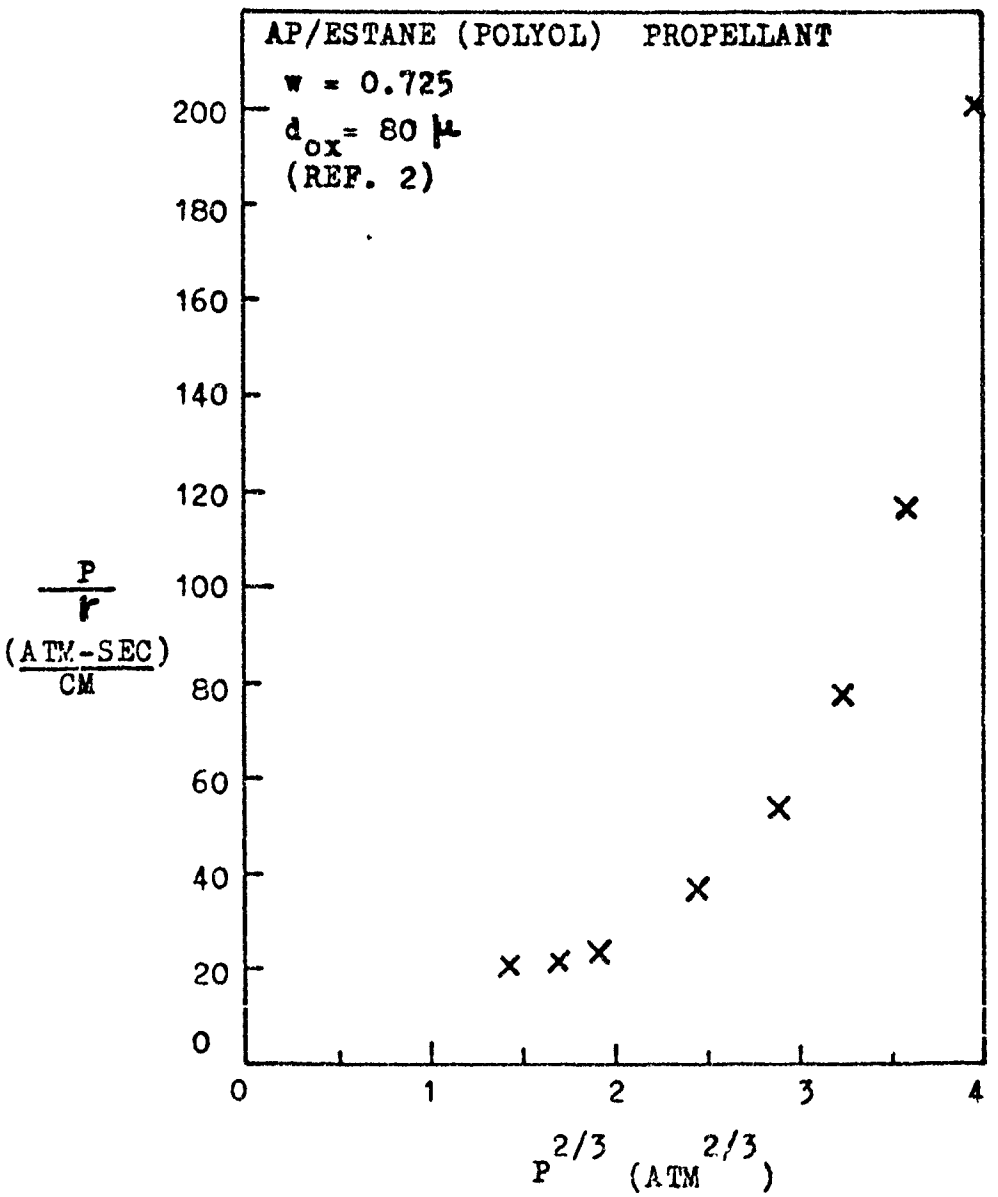

FIGURE II-8 ; BURNING RATE DATA OF A PROPELLANT WHICH DOES NOT CORRELATE WITH EQATION II-1

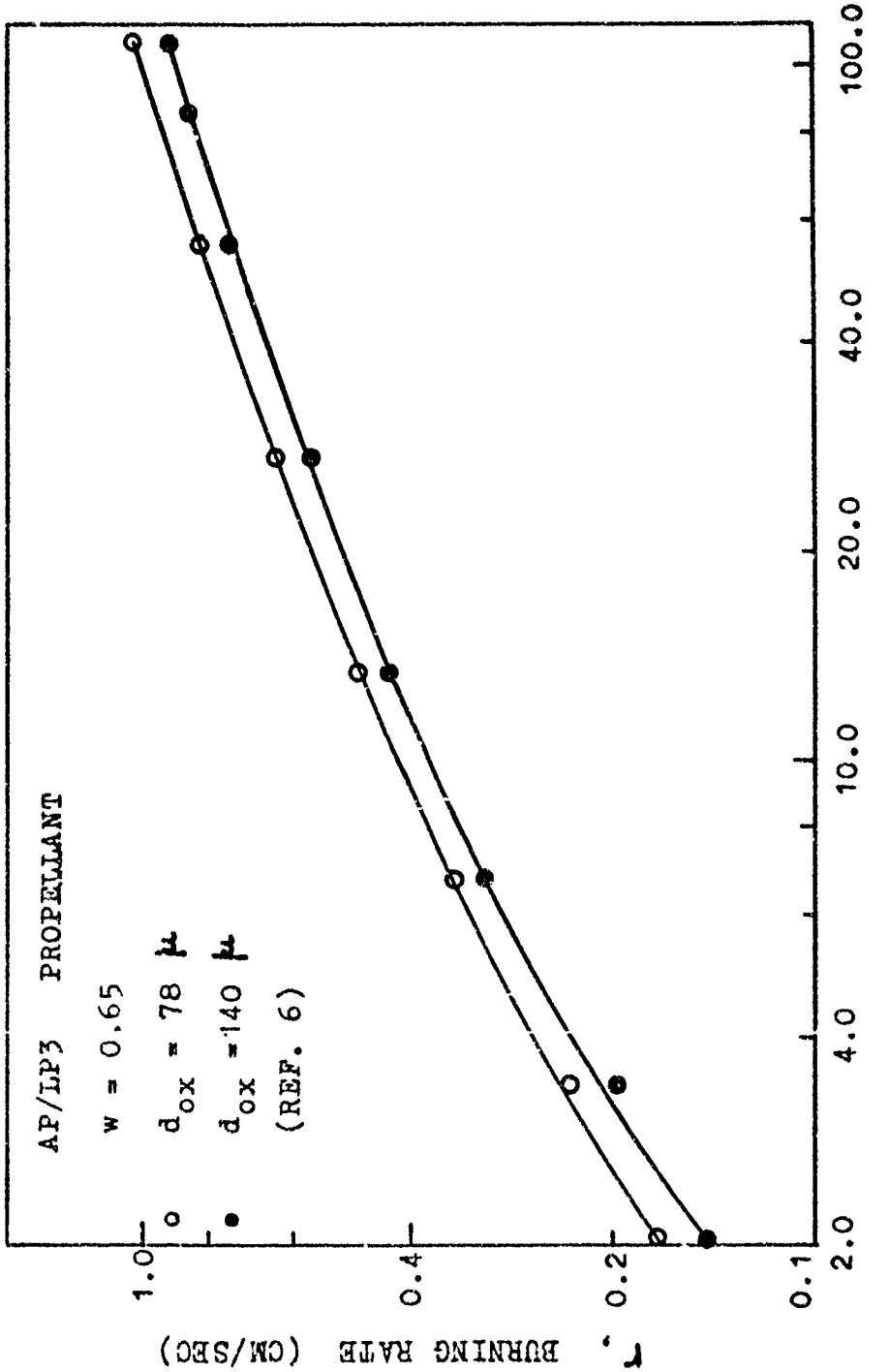

FIGURE II-9 : Vs. P CURVES OF PROPELLANTS WHICH OBEY EQUATION II-1

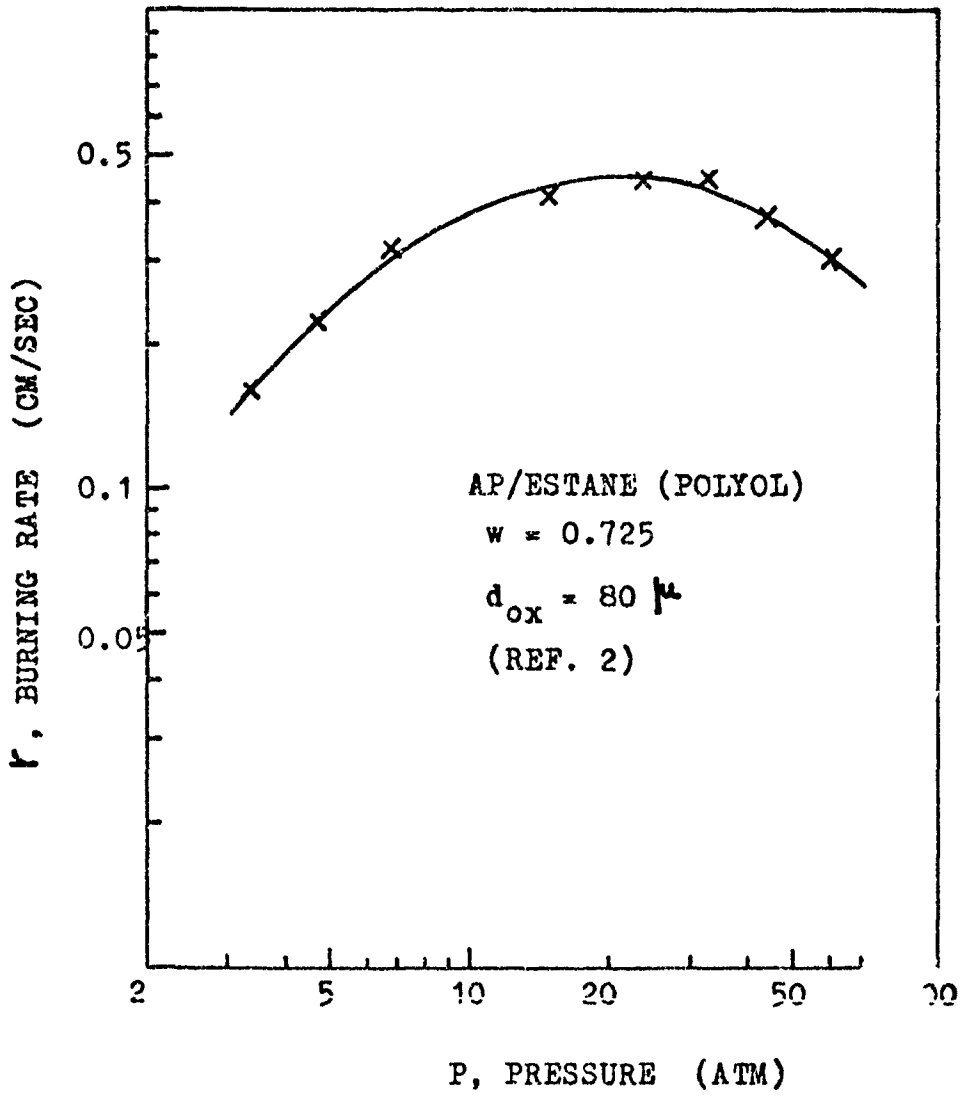

FIGURE II-10 : Vs. P CURVES OF A PROPELLANT WHICH DOES NOT OBEY EQUATION II-1

II. A. 4 Critique of Experimental Investigations

Based on a review of prior experimental investigations, the following observations can be made:

(i) In general, there is a lack of comprehensive experimental data available which deal with mixture-ratio influences. In order to assess existing and/or new models of propellant burning more comprehensive data is needed.

(ii). None of the propellants which follow equation II-1 were tested previously with more than two variations in the mixture ratio (2). Since a number of propellants obey Summerfield's equation, additional r vs. w data should be obtained for such propellants.

II. B THEORETICAL INVESTIGATIONS

Theoretical models describing the steady-state burning of composite solid propellants can be classified into two categories as follows:

(i) simple, analytical diagnostic aids, and

(ii) comprehensive models.

The simple, analytical diagnostic aids neglect many of the physical processes and chemical reactions for the purpose of mathematically tractable solutions. They lay their emphasis on specific processes. The following models belong to this category:

(i) Phalanx flame model (11),

(ii) Premixed, laminar flame model (12),

(iii) Sub-surface reaction model (13),

(iv) Thermal layer theory (14),

(v) Columnar diffusion flame model (15), and

(vi) Quasi-laminar. diffusion, and monopropellant flame theory (16).

Since these models neglect many of the presumably important processes and do not explain the burning-rate beheviour completely, they are not considered further in the present investigation.

The comprehensive models, on the other hand, are based on more complete, detailed mechanistic grounds. They allow prediction of the burning-rate behaviour with respect to variations in important parameters.

Hence, in the present study, the following comprehensive models have been consi'ered:

(i) Granular diffussion flame models (GDF),

a. Original GDF model (1, 6).

b. GDF model with collapsed AP decomposition flame (GDFC) (2).

c. GDF model with distended AP decomposition flame (GDFD) (2).

(ii) Heterogeneous reaction model (HR) (17, 18),

(iii) Multiple flame model (MF) (19, 20).

II. B. 1 Granular Diffusion Flame Model (GDF)

II. B. 1. a Description

In the general formulation of the GDF model (2), the gasification of the solid surface was considered to be driven by the conductive heat feed back from a two-stage flame in the gas phase.

The first-stage flame was considered to be the AP decompostion flame, and the second-stage flame was considered to be the result of the reaction between pockets of fuel (granules) and the oxidant rich products of AP flame. It should be noted that there is no experimental evidence for the existence of the fuel pockets, and this assumption has been seriously questioned (3).

A schematic description of the GDF model is shown in Figure II-ii.

II. B. 1.b Assumptions

Itemized, the major assumptions of the GDF model are :

(i) One-dimensionality (planar surface and reaction zones in the gas phase).

(ii) Steady-state.

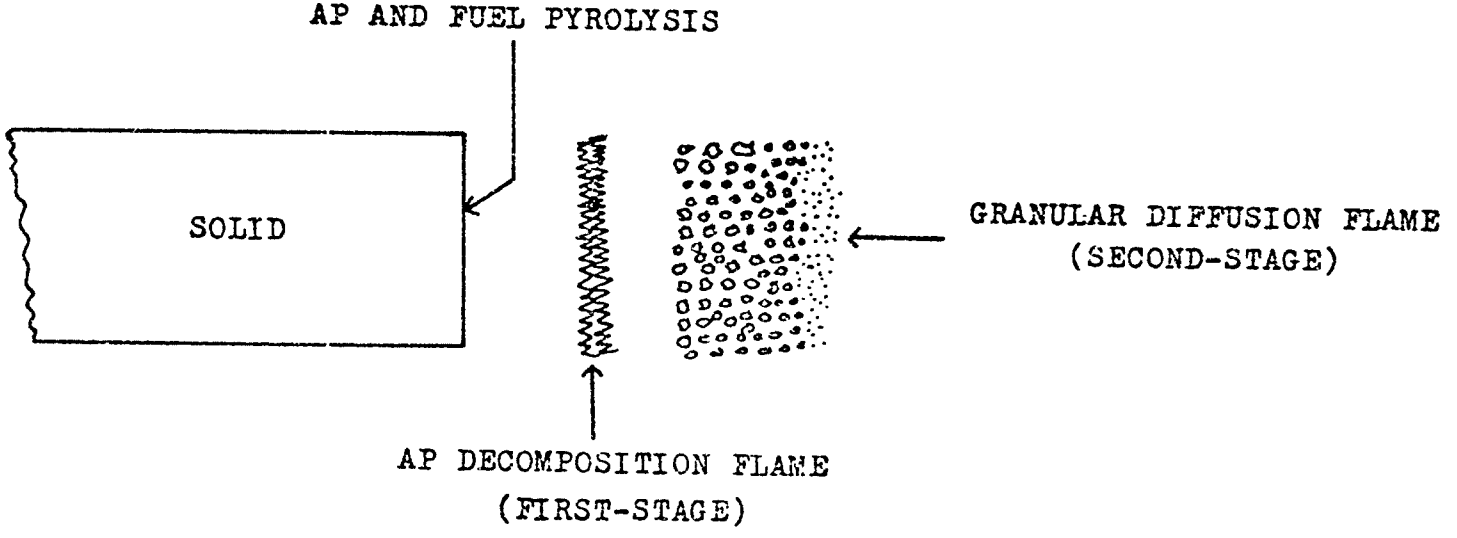

FIGURE II-11 : DESCRIPTION OF THE GDF MODEL

(iii) Specific physico-chemical processes:

The physical processes considered are heat conduction and granular diffusion.

The chemical reactions considered are fuel pyrolysis, dissociative sublimation of AP into ammonia and perchloric acid, AP decomposition flame (first-stage flame resulting from a second order, premixed reaction between ammonia and perchloric acid), and granular diffusion flame (second-stage flame resulting from the diffusional mixing and reaction between fuel pockets and oxidant rich products of AP flame).

(iv) Linear temperature distribution in the gas phase.

(v) Uniform thermal properties.

II.B.1.c Equations

From the description and the assumptions made in the formulation of the GDF model, the following equations can be written (2).

An energy balance at the surface, for the first-stage flame gives:

$$\lambda_g \left(\frac{T_f - T_s}{L_f}\right) = \rho_p r \left[c_g (T_s - T_0) + w Q_{AP} + (1-w) Q_s\right] \quad \ldots \text{II-2}$$

An energy balance at the first-stage flame, for the second-stage flame gives :

$$\lambda_g \left(\frac{T_s - T_1}{L_2}\right) = \rho_p r \left[c_g (T_s - T_o) + W Q_{AP} + (1-W) Q_f - W \Delta H_{AP}\right] \quad \ldots \text{ II-3}$$

where

λ_g - thermal conductivity of gases,

c_g - specific heats of solid and gases,

T_o - initial temperature,

T_s - surface temperature,

T_1 - first-stage flame temperature,

T_2 - second-stage flame temperature,

L_1 - first-stage flame height,

L_2 - second-stage flame height,

ρ_p - propellant density,

r - burning rate,

w - weight fraction of oxidant,

Q_{AP} - heat of sublimation of AP,

Q_F - heat of pyrolysis of fuel, and

ΔH_{AP} - heat of reaction of AP flame.

An Arrhenius expression is assumed to describe the surface pyrolysis of the propellant and is given by:

$$r = A_s \exp(-E_s/RT_s) \qquad \ldots \text{ II-4}$$

where A_s - pre-exponential factor,

E_s - activation energy, and

R - universal gas constant.

II.B.2 Original GDF Model

II.B.2.a Additional Assumptions

In the original GDF model (1), the following additional assumptions were made :

(i) Constant surface temperature, T_s.

(ii) An AP decomposition flame (first-stage flame) occuring entirely ("collapsed") at the regressing surface.

II.B.2.b Formulation of the Model

The collapsed AP flame assumption reduces Equation II-2 and Equation II-3 to a single equation :

$$\lambda_g \left(\frac{T_2 - T_s}{L_2}\right) = \rho_p r \left[c_g (T_s - T_o) + w Q_{AP} + (1-w) Q_f - w \Delta H_{AP}\right] \qquad \ldots \text{ II-5}$$

In Equation II-5, L_2 is unknown and is expressed by considering the detailed structure of the granular diffusion flame. To approximate

L_2, two extremes of low and high pressures were considered. At low pressures, chemical reaction was considered to be controlling; at high pressures, diffusional mixing was considered to be controlling.

Letting $L_{2,ch}$ denote the granular diffusion flame height, when chemical reactior is controlling (at low pressures), the chemical mass conversion rate in a zone of thickness $L_{2,ch}$ may be written as:

$$\rho_p r_{ch} = L_{2,ch} B \rho_g^2 \exp(-E_2/RT_2) \quad \ldots \text{II-6}$$

where r_{ch} - burning rate at low pressures,

B - pre-exponential factor, and

E_2 - activation energy for the gas-phase reaction

Substituting the value for $L_{2,ch}$ from Equation II-6 in Equation II-5, an expression for r_{ch} has been obtained (2) :

$$\frac{1}{r_{ch}} = \rho_p \sqrt{\frac{c_g (T_s - T_o) + W Q_{AP} + (1-W) Q_f - W \Delta H_{AP}}{\lambda_g (T_2 - T_s)}} \times \left(\frac{\alpha T_2}{P}\right) \exp(E_2/2RT_2) \quad \ldots \text{II-7}$$

where α is a constant.

On the other hand, considering high pressures and control of burning by the diffusional mixing of the fuel pockets, an expression for $L_{2,diff}$ has been obtained (2) :

$$L_{2,diff} = \beta^2(d_{ox}) \frac{\rho_p r_{diff} T_2^{5/3}}{T_s^{7/4} p^{2/3}} \quad \ldots \text{ II-8}$$

where β is a function of μ, the mass of each fuel pocket, and hence depends only on d_{ox}.

By substituting the value for $L_{2,diff}$ in Equation II-5, the burning rate at high pressures, r_{diff}, has been obtained (2) as:

$$\frac{1}{r_{diff}} = \rho_p \sqrt{\frac{c_g(T_s - T_o) + W Q_{AP} + (1-W) Q_f - W \Delta H_{AP}}{\lambda_g (T_2 - T_o)}} \times \left(\frac{\beta(d_{ox}) T_2^{5/6}}{p^{1/3} T_s^{7/8}} \right) \quad \ldots \text{ II-9}$$

With the two asymptotic forms for the burning rate, given by Equations II-7 and 9, the burning rate at an intermediate pressure was expressed by a relation which reduces to one of these limiting forms at either extreme of pressure.

The following form was proposed in reference (1):

$$\frac{1}{r} = \frac{1}{r_{ch}} + \frac{1}{r_{diff}} \quad \ldots \text{ II-10}$$

or, substituting from Equations II-7 and II-9 :

$$\frac{1}{r} = \rho_p \sqrt{\frac{c_g(T_s - T_o) + W Q_{AP} + (1-W) Q_f - W \Delta H_{AP}}{\lambda_g (T_2 - T_s)}} \times \left\{ \frac{\alpha T_2}{p} \exp\left(E_2/RT_2\right) + \frac{\beta(d_{ox}) T_2^{5/6}}{p^{1/3} T_s^{7/8}} \right\} \quad \ldots \text{ II-11}$$

or

$$\frac{1}{r} = \frac{a}{P} + \frac{b}{P^{1/3}} \qquad \ldots \text{ II-12}$$

where

$$a = \rho_p \sqrt{\frac{c_g (T_s - T_o) + W Q_{AP} + (1-W) Q_f - W \Delta H_{AP}}{\lambda_g (T_2 - T_s)}} \times \left\{ \alpha T_2 \exp \left(E_2 / R T_2 \right) \right\} \qquad \ldots \text{ II-13}$$

and

$$b = \rho_p \sqrt{\frac{c_g (T_s - T_o) + W Q_{AP} + (1-W) Q_f - W \Delta H_{AP}}{\lambda_g (T_2 - T_s)}} \times \left\{ \frac{\beta (d_{ox}) \, T_2^{5/6}}{T_s^{7/8}} \right\} \qquad \ldots \text{ II-14}$$

II. B. 2. c Discussion

In the preceding equations, the burning rate appears in a transcendental form requiring an iterative solution. The principal equations involved are Equations II-4 and II-11. The two unknowns are r and T_s, the burning rate and the surface temperature, respectively.

In the original formulation of the GDF model, these equations were not solved numerically. The assumption that the surface temperature, T_s, is constant allowed the Equation II-4 to be neglected, and the burning rate was related to the pressure by means of Equation II-12 only; this equation is sometimes known as

Summerfield equation. The validity of the GDF model was said to be established by showing that experimental burning-rate data (r vs. P) could be correlated by the Summerfield equation for many propellants (1, 2, 6).

II.B.3 GDFC Model

Steinz (2) has modified the GDF model by allowing the surface temperature to vary with pressure, in accordance with Equation II-4, but retained the collapsed AP decomposition flame assumption. This model was termed the "granular diffusion flame model with collapsed AP decomposition flame" (GDFC) model.

II.B.3.a Resulting Equations

The equations of the GDFC model are those of the GDF model:

$$r = A_s \exp(-E_s/RT_s) \qquad \ldots \text{II-4}$$

$$\frac{1}{r} = \rho_p \sqrt{\frac{c_g (T_s - T_0) + W Q_{AP} + (1-W) Q_f - W \Delta H_{AP}}{\lambda_g (T_2 - T_s)}}$$

$$\times \quad \frac{\alpha T_2}{P} \exp\left(\frac{E_2}{2RT_2}\right) + \frac{\beta (d_{ox})\, T_2^{5/6}}{P^{1/3}\, T_s^{7/9}} \qquad \ldots \text{II-11}$$

Equations II-4 and II-11 contain two unknowns, r and T_s. They can be solved numerically by using the method described below.

II.B.3.b Method of Solution

The input values required to solve Equations II-4 and II-11 are classified as :

(i) environmental input values (P and T_o),

(ii) compositional input values (w, d_{ox}, ρ_p, T_2, Q_{AP}, Q_f, ΔH_{AP}),

(iii) kinetic input values (E_s, E_2, etc.,), and

(iv) empirical input values (A_s, α, and β).

The empirical input values are obtained as follows :

(i) Determine values for a and b from a plot of $\frac{P}{r}$ vs. $P^{2/3}$.

(ii) Choose a pressure (matching point), determine the corresponding value for r, and select an appropriate value for T_s.

(iii) Use Equations II-4 to determine A_s.

(iv) Use Equations II-13 and II-14 to determine α and β.

Equations II-4 and II-11 can now be solved numerically for various other pressures.

Figure II-12 describes the method used to solve the GDFC model equations.

II.B.3.c Results and Discussion

In Reference 2, numerical solutions were obtained for a typical propellant by considering only pressure variations. The predicted r vs. P results were shown to have the same form as that of Summerfield Equation (Equation II-12) in 1.0 to 100 atm. range.

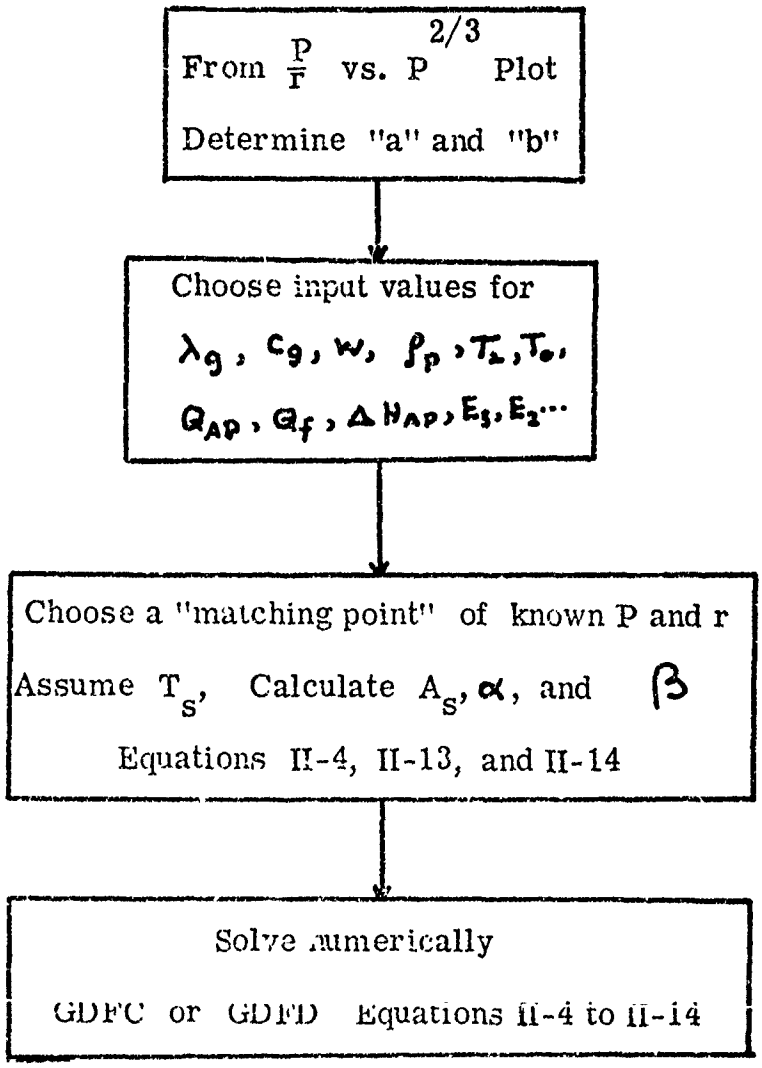

FIGURE II-12 FLOW CHART OF THE METHOD OF SOLUTION FOR GDF MODEL

The predicted results were not compared with any experimental data. The matching point needed to obtain the empirical constants A_s, α, and β, was chosen arbitrarily at a low pressure. The possible effects of alternative selections for the matching point (at different pressures) was ignored. Furthermore, the influences of oxidant particle size, mixture ratio and initial temperature on the burning rate were not discussed.

Therefore, as part of the present investigation, the following comprehensive numerical tests were made to assess the GDFC model :

(i) A comparison of the predicted GDFC results with experimental results (r vs. P).

(ii) An investigation of the effect of the matching point selected.

(iii) An investigation of the influence of mixture ratio on the burning rate as predicted by the GDFC model.

II.B.4 GDFD Model

The collapsed-AP-flame assumption made in the GDFC model was found by Steinz (2) to be invalid at low pressures. Hence, Steinz proposed a GDF model with "distended" AP flame (GDFD). The GDFD model is supposed to be valid at low combustion pressures.

II. B. 4. a Resulting Equations

As a consequence of the above-mentioned assumption, the GDFD model is described by Equations II-2, II-3, and II-4. In order to solve these equations, the flame height L_1 of the first-stage flame must be specified.

Considering mass conservation, L_1 can be written as (2) :

$$L_1 = \frac{\rho_p r}{\rho_g} \cdot \tau_{AP} \qquad \ldots \text{ II-15}$$

where τ_{AP} is the reaction time of the AP flame. Assuming the AP flame to be a premixed and second-order reaction, τ_{AP} was found to be (2) :

$$\tau_{AP} = \frac{6.5 \times 10^{-6}}{P} \quad (sec) \qquad \ldots \text{ II-16}$$

The flame height, L_2, has been taken to be the same as that considered in the GDFC model.

The following equations resulted after simplification (2) :

$$r = A_s \exp(-E_s/RT_s) \qquad \ldots \text{ II-4}$$

$$T_1 = \frac{T_s}{\left[1 - \frac{r^2 \tau_{AP} R \rho_p^2}{P \lambda_g M}\left\{c_g(T_s - T_0) + w Q_{AP} + (1-w)Q_f\right\}\right]} \qquad \ldots \text{ II-17}$$

$$r = \frac{1}{L_2 \rho_p} \left\{ \frac{\lambda_g (T_2 - T_1)}{C_g (T_1 - T_0) + W Q_{AP} + (1-W) Q_f - W \Delta H_{AP}} \right\}$$

... II-18

II. B. 4. b Method of Solution

The resulting equations, viz. Equations II-4, 17, and 18 of the GDFD model contain three unknowns r, T_s, and T_1. The numerical procedure used to solve these three equations is the same as that described in Section II. B. 3. b and also in Figure II-12.

II. B. 4. c Results and Discussion

The results reported in Reference 2 for the GDFD model were obtained for the same typical propellant used for the GDFC model calculations described earlier (Section II. B. 3. c). The burning rates predicted by the GDFD model in the 1. 0 to 100. 0 atm. range were found to be less than those predicted by the GDFC model. The GDFD model results were not compared with any experimental data. The influences of matching point selection, oxidant particle size, mixture ratio, and initial temperature were not reported in Reference 2.

Therefore, as part of the present investigation, the following numerical tests were made to assess the GDFD model:

(i) A comparison of the predicted GDFD results with experimental data (r vs. P).

(ii) An investigation of the influences of matching points.

(iii) An investigation of the influence of mixture ratio on the burning rate as predicted by the GDFD model.

These tests and their results are discussed in Chapter IV.

II.B.5 Heterogeneous Reaction Model (HR)

II.B.5.a Description of the HR Model

Hermance (17, 18) developed a model of composite - solid - propellant burning by incorporating effects of propellant surface heterogeneity and of heat released at the surface due to a heterogeneous reaction between the oxidant pyrolysis products and solid fuel binder. This model can be used to predict known combustion characteristics like the burning rate, surface temperature, etc., a priori , using only the propellant composition and component decomposition characteristics as input data.

Figure II-13 describes schematically the structure of the surface and the sites of heat generation considered in the HR model.

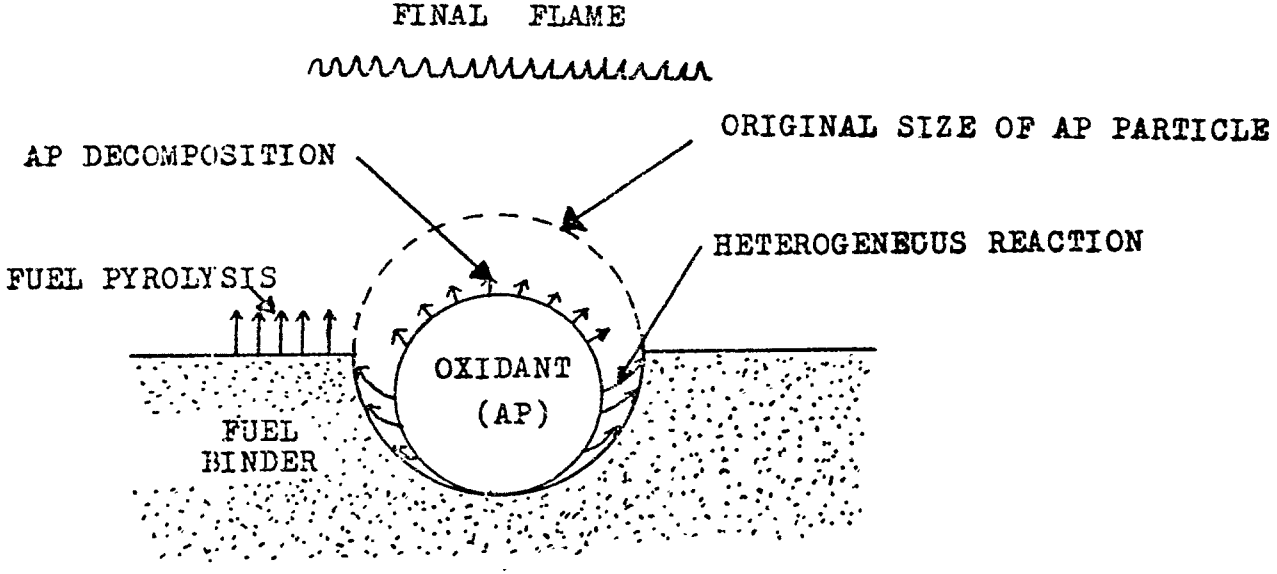

FIGURE II-13 : DESCRIPTION OF THE HETEROGENEOUS REACTION MODEL

II.B.5.b Major Assumptions

(i) Geometry :

solid phase - one dimensional

surface - three dimensional

gas phase - one dimensional

(ii) Steady state.

(iii) Uniform thermal properties.

(iv) Specific physico-chemical processes :

The physical processes considered are heat conduction, and diffusion.

The chemical reactions considered are fuel pyrolysis, dissociative sublimation of AP into ammonia and perchloric acid, exothermic reaction between fuel binder and products of AP sublimation (heterogeneous reaction), and exothermic reaction between final AP decomposition products and fuel vapors.

II.B.5.c Resulting Equations

Due to the complexity of the model and the numerous equations involved, a detailed review is not given here. Hence, only the final equations are listed below :

$$r = a_1 \exp\left(-\frac{E_f}{E\theta_s}\right) + \frac{b_1 P^{\delta}}{\theta_s^{1/2}}\left[\frac{c_3}{r} - \frac{d_1}{P^m}\right] \times \exp\left(\frac{-E_{ox} - E_{sr}}{E\theta_s}\right) \quad \ldots \text{ II-19}$$

$$\theta_s = b_2 + \left(\frac{b_3 P^{\delta}}{r\theta_s^{1/2}}\right)\left[\frac{c_3}{r} - \frac{d_1}{P^m}\right] \exp\left[\frac{-(E_{ox} + E_{sr})}{E\theta_s}\right] + \frac{a_2}{r}\exp\left(-\frac{E_s}{E\theta_s}\right) + a_3 \exp\left(-\beta_f \theta_f^2 e^{\frac{1}{\theta_f}\left(\frac{r}{P}\right)^2}\right] \quad \ldots \text{ II-20}$$

$$\theta_f = \theta_s + a_3\left\{1 - \exp\left[-\beta\theta_f^2 e^{\frac{1}{\theta_f}\left(\frac{r}{P}\right)^2}\right]\right\} \quad \ldots \text{ II-21}$$

where $\theta = \frac{RT}{E}$, and the constants a_1, a_2, a_3, b_1, b_2, b_3, c_3, d_1, and other parameters involved are defined in References 17 and 18.

II.B.5.d Method of Solution

The above equations contain three unknowns, viz. r, T_S, and T_F. Numerical solutions were obtained by an iterative procedure described in Reference 17.

II.B.5.e Results and Discussion

The results of the HR model were compared with experimental data of AP/LP3 (6) propellants only. The model has been tested comprehensively, and qualitative agreement has been found between the predictions of the model and experimental data with regard to the influences of P, d_{ox}, w and T_o on r (17, 18). Since the experimental data available for mixture ratio variation were confined to a narrow range of w (0.6 to 0.7), the results of the HR model were not considered beyond w=0.7. Hence, an additional test useful for evaluating this model would be to obtain more results beyond w = 0.7 and to study the predicted trends of r vs. w curves.

One of the most severely criticised assumptions of the HR model is the heterogeneous reaction considered to be occuring in the cusps. There is no experimental evidence for the occurrence of such a reaction.

II.B.6 Multiple Flame Model (MF)

II.B.6.a Description of the MF Model

The multiple flame model has been based on a flame structure surrounding individual oxidant particles. Three seperate flames have been considered to supply the heat required for surface gasification. They are as follows :

(i) A primary flame (PF) surrounding the AP particle caused by the reaction between a fraction of AP sublimation products and a fraction of fuel vapors. Both kinetics and diffusion are assumed to be controlling.

(ii) The AP decomposition flame (AP flame) controlled by kinetics alone .

(iii) A final flame (FF) caused by the reaction between AP decomposition products and fuel vapors and is controlled by diffusion alone.

In Figure II-14, a schematic description of the MF model is given.

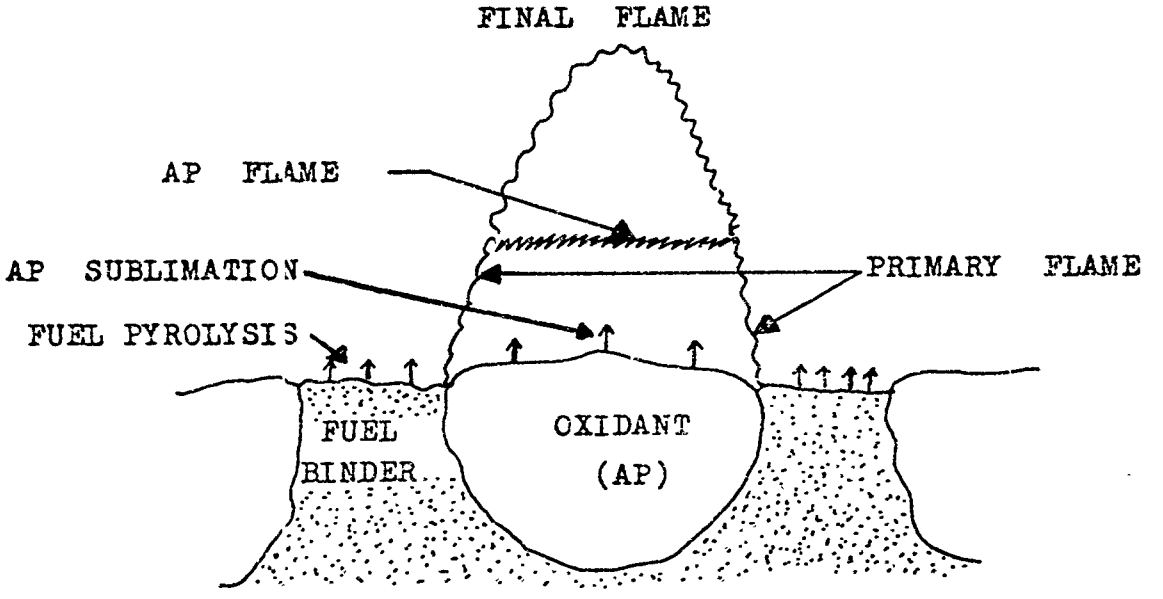

FIGURE II-14 : DESCRIPTION OF THE MULTIPLE FLAME MODEL

II.B.6.b Major Assumptions

(i) Geometry :

Solid phase - one dimensional

Surface - three dimensional

Gas phase - primary and final flames- three dimensional, and AP flame - one dimensional.

(ii) Steady state.

(iii) Uniform thermal properties.

(iv) Specific physico-chemical processes :

The physical processes considered are heat conduction and diffusion.

The chemical reactions considered are fuel pyrolysis, AP sublimation, primary flame, AP decomposition flame, and final flame.

II.B.6.c Equations

Mass conservation at the surface gives :

$$\dot{m}''_T = \rho_p r = \dot{m}''_{ox}\left(\frac{s_{ox}}{s_o}\right) + \dot{m}''_f\left(\frac{s_f}{s_o}\right) \quad \ldots \text{ II-22}$$

where $\dot{m}''_T$ - mass flux of the propellant,

$\dot{m}''_{ox}$ - mass flux of the oxidant,

$\dot{m}''_f$ - mass flux of the fuel,

$\frac{S_{ox}}{S_o}$ - surface area ratio of oxidant to total propellant, and

$\frac{S_f}{S_o}$ - surface area ratio of fuel to total propellant.

$\dot{m}''_{ox}$ and $\dot{m}_f$ have been expressed in terms of pre-exponential factors, A_{ox} and A_f, and activation energies, E_{ox} and E_f, and the surface temperature, T_s, as given below :

$$\dot{m}''_{ox} = A_{ox} \exp\left(-E_{ox}/RT_s\right) \quad \ldots \text{II-23}$$

$$\dot{m}''_f = A_f \exp\left(-E_f/RT_s\right) \quad \ldots \text{II-24}$$

$\frac{S_{ox}}{S_o}$ and $\frac{S_f}{S_o}$ were expressed as functions of w and other factors which influenced the surface geometry.

An energy balance at the surface was given by :

$$T_s = T_o - w\frac{Q_L}{c_p} - (1-w)\frac{Q_f}{c_p} + (1-\beta_F)w\left[\frac{Q_{AP}}{c_p}\exp(-\xi^*_{AP}) + \frac{Q_{FF}}{c_p}\exp(-\xi^*_{FF})\right] + \beta_F\frac{Q_{PF}}{c_p}\exp(-\xi^*_{PF}) \quad \ldots \text{ II-25}$$

where Q's represent the heat of vaporization of solids and heats released by various flames, β_F is the fraction of oxidant reactants that react in the primary flame (PF), and ξ^*'s are the nondimensional flame stand-off distances of various flames, ($\xi^* = \frac{c_p \dot{m}'' x^*}{\lambda}$).

The flame heights, x^*'s, were obtained for kinetic-controlled flames and diffusion-controlled flames in the following forms :

$$x^*_{\text{(kinetic-controlled flame)}} = \frac{\dot{m}''}{k P^{\delta}} \quad \ldots \text{ II-26}$$

where k is the pseudo-rate constant and δ is the reaction order.

$$x^*_{\text{(diffusion-controlled flame)}} = f(\eta', \ldots) \quad \ldots \text{ II-27}$$

where η' is the nondimensional flame height given by Burke and Schumann's thin-flame analysis (22).

II.B.6.d Method of Solution

The equations of the MF model contain basically two unknowns, r and T_s, and can be solved numerically by an iterative procedure. The burning rate behaviour with pressure, oxidant particle size, mixture ratio, and initial temperature has been studied (19, 20).

II.B.6.e Results and Discussion

The formulation of the MF model is found in two publications (19, 20). The major assumptions, the resulting equations, and the method of solutions were the same in both these references, but the input values used were different.

The following comments are made with regard to these two presentations :

(i) Reference 19 contains a complete set of input data needed for numerical calculations of the MF model; Reference 20 contains incomplete input data.

(ii) The results reported in Reference 19 are poorly supported by experimental data. The results of Reference 20 are somewhat improved.

In order to assess this model, a complete set of input data used in Reference 20 has been obtained from one of the authors(23), and further tests have been made on the MF model as part of the present

study.

Mixture ratio effects considered in References 19 and 20 were confined to a narrow range of w (0.6 to 0.7). In order to study the trends of r vs. w predicted by the MF model more calculations are needed, and new numerical tests made on the MF model in the present investigation are discussed in Chapter IV.

II.C CONCLUDING REMARKS

The preceeding review of the prior experimental and theoretical investigations of the burning of AP propellants has established the need for futher consideration of the influences of mixture ratio, and the need for further assessment of the existing models by more numerical tests.

In Chapter III, new experimental and theoretical investigations undertaken in the present investigation with regard to the mixture-ratio influences are presented.

In Chapter IV, an assessment of the important theoretical models is made based on a number of new numerical test.

CHAPTER III - PRESENT INVESTIGATIONS INVOLVING MIXTURE-RATIO INFLUENCES

III. A BURNING RATE MEASUREMENTS ON PROPELLANT ANALOGS

The influences of fuel and oxidant particle size on the mixture ratio for maximum burning rates, $w_{r(max)}$, were studied previously by Bakhman et al. (4), and McAlevy et al. (10) by varying w over a wide range (beyond w_{st} on the oxidant rich side). But the data obtained by Bakhman et al. (4) to study similar influences of pressure, were not taken beyond w_{st}. The occurrence of maxima in r vs. w curves has also not been well confirmed above 10 atm. (see Figure II-6). Hence, burning rates have been measured in the present investigation over a wide range of w (beyond w_{st}), for different pressures, by using a loose-granule burner. The purpose of these measurements is to supplement the previously obtained data (4) and to verify those results.

The fabrication of the loose-granule burner, the apparatus used, and the techniques used to measure the burning rate are described in detail in Reference 10, and hence, only new experimental results are discussed at present.

III. A. 1 Results and Discussion

The results of the present investigation together with those of reference 9 are plotted in Figure III-1. It is seen clearly that $w_{r(max)}$ shifts from the fuel-rich side towards the stoichiometrically correct mixture-ratio as pressure is increased. This behaviour is in conformity with the results of Bakhman et al. (4).

III. B EXTENSION OF A SIMPLIFIED PREMIXED FLAME MODEL TO ENCOMPASS COMPOSITE PROPELLANT BURNING

In the past, solid propellant burning models were based on simple extensions of laminar, premixed flame theories to predict burning rate characteristics, such as, the dependence of the burning rate on pressure, flame temperature, etc., (3, 12, 16). Since the mixture ratio influences the structure of a premixed flame via flame temperature a simplified, premixed, and laminar flame model has been formulated as part of the present investigation to explore mixture-ratio influences on the burning rate of composite solid propellant.

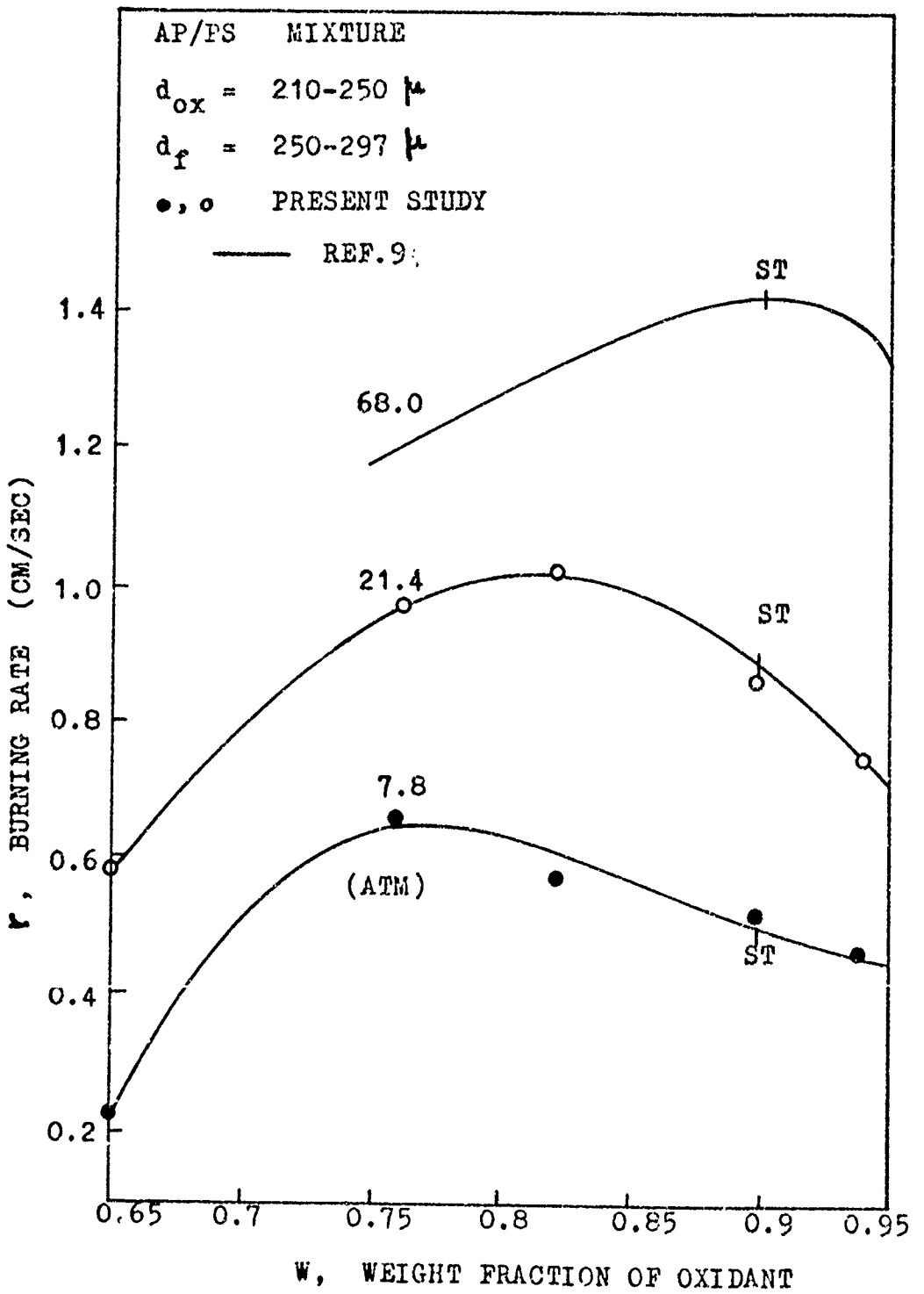

FIGURE III-1 : INFLUENCE OF PRESSURE ON THE POSITION OF MAXIMM BURNING RATE

III. B. 1 Description of the Model

Figure III-2 illustrates the simple, premixed, laminar-flame model considered. A single premixed flame in the gas phase is considered to release heat which, conducted to the solid surface, causes regression of the solid surface. The temperature of this flame is assumed to be equal to the adiabatic flame temperature of the propellant.

III. B. 2 Major Assumptions

(i) The solid surface and the flame are planar and parallel to each other (one dimensional).

(ii) Steady state.

(iii) Uniform thermal properties.

(iv) An Arrhenius type expression describes the surface pyrolysis of both AP and fuel.

(v) A premixed, laminar flame of second order exists in the gas phase.

(vi) The temperature distribution in the gas phase is linear.

III. B. 3 Equations

The surface pyrolysis of the propellant is assumed to be described by an Arrhenius type expression given below:

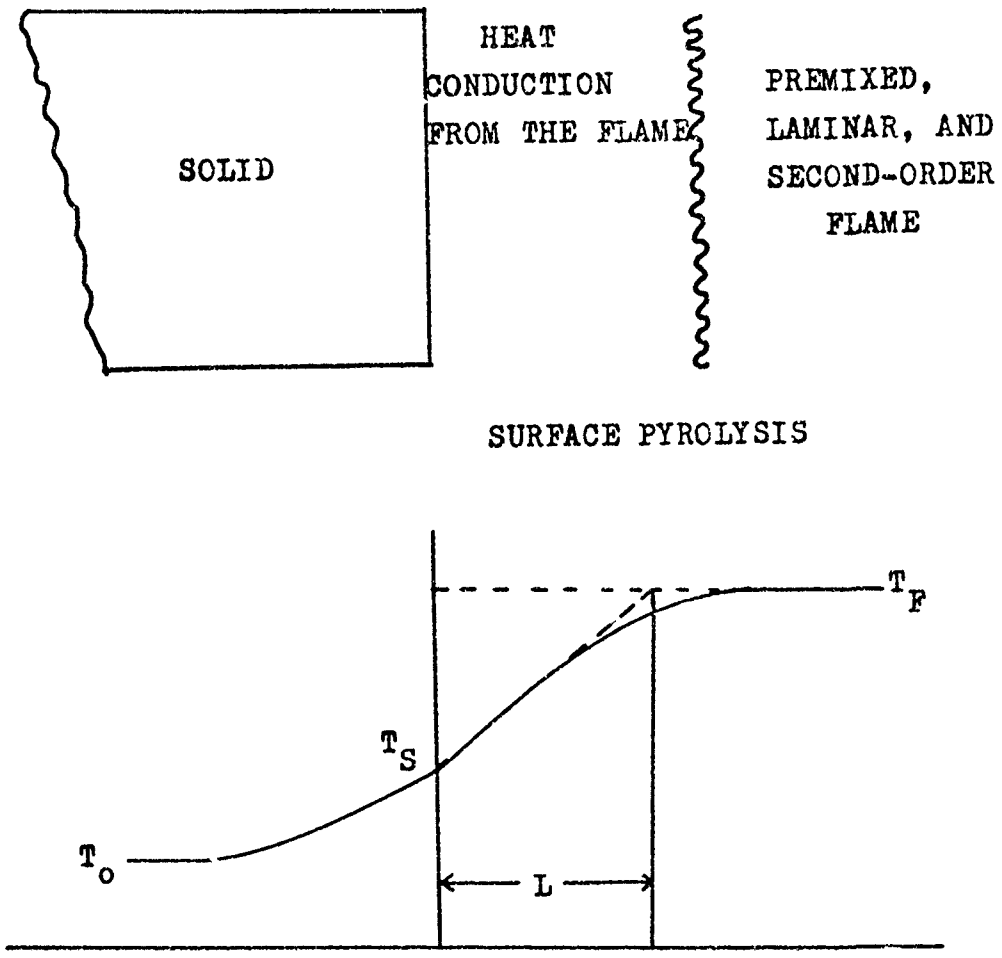

FIGURE III-2 : THE SIMPLIFIED, PREMIXED AND LAMINAR FLAME MODEL

$$r = A_s \exp(E_s/RT_s) \qquad \ldots \text{ III-1}$$

The notations used here are explained in Chapter II.

With the above assumptions, the energy balance at the surface is given by :

$$\lambda_g \left(\frac{T_F - T_s}{L}\right) = \rho_p r \left[c_g (T_s - T_o) + w Q_{AP} + (1-w) Q_f\right] \qquad \ldots \text{ III-2}$$

If the thickness of the reaction zone, L, is specified as a function of pressure (P), flame temperature (T_F), mixture ratio (w), etc., then Equations III-1 and III-2 can be solved for burning rates as functions of P and w.

The thickness of the reaction zone, L, has been estimated as follows :

For a second-order reaction, the reaction rate can be written as

$$\text{reaction rate} = B \rho_g^2 w(1-w) \exp(-E_2/RT_F) \qquad \ldots \text{ III-3}$$

From mass continuity, we get

$$r \rho_p = L B' \rho_g^2 w(1-w) \exp(-E_2/RT_F) \qquad \ldots \text{ III-4}$$

It should be noted here that the reaction zone thickness, L, considered is similar to $L_{2,ch}$ considered in the GDF model, except that a term, w (1-w), is included in the present model to account for the dependence of reaction rate on the concentrations of fuel and oxidant.

Substituting the expression for L, given by Equation III-4 in Equation III-2, the following equation for the burning rate, r, has been obtained :

$$\frac{1}{r} = \frac{\alpha'}{\sqrt{w(1-w)}} \frac{T_F}{P} \exp\left(E_2/2RT_2\right) \times \sqrt{\frac{C_g (T_s - T_o) + w Q_{AP} + (1-w) Q_f}{\lambda_g (T_F - T_s)}} \quad \ldots \text{ III-5}$$

Equation III-1 and III-2 were solved numerically for r as a function of w at various pressures. The input values used are listed in Table III-1. The results are plotted in Figure III-3 and are discussed in the following section.

III. B. 4 Discussion

In Figure III-3, the burning rates, r, predicted by the simplified model for a polyester/AP propellant are plotted against mixture ratio, w, for different pressures (P), and these r vs. w curves are compared with a plot of flame temperature, T_2 vs. w.

λ_g	=	2.0×10^{-4}	cal/°C-sec-cm
c_g	=	0.3	cal/°C-gm
ρ_{AP}	=	1.95	gm/cc
ρ_f	=	1.27	gm/cc
Q_{AP}	=	480	cal/gm
Q_f	=	175	cal/gm
A_s	=	780	cm/sec
E_s	=	15	Kcal/mole
E_2	=	20	Kcal/mole
T_o	=	300	°K
α'	=	3.75×10^{-6}	
T_2	=	2000°K	(w= 0.70)*
T_2	=	2450°K	(w= 0.75)
T_2	=	2800°K	(w= 0.80)
T_2	=	3030°K	(w= 0.85)
T_2	=	2960°K	(w= 0.90)
T_2	=	2500°K	(w= 0.95)

* Calculated values assuming equilibrium among combustion products

TABLE III-1 LISTING OF INPUT VALUES USED FOR PREMIXED-LAMINAR FLAME MODEL

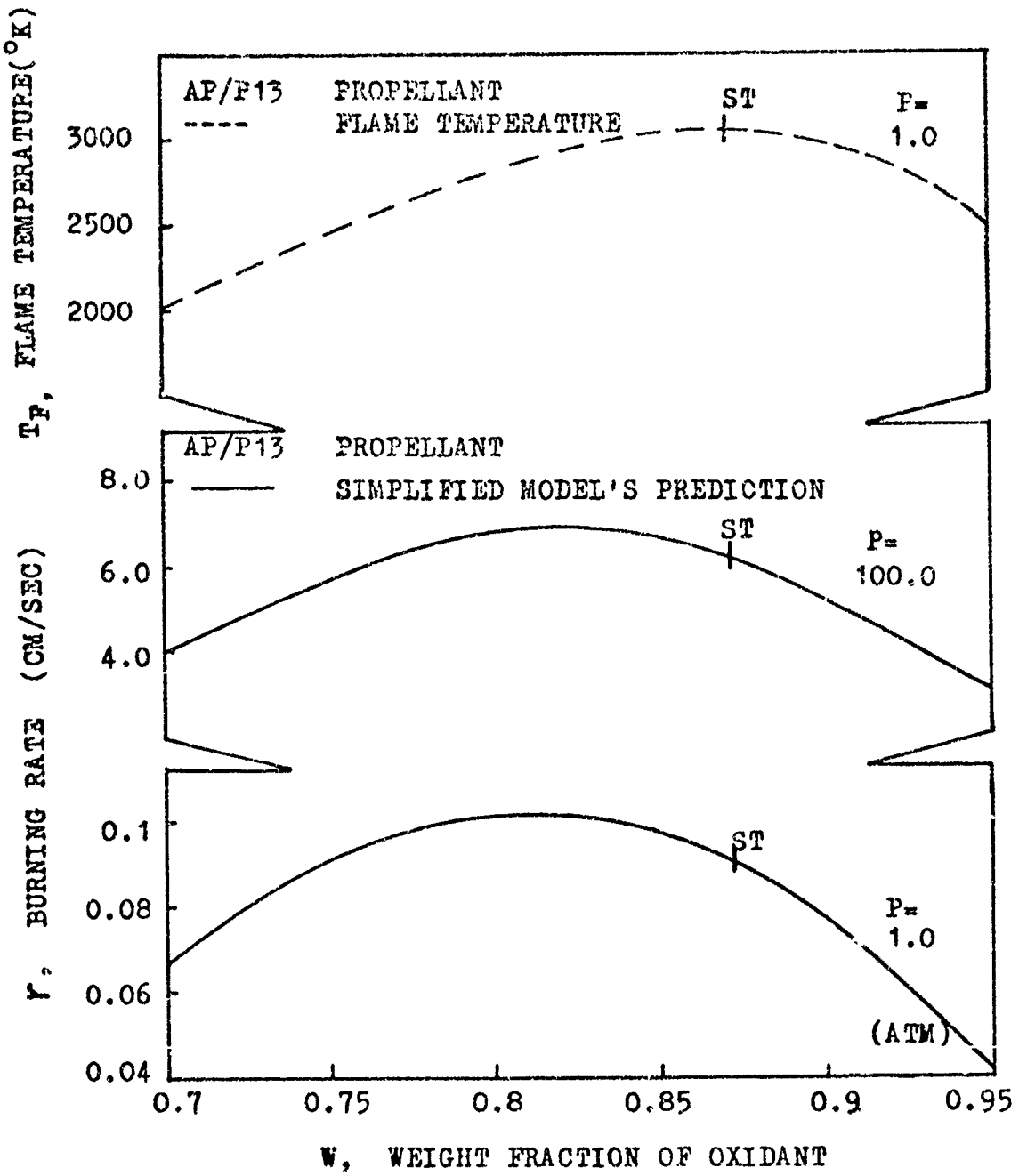

FIGURE III-3 COMPARISON OF PREDICTED BURNING RATE VARIATION AND ADIABATIC FLAME TEMPERATURE VARIATION WITH MIXTURE RATIO

The following observations are made :

(i) The predicted burning rates attain a maximum value at a mixture ratio, $w_{r(max)}$, which is less than the stoichiometrically correct mixture ratio, w_{st}.

(ii) The pressure does not seem to affect the positions of the mixture ratio, $w_{r(max)}$'s, corresponding to maximum burning rates.

(iii) The flame temperature, T_F, however, has a maximum value at a mixture ratio near the stoichiometrically correct mixture ratio, w_{st}, independent of pressure.

These observations imply that although the premixed flame model can predict the maximum burning rates at mixture ratios different from w_{st}, it is unable to predict the shifts in $w_{r(max)}$ with pressure variations such as are observed in experimental investigations.

Hence, two possibilities were considered.

(i) Due to nonequilibrium chemical effects, actual flame temperatures may be different from those calculated by assuming chemical equilibrium among the combustion products, or

(ii) The surface of the solid propellant may not be driven by the heat conducted from a single premixed, laminar flame, as assumed in the simplified model, but by multiple flames occuring in the gas phase.

III. C. FLAME TEMPERATURE MEASUREMENT

In order to check the possibility of nonequilibrium chemical effects, flame temperatures of loose-granule burners were measured at atmospheric conditions, for various mixture ratios. The measured flame temperatures were then compared with theoretical flame temperatures calculated by assuming equilibrium among the combustion products.

A modified Sodium-D line (Na-D line) reversal technique was found suitable for flame temperature measurements. Since the technique requires the flame to be optically accessible, loose-granule burners were fabricated by compacting mixtures of AP and polystyrene in lead foil tubes rather than into stainless tubes or glass tubes as had been used previously (10). The thickness of the lead foil tube was chosen so that the regressing surface of the mixture and the melting rate of the lead foil were the same. The possibility of chemical effects of lead on the flame was checked by measuring the burning rate, which is very sensitive to the flame temperature, for loose-granule burners in lead and in stainless steel tubes. These two burning

rates agreed within two percent. The thermal effects of the lead tube were also determined to be negligible since the heat required to melt the lead is considerably less than that required to pyrolyse AP and fuel (e.g, 480 cal/gm for AP, 175 cal/gm for a typical fuel, and 6 cal/gm for lead).

The details of the modified Na-D line reversal technique, description of the apparatus used, and the errors involved in the measurements are discussed in Appendix A.

For comparison with experimental values, the adiabatic flame temperatures of AP/polystyrene systems were calculated for various mixture ratios using a computer program developed by NASA (22) and modified for use on Stevens' PDP 10 computer.

III.C.1 Results and Discussion

Experimentally measured flame temperatures are compared with numerically calculated flame temperatures in Figure III-4. The maximum flame temperature in both cases occurs at the same mixture ratio. This excludes the possibility of nonequilibrium chemical effects being responsible for the maximum burning rate occuring at mixture ratios away from w_{st}.

Hence, the second possibility, that of multiple flames in the

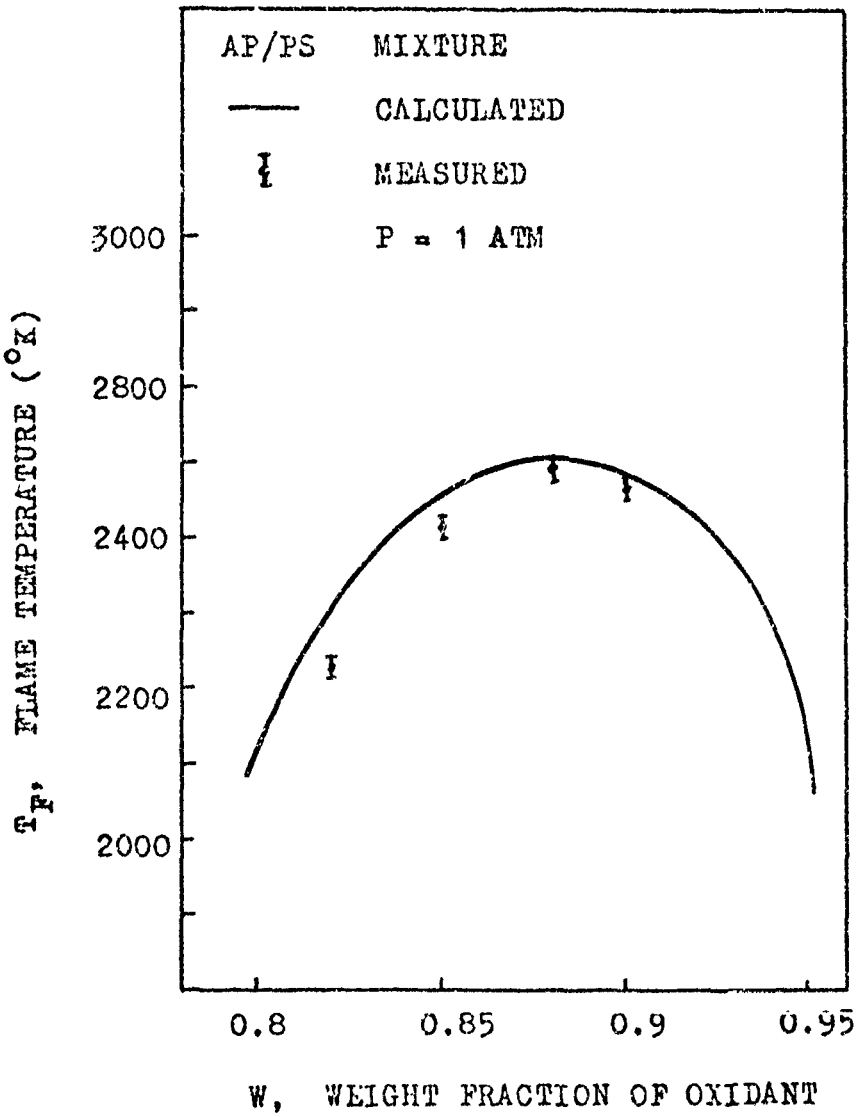

FIGURE III-4 : COMPARISON OF MEASURED AND CALCULATED FLAME TEMPERATURES OF AP/PS MIXTURES

gas phase which supply the heat energy needed to pyrolyse the solid surface of the propellant, has been considered to be a reasonable one.

As a first step, the comprehensive models which include more than one heat source were investigated further.

CHAPTER IV - NUMERICAL DIAGNOSTIC TESTS MADE ON COMPREHENSIVE MODELS

IV.A INTRODUCTION

In the previous Chapters (II and III), the reasons were stated for making numerical tests on the existing comprehensive models of AP composite propellant burning. These many such tests were not made by the originators of these models. Therfore, as part of the present investigation, a number of numerical tests were made on the GDFC model, the GDFD model, the HR model, and the MF model.

IV.B GDFC MODEL TESTS

The following tests have been made on the GDFC model :

(i) A comparison of the GDFC-model results with experimental data (r vs. P).

(ii) An investigation of the influences of different matching points on the predicted results of the GDFC model.

(iii) An investigation of the influence of mixture ratio on the burning rate as predicted by the GDFC model.

IV.B.1 Comparison with Experimental Data

While presenting predicted results of the GDFC model, Steinz (2) did not compare them with any experimental data. Hence, for the purpose of comparison, a propellant (AP/LP3, $d_{ox} = 78\,\mu$, and $w = 0.65$) for which data have been found to correlate well with Summerfield equation (2, 6) (see Figure II-7) was chosen. Following Steinz (2), a matching point at $P = 2.04$ atm. was chosen to determine the empirical constants A_s, α, and β. Using the method of solutions described in Figure II-12. GDFC equations were solved for the burning rate, r. as a function of P. The input values used are given in Table IV-1.

The results of the GDFC model. using Steinz's matching point ("low-pressure matching"). are compared in Figure IV-1. It is found that the GDFC model predicts lower burning rates above 2.04 atm. and higher rates below 2.04 atm. The error in correlation between the model and experimental data is about 30% at 100 atm.

IV.B.2 Influence of Matching Points

In order to study the influence of matching points on the predictions of the GDFC model. two matching points other than that used by Steinz (13.6 atm. and 100 atm.) were tested. The empirical constants A_s, α, and β, were determined at these matching points

λ_g	=	2.0×10^{-4}	cal/^{o}C-cm-sec
c_g	=	0.3	cal/^{o}C-cm-sec
ρ_{AP}	=	1.95	gm/cc
ρ_f	=	1.27	gm/cc
Q_{AP}	=	480	cal/gm
Q_f	=	175	cal/gm
ΔH_{AP}	=	810	cal/gm
T_o	=	300	^{o}K
d_{ox}	=	78	microns
w	=	0.65	
T_2	=	2351	^{o}K
E_s	=	15	Kcal/mole
E_2	=	20	Kcal/mole

MATCHING POINT P (ATM)	T_s (^{o}K)	A_s (cm/sec)	α	β
2.04	900	780	1.161×10^{-5}	0.152
13.6	1000	920	1.067×10^{-5}	0.110
100.0	1100	1073	8.32×10^{-6}	0.093

TABLE IV-1 INPUT VALUES USED FOR "GDFC" AND "GDFD" MODELS

(see Table IV-1), and the GDFC equations were numerically solved. These results also are plotted in Figure IV-1, which show that for the high-pressure matching point (100 atm.) the predicted burning rates are higher than the experimental values. and the percentage error in r at 2.04 atm. is about 60%. For a mid-pressur matching point (13.6 atm.). the GDFC results were in considerable disagreement with experimental data .

IV.B.3 Influence of Mixture Ratio

A further test involving the mixture ratio influence on r as predicted by the GDFC model was considered. Numerical solutions to the GDFC equations were obtained by considering a typical propellant which was considered earlier by Steinz (2). Steinz's values for the constants α, β . and A_s were used for calculations at other mixture ratios (w ranging from 0.7 to 0.95). The flame temperatures used as input values are listed in Table III-1. The resulting predictions of the GDFC model and experimental data are compared in Figure IV-2. The following conclusions can be drawn :

(i) r increases monotonically with w. and no maximum burning rate is predicted by the GDFC model. This is a consequence of the collapsed AP flame assumption, which allows more heat to be generated at the surface as w is increased.

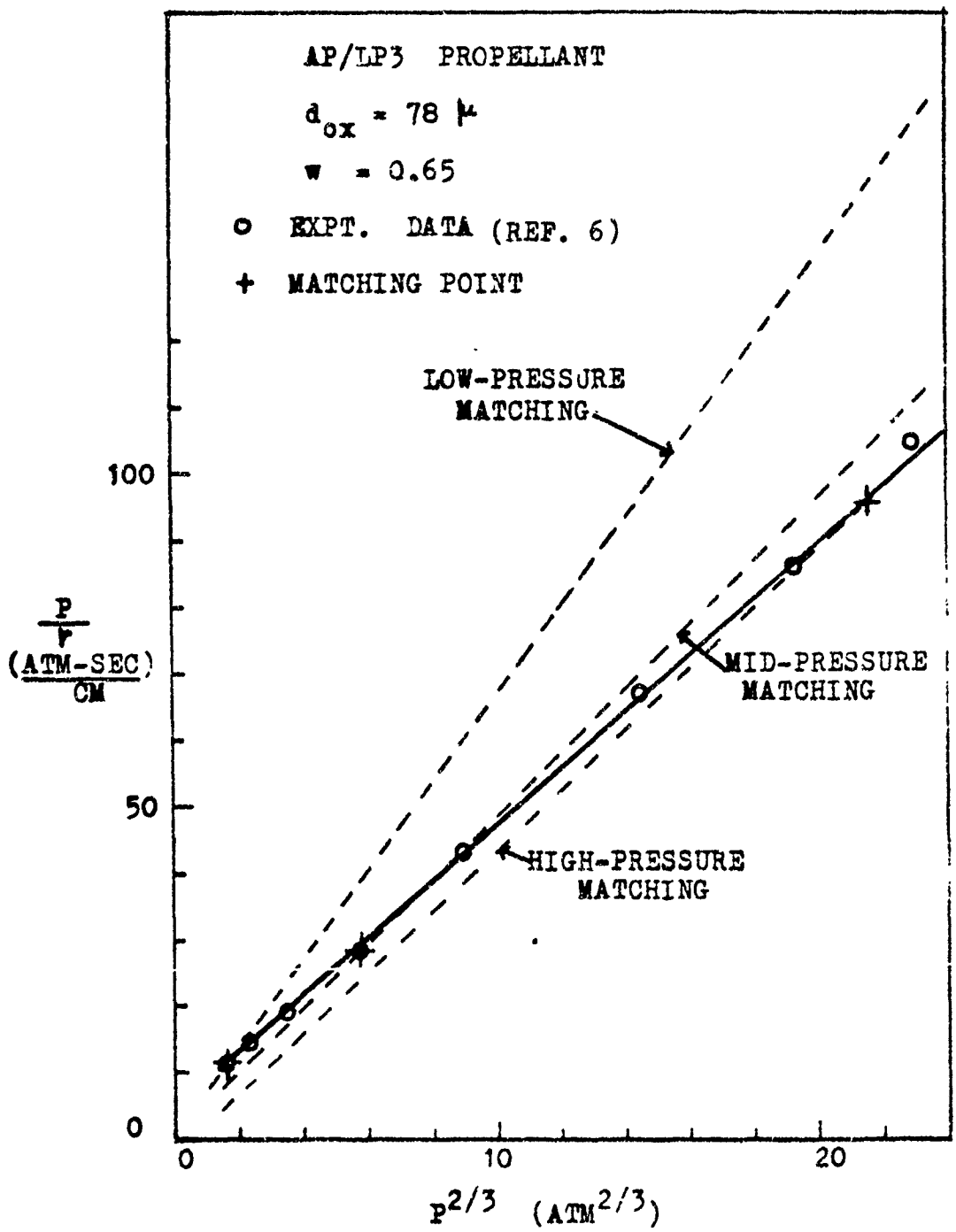

FIGURE IV-1 : INFLUENCE OF MATCHING POINTS ON THE GDFC MODEL PREDICTIONS

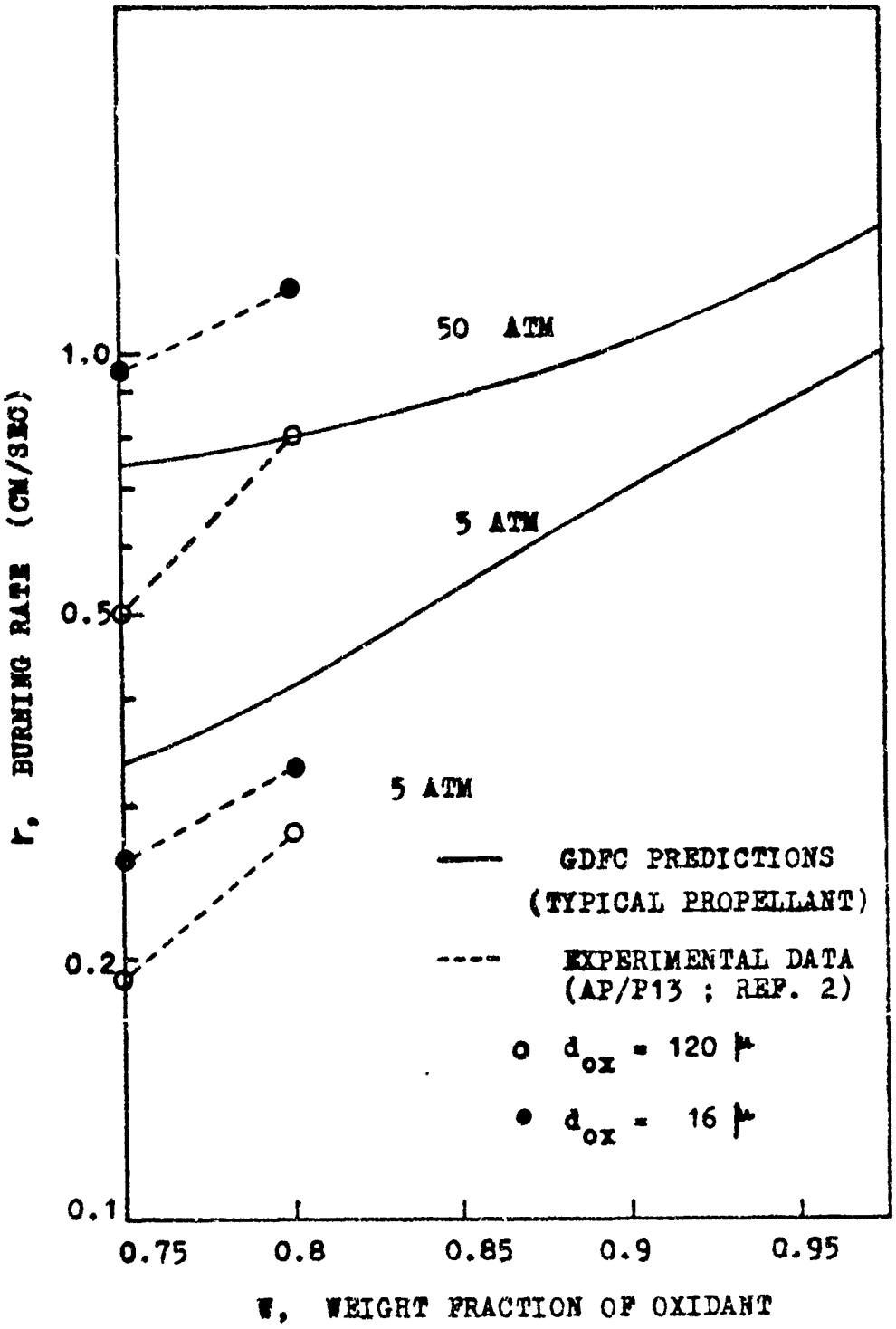

FIGURE IV-2 : MIXTURE RATIO INFLUENCES . COMPARISON OF GDFC RESULTS WITH EXPERIMENTAL DATA

(ii) The mixture-ratio sensitivity, $\frac{\partial \ln r}{\partial w}$, predicted by the model is of the same order of magnitude as those shown by experimental data at low pressures, but at higher pressures, it is too low.

From these tests, it was concluded that the GDFC model is not a very reasonable model. Therefore, it was not considered for any further tests or modifications.

IV.C GDFD MODEL TESTS

The GDFD model was also subjected to the same tests which were made on the GDFC model. Figure IV-3 shows a comparison between GDFD results and experimental data for various matching points. The matching points used in the GDFD-model calculations were obtained from the GDFC-model calculations. Since the GDFD-model predictions of r are always less than the corresponding GDFC-model predictions, burning rates given by the experimental data and those predicted by the GDFD model are not the same at various matching points. It is clear from Figure IV-3 that the disagreement between GDFD results and experimental data is great at low pressures, where the distended AP flame assumption is supposed to be reasonable. Hence, any modification to be made on the GDFD model should be aimed at improving it in the low pressure range.

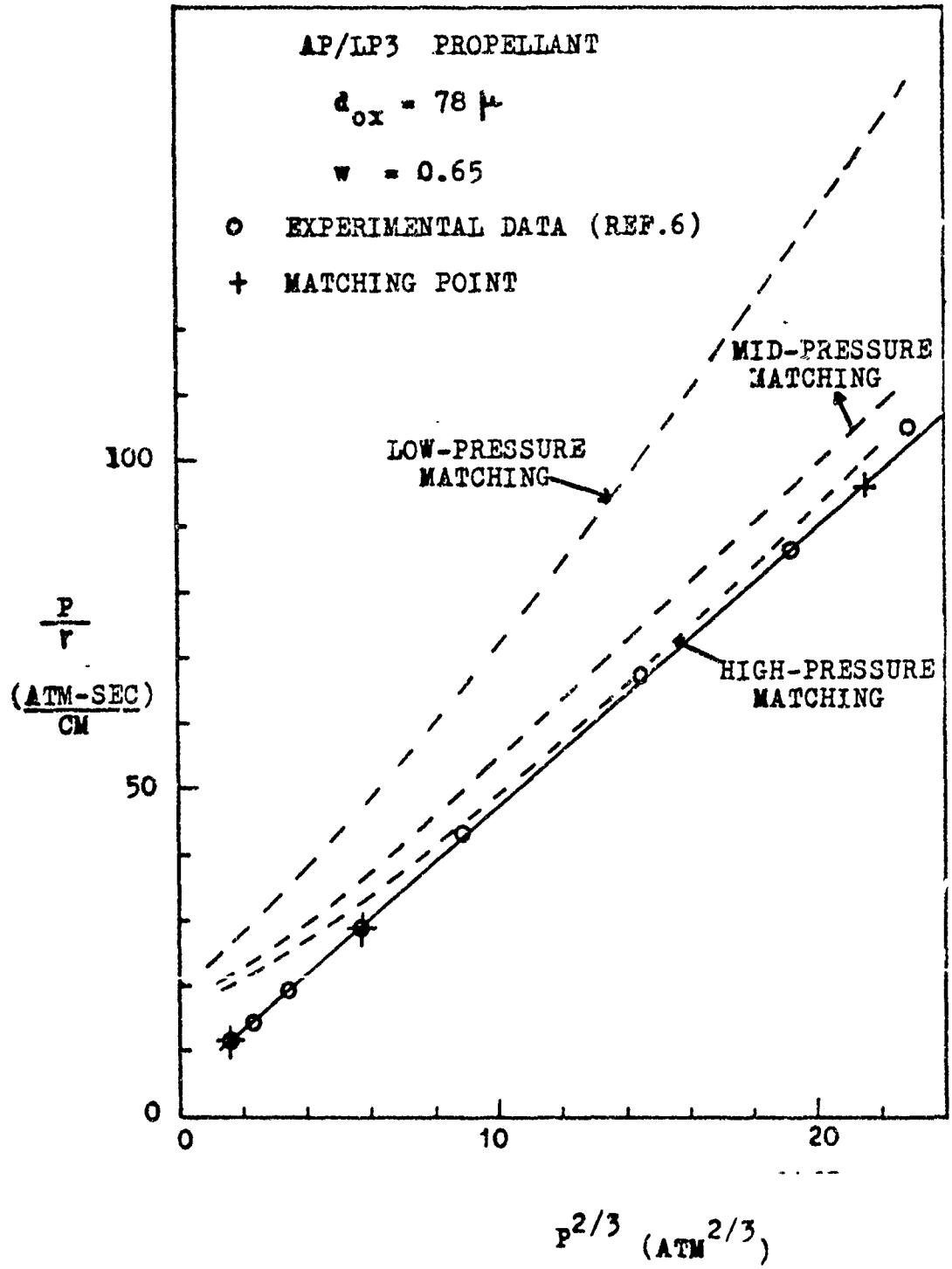

FIGURE IV-3 : INFLUENCE OF MATCHING POINTS ON THE GDFD MODEL PREDICTIONS

IV.C.1 Influence of Mixture Ratio

The results of the GDFD model with regard to the mixture-ratio influences on the burning rate are shown in Figure IV-4. The following observations are made :

(i) r vs. w results predicted by the GDFD model attain a maximum at w's different from w_{st} at low pressures. This trend is in accordance with those shown by experiments.

(ii) The mixture ratio-sensitivities, $\frac{\partial \ln r}{\partial w}$, predicted by the GDFD model are much lower than those observed experimentally.

Because of the observed qualitative agreement between predicted and experimental trends, a few more numerical diagnostic tests were made. The purpose of these tests was to establish a basis for modifying the model in order to increase the too-low mixture-ratio sensitivity of the model, while still maintaining its qualitative correct predicted trends.

IV.C.1.a Modified "a" and "b"

Two possible sources of mixture-ratio effects, which do not appear in the GDFD model were introduced by modifying the GDFD model expressions for "a" and "b" (Equations II-13 and II-14).

Though not accounted for in the original GDF model formulation (2), the chemical-time parameter "a" , is sensitive to mixture-ratio

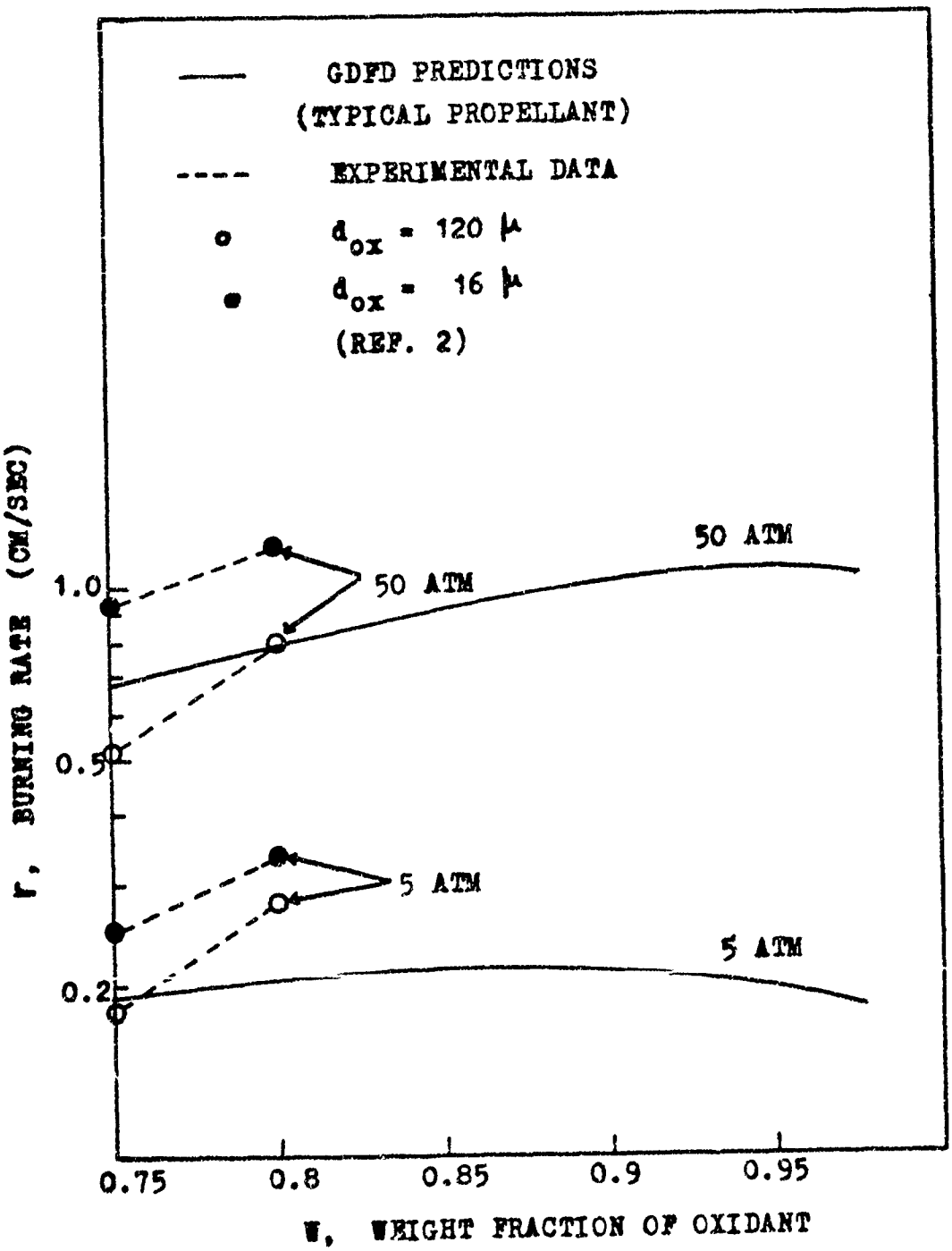

FIGURE IV-4 : MIXTURE-RATIO INFLUENCES : COMPARISON OF GDFD RESULTS WITH EXPERIMENTAL DATA

variations because "a" depends on the reaction rate of the granular diffusion flame. In the original formulation of the GDFD model, the reaction rate was expressed in terms of the flame temperature, pressure, and other parameters (see Equation II-6). Because the reaction rate is expected to depend on the concentration of the reactants, a modified expression for the reaction rate, given by Equation III-4, has been considered in the present investigation. Denoting the modified a by a', the following relation can be established between a and a' :

$$a' \sim \frac{a}{\sqrt{w(1-w)}} \qquad \ldots \text{ IV-1}$$

Since the empirical constant, α, varies directly with a, a modified α, viz., α' can be written as :

$$\alpha' \sim \frac{\alpha}{\sqrt{w(1-w)}} \qquad \ldots \text{ IV-2}$$

The diffusion-time parameter, "b", considered in the original GDF model was assumed to be sensitive to d_{ox}, only, since μ, the mass of each fuel pocket, depended only on d_{ox}. It is reasonable to assume that the mass of each fuel pocket can vary with the mixture ratio also. μ is expected to decrease as w increases. The following functional relationship has been considered between μ

and w :

$$\mu \sim (1-w)\, f(d_{ox}) \qquad \ldots \text{IV-3}$$

Since, $b \sim \mu^{1/3}$, $b \sim (1-w)^{1/3}$ as $b \sim \beta$, then

$$\beta' \sim \beta (1-w)^{1/3} \qquad \ldots \text{IV-4}$$

The GDFD equations (Equations II-4, II-17, and II-18) were solved with both old and new empirical constants viz., α, β, α', and β'. The following values were used :

$\alpha = 8.2 \times 10^{-6}$; $\beta = 0.1099$ (Calculated from data of Ref. 1)

$\alpha' = 3.75 \times 10^{-6}$; $\beta' = 0.1642$ (From Equations IV-2 and IV-4)

The predicted results of the GDFD model for both new and old parameters α and β are compared in Figure IV-5. Although the trends of the r vs. w curves have been preserved, the modification has not improved the mixture-ratio sensitivity, $\frac{\partial \ln r}{\partial w}$.

IV.C.1.b Modified "Pyrolysis Rate Equation"

In the original GDFD model, an overall surface-pyrolysis rate equation was assumed to describe the surface pyrolysis (Equation II-4). This equation does not contain any term involving the mixture ratio, w. In the MF model (19, 20), a different surface pyrolysis

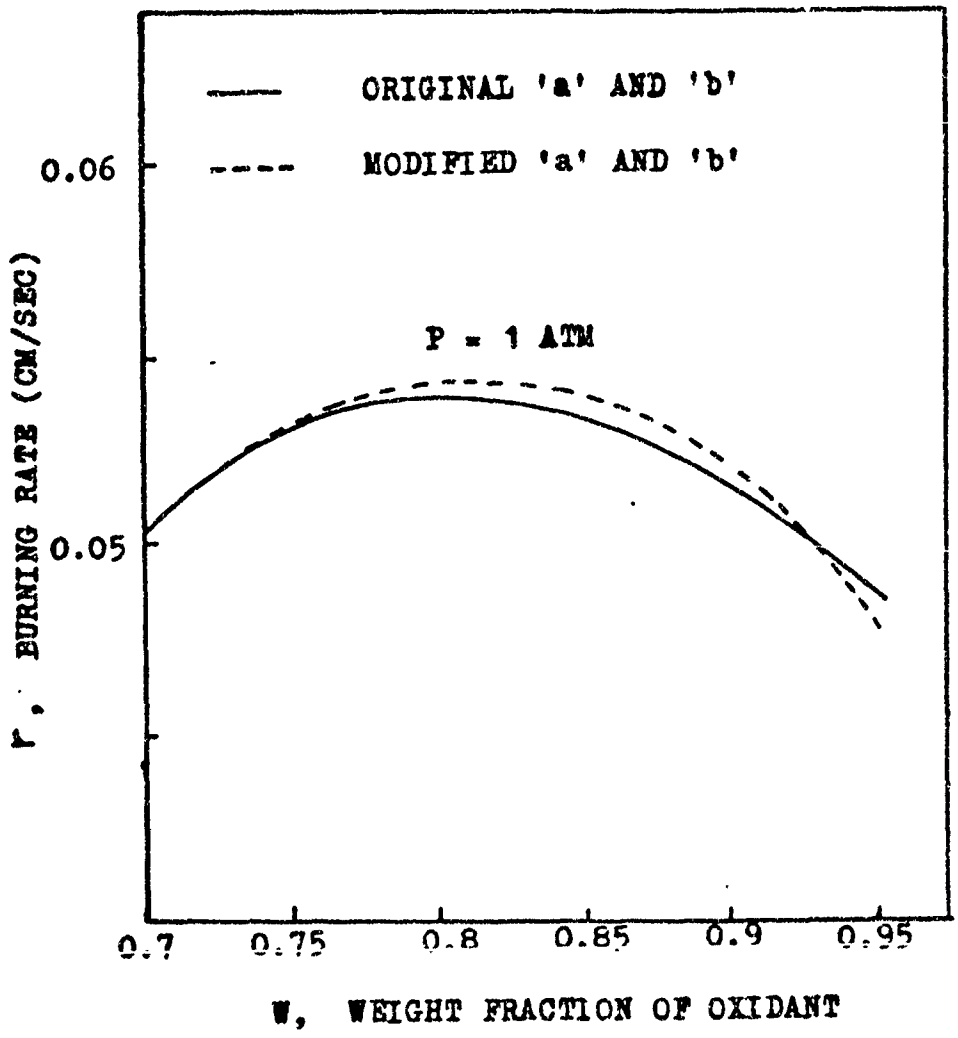

FIGURE IV-5 INFLUENCES OF MODIFIED 'a' AND 'b' ON r VS. W CURVE

rate equation containing mixture ratio, w, was considered (Equation II-22). Hence, Equation II-4 was replaced by Equation II-22 and the resulting equations of the GDFD model (Equations II-17 and II-18) were solved for the burning rate while varying the mixture ratio.

The results obtained using both the original and modified pyrolysis - rate laws are shown in Figure IV-6. This modification basically changes only the magnitude of burning rates while preserving the trends of r vs. w curves. It has not increased the predicted mixture-ratio sensitivity, $\frac{\partial \ln r}{\partial w}$.

IV.C.2 Further Numerical Diagnostic Tests (Inverse Procedure)

As the previous tests failed to improve the GDFD model, with respect to mixture-ratio sensitivity, the following diagnostic tests were made to isolate particular mechanisms which, when included, might improve the GDFD model. It was observed that both the energetics (heat generated at the first-stage flame, ΔH_1) and kinetics (reaction time of the first-stage flame, τ_1) play important roles in the predictions of the GDFD model. These roles were investigated by means of an "Inverse Procedure".

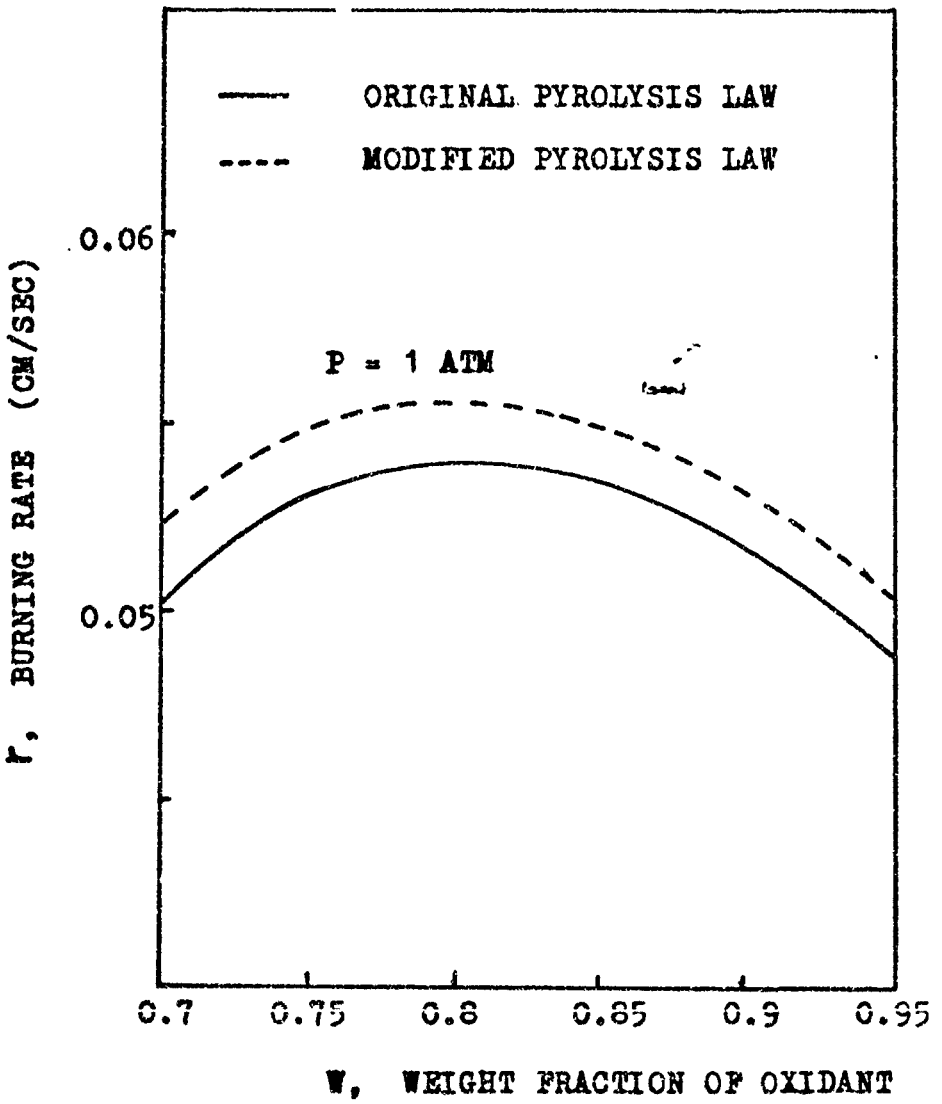

FIGURE IV-6 INFLUENCE OF MODIFIED PYROLYSIS LAW ON r VS. W CURVES

The inverse procedure involves using experimental burning-rate data for various pressures, particle sizes, and mixture ratios as input values in the GDFD equations to calculate the heat generated at the first-stage flame, ΔH_1, and the reaction time of the first-stage flame τ_1.

The experimental data used here were taken from Reference 1 for AP/P13 propellants with w = 0.7, and d_{ox} = 16 μ and 120 μ. The GDFD model was forced to predict r vs. w values for w = 0.75 and d_{ox} = 16 μ and 120 μ by suitable choices of α and β. Such a method had to be used since the GDFD-model-predicted-values were lower than the experimental data (see Figure IV-3). This selective choosing of values for α and β can be justified: The purpose of the inverse procedure is not to obtain quantitative results but rather qualitative results which can provide clues for improving the model.

The set of values used for α and β so obtained for w = 0.75 and d_{ox} = 16 μ and 120 μ, were used along with r vs. P data for w = 0.8 in the GDFD equations to calculate ΔH_1 and τ_1.

In calculating ΔH_1, τ_1 was assumed to be a constant with respect to d_{ox} and w but was varied inversely with P, as given by Equation II-16. The results of the inverse procedure for calculating ΔH_1 are shown in Figure IV-7. These results indicate that if the heat generated at the first-stage flame were higher, depending on P, d_{ox}, and

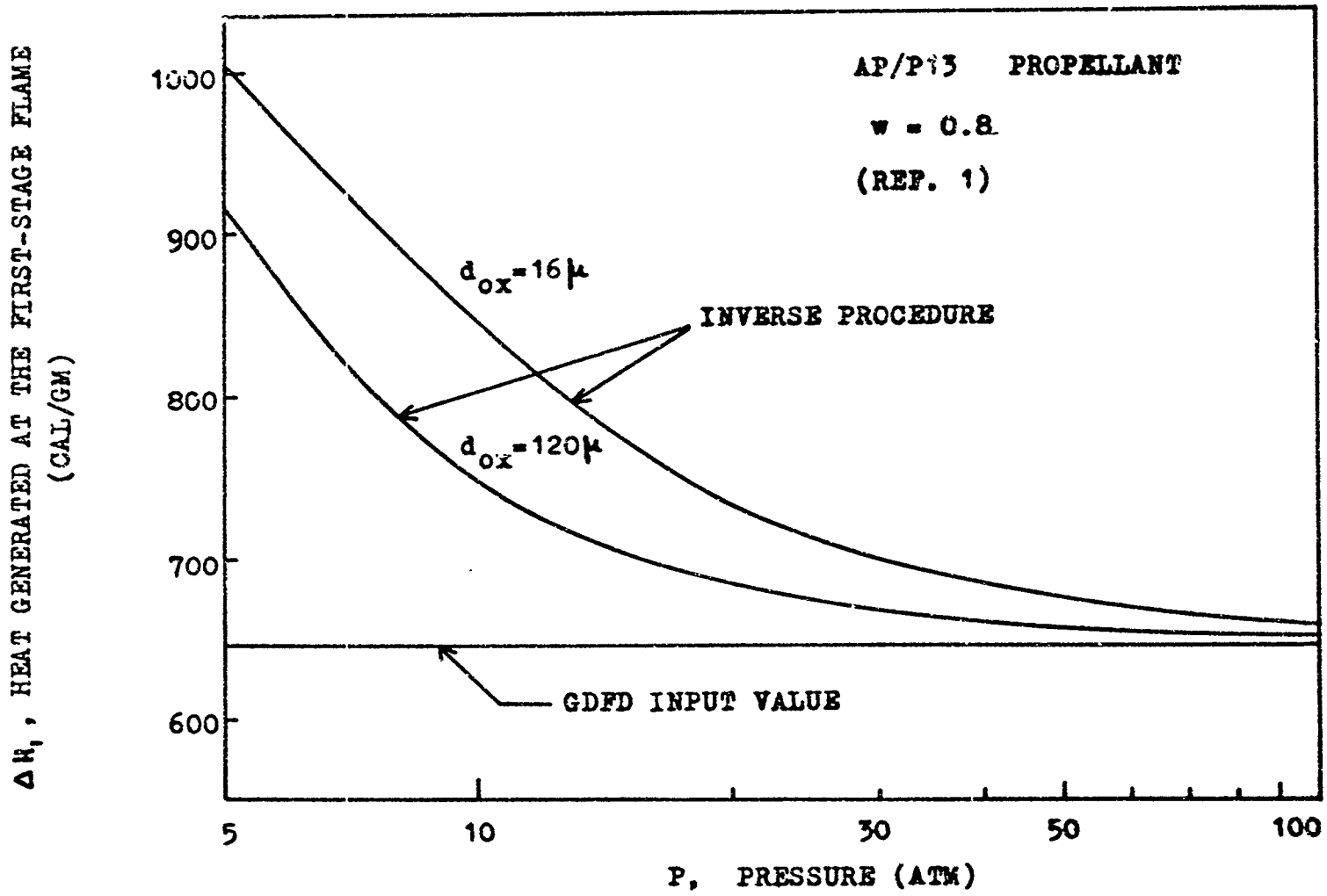

FIGURE IV-7 : RESULTS OF THE INVERSE PROCEDURE

w, the GDFD model would have predicted reasonable results.

The inverse procedure was also used to calculate the reaction time of the first-stage flame, τ_1, from the GDFD equations by assuming ΔH_1 to be constant with respect to P but by assuming a linear variation with respect to w (as assumed in the GDFD model). These calculations yielded unrealistic values for τ_1, (sometimes negative values were obtained). Therefore, it was decided to vary the reaction time for the first-stage flame, τ_1, in a reasonable way with respect to w and to solve the GDFD equations with the modified τ_1. It was noted that from the results reported in Reference 2 that the reaction time for the second-stage flame in the GDFD model viz., τ_2, varied with both w and P. τ_2 is given by

$$\tau_2 = \frac{PM}{RT_2}\left\{\frac{\alpha T_2}{P}\exp\left(\frac{E_2}{2RT_2}\right) + \beta(d_{ox})\frac{T_2^{5/6}}{P^{1/2}T_5^{7/8}}\right\}^2 \quad \ldots \text{IV-5}$$

where M is the average molecular weight of the gases, and R is the universal gas constant. All the other quantities in Equation IV-5 have the same meaning as those described in Chapter II. At low pressures, it was also observed that τ_2 was about 10 times greater than τ_1. Hence, in order to vary τ_1 with both P and w, the following relation between τ_1 and τ_2 was considered.

$$\tau_1 = 0.1\ \tau_2 \quad \ldots \text{IV-6}$$

The GDFD model equations were solved numerically with $\tau_1 = 0.1\tau_2$ and $\tau_1 = \tau_{AP}$. The results are plotted as r vs. w for P 1 atm. and are compared in figure IV-8. It is clearly seen that the r vs. w curves corresponding to $\tau_1 = 0.1\tau_2$ have a steeper slope than the r vs. w corresponding to $\tau_1 = \tau_{AP}$. These results show that if the kinetics of the first-stage flame can also be varied by some mechanism, then the GDFD model can predict increased mixture-ratio sensitivities, $\frac{\partial \ln r}{\partial w}$.

The results of the inverse procedure clearly indicate that the GDFD model can be improved if the first-stage flame were perturbed by some mechanism which would change the heat generated at the first-stage flame and the reaction time of the first-stage flame.

IV.D HR MODEL TESTS

The heterogeneous reaction model (HR) has been tested in a comprehensive manner previously (17, 18). These tests showed the model to predict burning rate behaviour, which is qualitatively in agreement with experimental results. However, in these tests, mixture ratio influences were considered only for a narrow range of variations in w (0.6 to 0.7). Hence, the trends of r vs. w curves were not evident in these numerical model tests. Therefore, as part of the present investigation, a further test involving mixture-

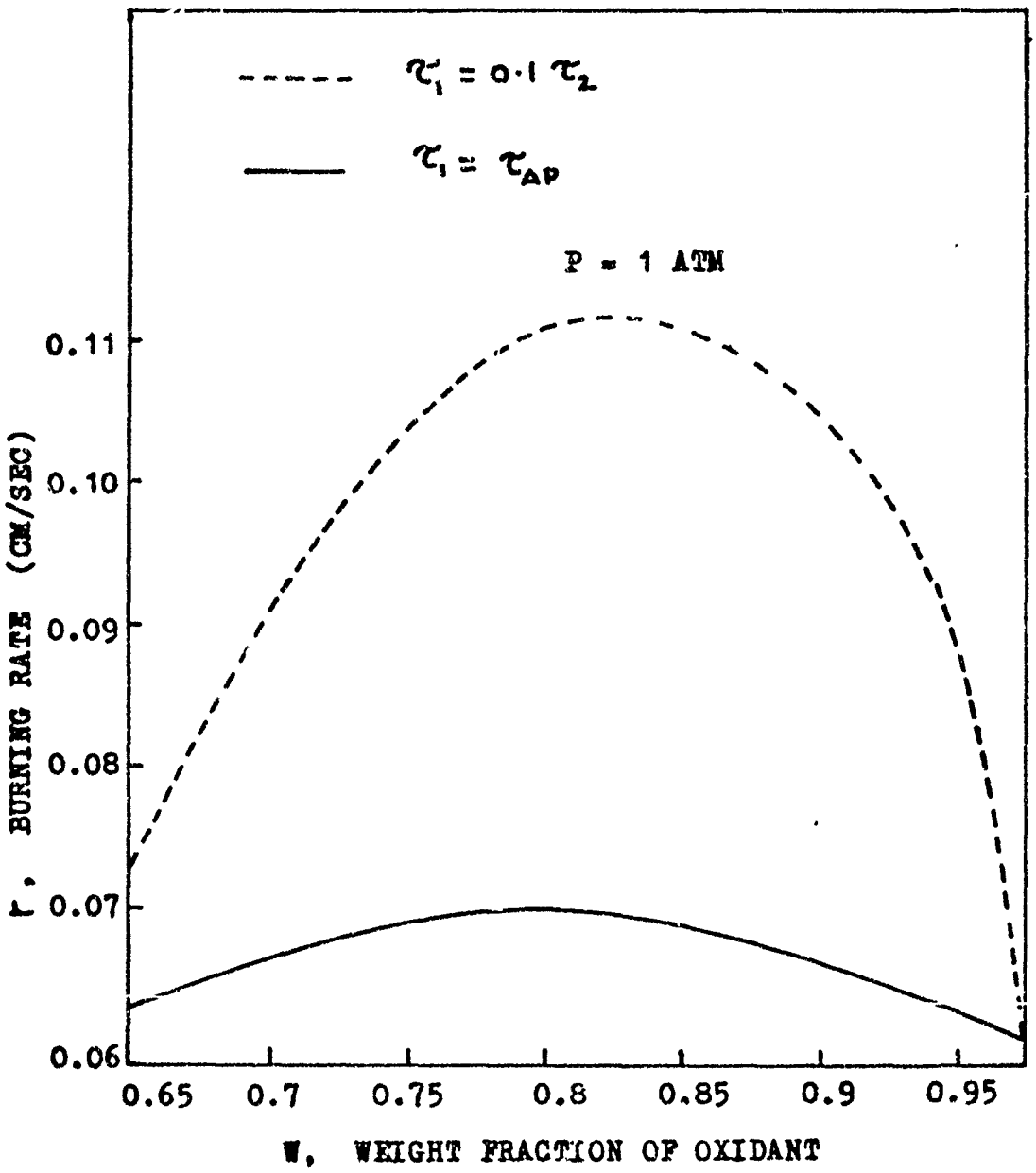

FIGURE IV-8 : INFLUENCE OF VARYING τ_1 ON r Vs. W CURVES

ratio influences was made.

IV.D.1 Influence of Mixture Ratio

The equations of the HR model were numerically solved for mixture ratios beyond w=0.7. The program for numerical calculations was supplied by the model's originator. The basic equations employed in the HR model, viz., mass conservation and energy conservation, allow the model to be extended to the limiting case when w= 1.0 (pure AP). However, an error developed in the program prevented the calculations from being carried beyond w= 0.95 for d_{ox} = 20μ and w = 0.9 for d_{ox} = 200μ. Hence, the numerical calculations were not carried beyond w= 0.95 for d_{ox} = 20μ and w= 0.9 for d_{ox} = 200μ.

The results of the HR model are plotted as r vs. w in Figure IV 9 for varying P and d_{ox}. It can be seen clearly that the HR model does not predict maximum values for r. This trend is contradictory to the experimental data trends.

IV.D.2 Discussion

The major objection to considering the HR model any further is that the heterogeneous reaction assumed in the model seems to be an important mechanism which influences the burning rate prediction

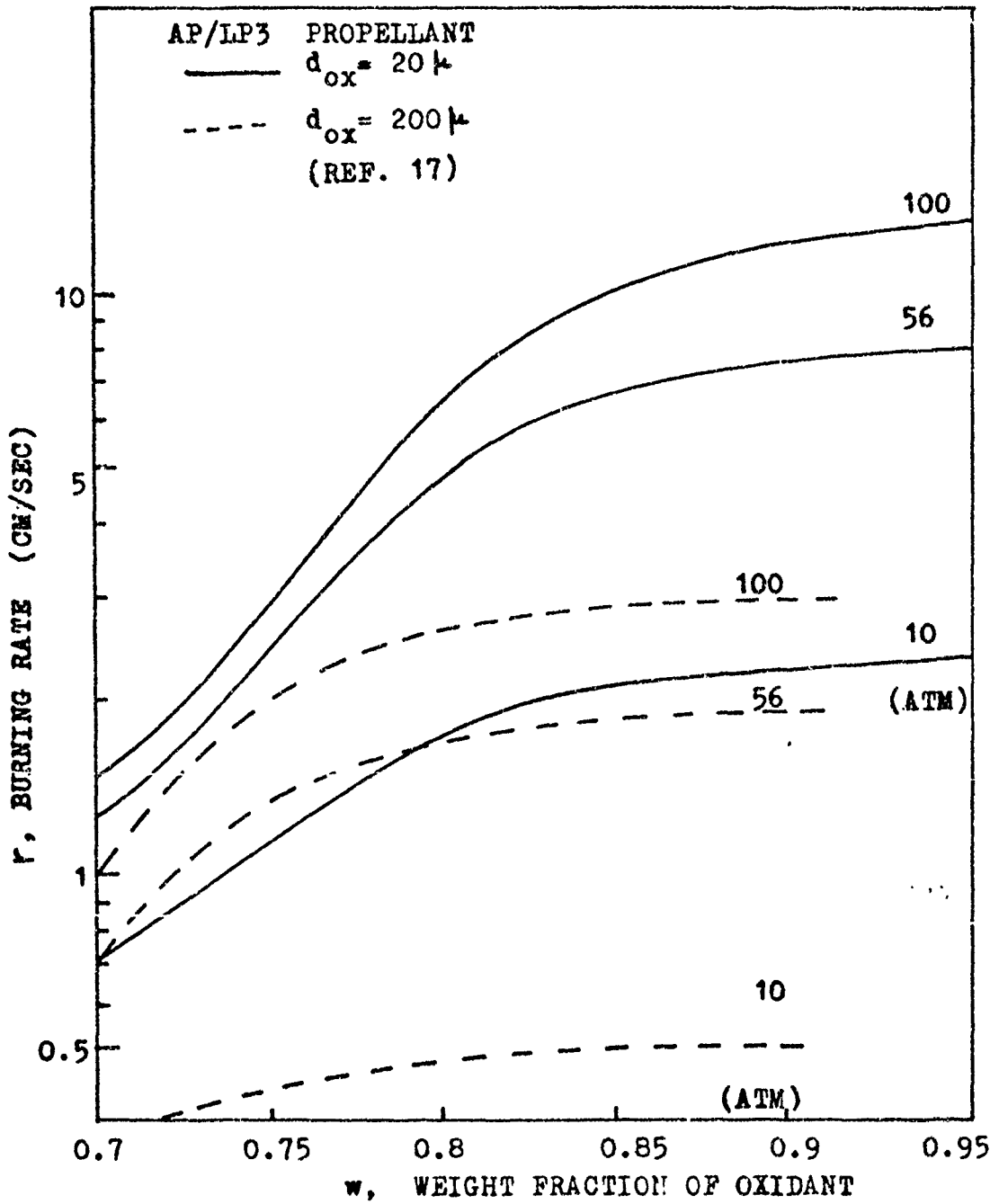

FIGURE IV-9 INFLUENCE OF MIXTURE RATIO AS PREDICTED BY THE HETEROGENEOUS REACTION MODEL

of this model. However, no experimental evidence has been found so far to support the existence of such reaction. This fact coupled with the fact that the model predicts no maximum for the burning rate, led toward abandonment of this model as a basis for any modifications or additional tests.

IV.E MF MODEL TESTS

Numerical solutions were obtained for the multiple flame model (MF) equations by using a computer program supplied by the originators of the MF model. The complete set of input data found in Reference 19 were used, and the results reported in Reference 19 were reproduced. However, numerical calculations made with the incomplete set of input data found in Reference 20 and additional data suggested by an originator of the MF model (23) yielded results which did not agree with those reported in Reference 20. In Figure IV-10 the results obtained presently and those reported in Reference 20 are shown. Two possibilities may be considered for the discrepency shown :

(i) an error might have developed in the program, or

(ii) a still different set of input data might have been used to get the results reported in Refernce 20.

In any case, the results of Reference 20 should not be considered

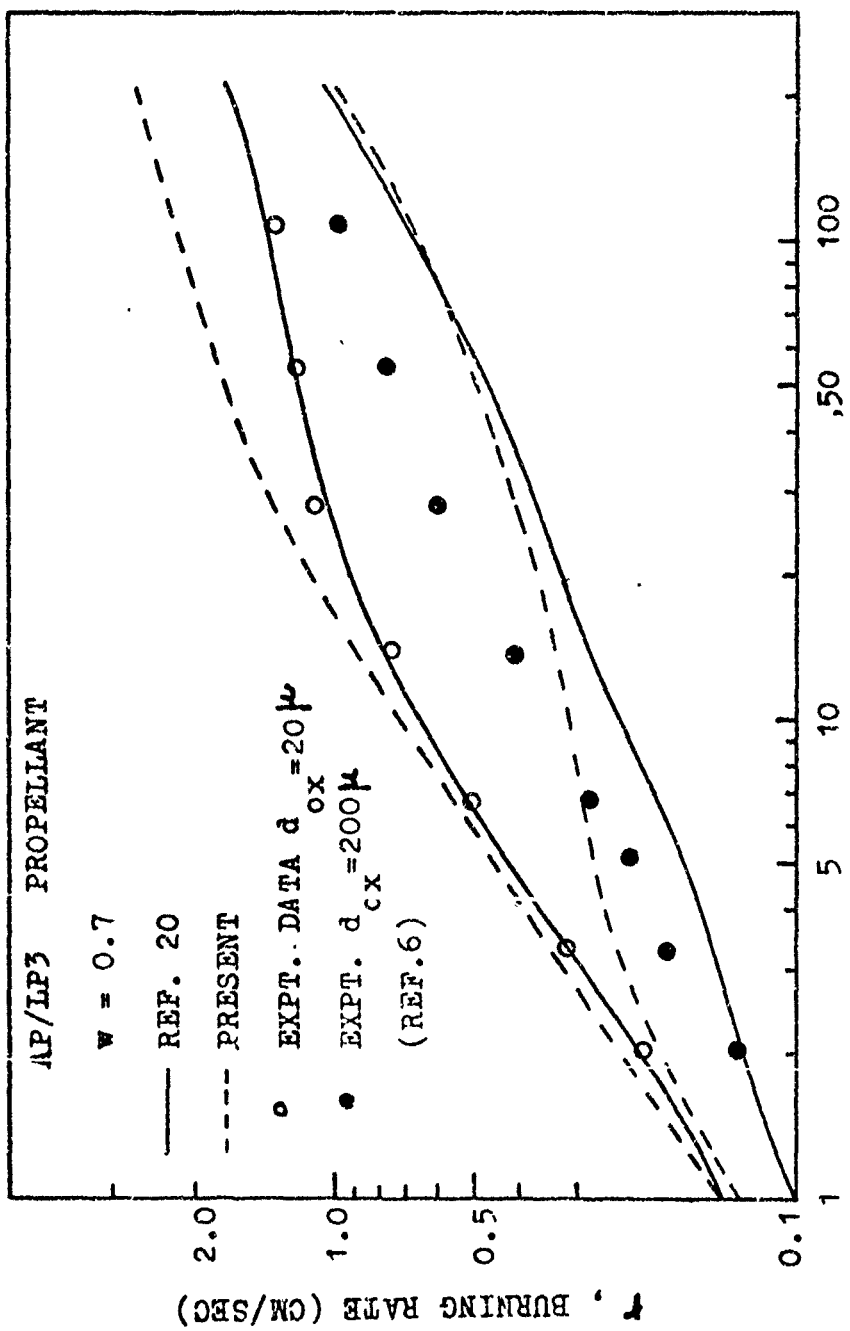

FIGURE IV-10 : RESULTS OF THE MULTIPLE FLAME MODEL

useful until a complete set of input data is available.

Besides the above mentioned discrepency, there are a few other demerits of the MF model.

In estimating the diffusion flame heights, the analysis of Burke and Schumann was used (22). Since the flame structure assumed in this model requires all the flames to envelope the oxidant particle, only fuel-rich diffusion flames ("underventilated") can be considered. This restricts the propellant composition that can be described by the MF model to fuel-rich compositions. Hence, mixture-ratio variations cannot be considered over a wide range.

Another major drawback of this model is the assumption that the primary flame temperature is equal to the adiabatic flame temperature of the propellant. The primary flame is the reaction between a fraction of AP products and a fraction of fuel vapors. The fraction of AP products that react in the primary flame, β_F, is a function of pressure and particle size. Therefore, the primary flame temperature should depend on these variables. The adiabatic flame temperature does not, however, depend on either the pressure or the oxidant particle size. Thus the validity of assuming the calculated adiabatic flame temperature and primary flame temperature as equal is questionable.

For the reasons stated above, the MF model was not considered for any further modifications or tests.

IV. F CONCLUSIONS

The results of numerical diagnostic tests made on several comprehensive models have indicated the GDFD model to be a promising one, i. e., one which might possibily be modified to predict results in better accord with experimental data. Such improvement should be in two categories :

(i) an increase in the predicted burning rates at lower pressures, and

(ii) an increase in the mixture-ratio sensitivity of the burning rates.

The results obtained by the "inverse procedure" indicated that the GDFD model could be substantially improved if the first-stage flame were perturbed. A mechanism for such perturbation is that of intermixing of fuel vapors into the AP decomposition flame and of consequent additional reaction. This mechanism was long ago suggested by Chaiken and Anderson (19, 20) and quite recently accounted for in the MF model (19, 20).

A modified granular diffusion flame model incorporating the above mentioned has been formulated and tested in the present study.

CHAPTER V - MODIFIED GRANULAR DIFFUSION FLAME MODEL

A modified granular diffusion flame model (MGDF), incorporating the intermixing of fuel-vapors into the AP decomposition flame and the consequent additional reaction with the AP decomposition flame, is described below. The major assumptions made, the resulting equations, and the numerical tests made on the MGDF model to assess its validity are also described in the following sections.

V.A DESCRIPTION OF THE MGDF MODEL

The MGDF model considers a two-stage flame in the gas phase to provide the necessary heat required to gasify the surface. The first-stage flame is a perturbed AP decomposition flame and the second-stage flame is a granular diffusion flame. The perturbation of the AP flame is due to the intermixing of fuel vapors into the AP flame and the additional reaction with the AP flame. Figure V-1 describes the MGDF model.

V.B MAJOR ASSUMPTIONS

The following assumptions are made :

(i) One dimensional.

(ii) Steady state.

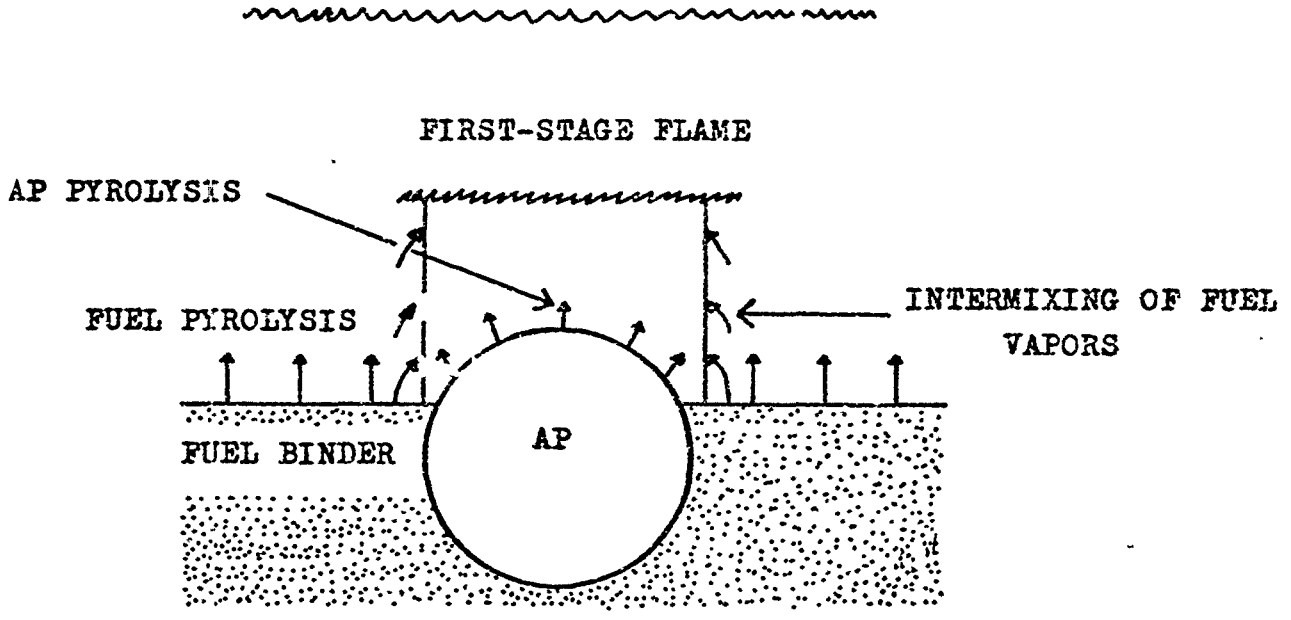

FIGURE V-1 : DESCRIPTION OF THE MGDF MODEL

(iii) Specific physico-chemical processes :

The physical processes considered are heat conduction and granular diffusion.

The chemical reactions considered are fuel pyrolysis, dissociative sublimation of AP into ammonia and perchloric acid, a perturbed AP decomposition flame, and a granular diffusion flame.

(iv) Linear temperature distribution in the gas phase.

(v) Uniform thermal properties.

V.C EQUATIONS

As a consequence of the above mentioned assumptions and modification, the resulting equations for the MGDF model are the same as those for the GDFD model (Equations II-4, II-17, and II-18) Only the input values related to the first-stage flame, viz., ΔH_1, the heat generated at the first-stage flame, and τ_1, the reaction time of the first-stage flame, are different. In the GDFD model these two input values are determined from the deflagration data for pure AP, but in the MGDF model, they are determined from the intermixing mechanism of fuel vapors as functions of pressure, oxidant particle size, and weight fraction of oxidant, as described below.

Following the notations used in Chapter II, the set of equations to be solved in the MGDF model are :

$$r = A_s \exp(-E_s/RT_s) \qquad \ldots \text{ V-1}$$

$$T_1 = \frac{T_s}{\left[1 - \frac{r^2 \tau_1}{p_0}\left(\frac{R\rho_p^2}{\lambda_g M}\right)\left\{c_g(T_s - T_0) + W Q_{AP} + (1-W) Q_f\right]\right.} \qquad \ldots \text{ V-2}$$

$$r = \frac{1}{L_2 \rho_p}\left\{\frac{\lambda_g (T_2 - T_0)}{c_g (T_1 - T_0) + W Q_{AP} + (1-W) Q_f - W \Delta H_1}\right\} \qquad \ldots \text{ V-3}$$

The modified input values ΔH_1 and τ_1 were determined as follows.

Let T_1^* denote the true temperature of the perturbed AP flame. Due to the additional reaction between the fuel vapors that intermixed with the AP flame, T_1^* could be determined if the amount of fuel vapor that reacted with the AP products could be specified. Once T_1^* has been determined, then following the original GDFD model, the following equation could be used to determine ΔH_1 :

$$\Delta H_1 = c_g (T_1^* - T_0) + Q_{AP} \qquad \ldots \text{ V-4}$$

Assuming that the perturbed AP flame is a second order reaction, τ_1 is given by;

$$\tau_1 \sim \frac{1}{\rho_g \exp(-E/RT_1^*)}$$

or

$$\tau_1 = C_1 \frac{T_1^*}{P \exp(-E/RT_1^*)} \quad \ldots \text{V-5}$$

The constant C_1 is determined from the condition that, for $T_1^* = T_{AP}$, $\tau_1 = \tau_{AP} = \frac{6.5 \times 10^{-6}}{P}$ (Equation II-16).

C_1 was found to be 1.8×10^{-12} $(\frac{\text{sec-atm}}{^oK})$.

In order to determine the amount of fuel vapor that intermixes with the AP flame and hence, T_1^*, the following model was considered. Following Figure V-1, let d_{ox} denote the oxidant particle diameter, L_1 be the height of the first-stage flame above the surface of the propellant. If $\dot{m}_f$ represents the mass flow rate (gm/sec) of the fuel that intermixes through the cylindrical surface area surrounding the AP particles, then

$$\dot{m}_f = \rho_g V A \quad \ldots \text{V-6}$$

where ρ_g is the average gas phase density, V is the diffusion velocity, and A is the area available for mixing.

V can be written as :

$$V \simeq \frac{D}{d_{ox}} \qquad \ldots \text{ V-7}$$

where D (the diffusion coefficient) $\propto \left(\frac{T^{1.75}}{P}\right)$ ... V-8

$$A = \pi d_{ox} L_1 \qquad \ldots \text{ V-9}$$

Using Equations V-7 and V-9 in Equation V-6, we get

$$\dot{m}_f \simeq \rho_g D L_1 \qquad \ldots \text{ V-10}$$

In Equation V-10, ρ_g and D are related to P and T by the perfect gas law and by Equation V-8, respectively, and L_1 is given by,

$$L_1 \simeq \left(\frac{\dot{m}''_T}{\rho_g}\right) \tau_1 \qquad \ldots \text{ V-11}$$

where $\dot{m}''_T$ is the mass flux of the propellant $(\simeq \rho_p r)$.

The reaction time τ_1 appearing in Equation V-11 is given by Equation V-5. Since T_1^* is an unknown quantity, introducing it into the expression for τ_1, would involve an iterative method to determine T_1^*. Hence, for mathematical simplicity, it was assumed that an average temperature T_{av}, given by the following equation be used in the

place of T_1^* in Equation V-11,

$$T_{av} = \frac{T_2 + T_{AP}}{2} \qquad \ldots \text{ V-12}$$

where T_2 and T_{AP} are the propellant and AP flame temperatures, respectively.

The reaction time, τ_1, used in the present model is given by;

$$\tau_1 = C_1 \frac{1}{\rho_g \exp(-E/RT_{av})} \qquad \ldots \text{ V-13}$$

Equation V-10 can be reduced to the following form by using Equations V-11 , II-12, and II-13 :

$$\dot{m}_f \simeq \dot{m}_r'' \frac{T_{av}^{2.75}}{P^2 \exp(-E/RT_{av})} \qquad \ldots \text{ V-14}$$

Letting $\dot{m}_{ox}''$ represent the mass flux of AP, then the mass flow rate $\dot{m}_{ox}$ (gm/sec) for a single particle is given by :

$$\dot{m}_{ox} = \dot{m}_{ox}'' \pi \left(\frac{d_{ox}}{2}\right)^2 \qquad \ldots \text{ V-15}$$

The ratio $\frac{\dot{m}_f}{\dot{m}_{ox}}$ can then be written as :

$$\frac{\dot{m}_f}{\dot{m}_{ox}} \simeq \left(\frac{\dot{m}_r''}{\dot{m}_{ox}''}\right) \cdot \frac{T_{av}^{2.75}}{d_{ox}^2 P^2 \exp(-E/RT_{av})} \qquad \ldots \text{ V-16}$$

The ratio $\frac{\dot{m}''_f}{\dot{m}''_{ox}}$ is given by :

$$\frac{\dot{m}''_f}{\dot{m}''_{ox}} = \frac{\rho_p}{\rho_{ox}} \qquad \ldots \text{ V-17}$$

Finally then, combining Equation V-16 and V-17, the ratio of fuel to oxidant in the first-stage flame is proportional to functions of pressure, oxidant particle size, and other propellant properties is given by :

$$\frac{\dot{m}_f}{\dot{m}_{ox}} = C_2 \frac{\rho_p T_{av}^{2.75}}{\rho_{ox} d_{ox}^2 P^2 \exp(-E/RT_{av})} \qquad \ldots \text{ V-18}$$

C_2 is a constant which can be determined empirically by matching the burning rates predicted by the model and given by experiments at a matching point. Details of the determination of C_2 are given in Section V.D.

Once the fuel-to-oxidant ratio of the first-stage flame is determined from Equation V-18, T_1^* can be determined from thermochemical calculations (22). It should be noted that the present model predicts that the amount of fuel mixing with the AP flame is greater at low pressures and for small oxidant particle sizes

(Equation V-18), which is in agreement with the results indicated by the inverse procedure in Chapter IV (see Figure IV-7).

V.D METHOD OF SOLUTION

The following steps were used in solving the MGDF-model equations :

(i) A propellant whose burning rate data correlated with Summerfield's equation was chosen. The empirical constants A_s, α, and β were determined as described in Chapter II.

(ii) A pressure (P) was chosen in the low pressure region, where the modification on the GDFD model would be effective. $\frac{\dot{m}_f}{\dot{m}_{ox}}$ was determined from Equation V-18 by assuming a reasonable value for C_2 and for the input values of w, d_{ox}, etc.,

(iii) For the $\frac{\dot{m}_f}{\dot{m}_{ox}}$ calculated in step (ii), the corresponding T_1^* was determined from thermo-chemical calculations.

(iv) The modified input values ΔH_1 and τ_1 were determined from Equations V-4 and V-13, respectively.

(v) With the appropriate input values (steps i and ii), the resulting equations (Equations V-1 to 3) were

solved numerically to obtain r_{MGDF} at the selected pressure (P). The listing of the computer program used is given in Appendix B.

(vi) The calculated r_{MGDF} was compared with r_{EXPT}, if they were different, a new C_2 was assumed and steps (iii) to (v) were repeated until agreement was reached.

(vii) The constant C_2 determined in step (vi) was used to calculate r as a function of P, d_{ox}, etc.,

V.E RESULTS AND DISCUSSION

The MGDF model has been subjected to the following tests in order to check its predictive capability for predicting burning rate variations with varying pressure (P), oxidant particle size (d_{ox}), mixture ratio (w), and initial temperature (T_0).

V.E.1 Pressure Effects as Predicted by the MGDF Model

The MGDF-model equations were solved for burning rates at various pressures for a propellant whose r(P) data correlated well with Summerfield's equation, viz. Equation II-1. The propellant chosen for this calculation was an AP/LP3 propellant with $w = 0.65$ and $d_{ox} = 78\,\mu$. The experimental data, i.e. r vs. P data, were taken from Reference 6.

The necessary input data needed for the numerical calculations are listed in Table IV-1. The empirical constants A_s, α, and β were obtained from a high pressure matching (P 100 atm.) proceedure described in Chapter II. The constant C_2, introduced in the MGDF model, was determined by the iterative procedure described in the previous section (Section V.D) by matching the burning rate predicted by the MGDF model with the burning rate given by experiment, at a low pressure (P = 2.04 atm.). The value of C_2 obtained by the iterative procedure was found to be 1.0×10^{-17} $\left(\frac{cm^2\text{-}atm^2}{^oK^{2.75}}\right)$.

Figure V-2 shows the predictions of the MGDF model compared with the results of both the GDFC and the GDFD models and also with experimental data.

The following conclusions can be drawn from this comparison :

(i) The burning rates predicted by the MGDF model are in good agreement with the experimental data in the pressure range of 1 to 100 atm. The maximum error in this range between the MGDF results and experimental results is about 10%.

(ii) The results of the MGDF model are clearly much better than those of GDFC and GDFD models. The improvement is quite significant at the low pressure

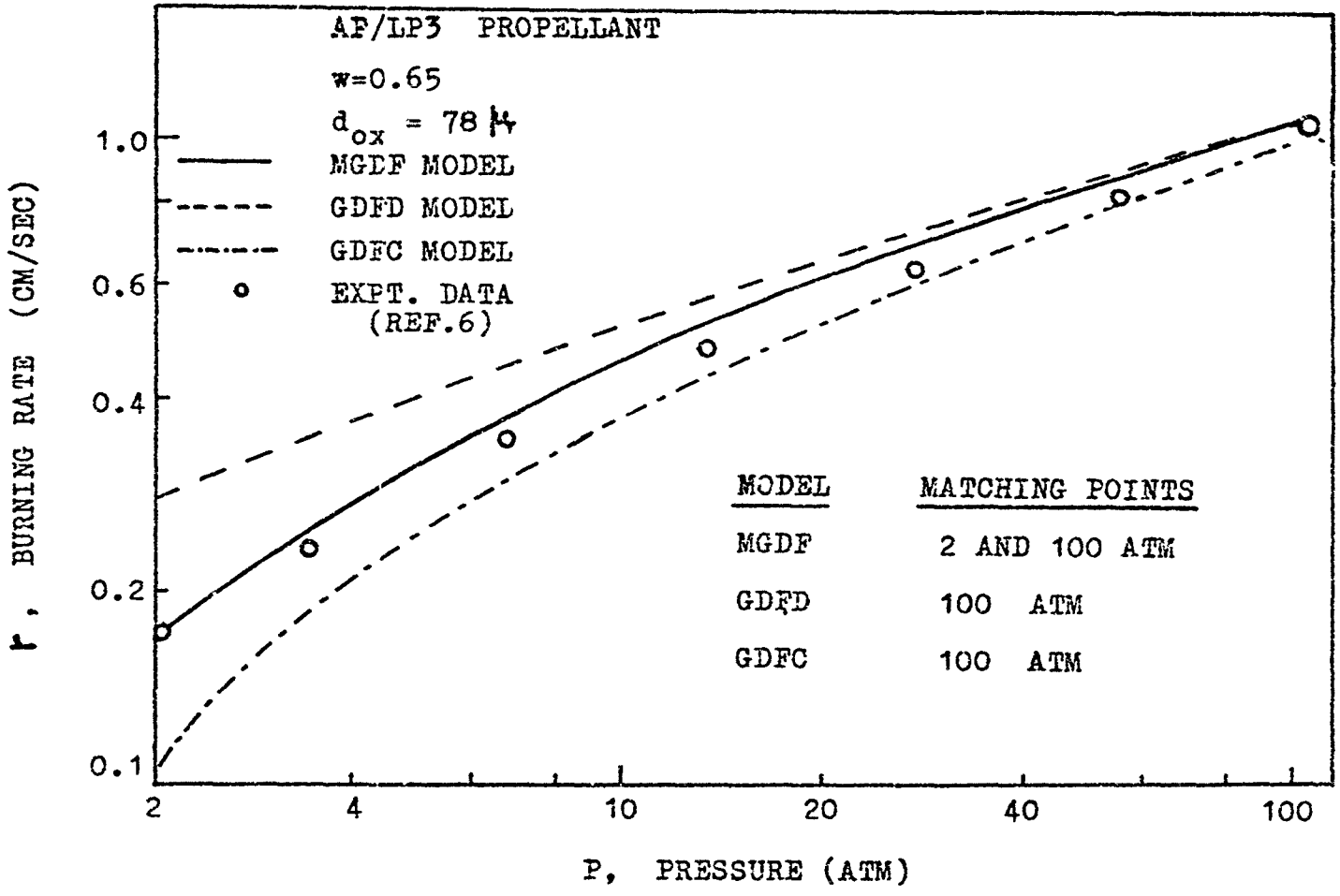

FIGURE V-2 : COMPARISON OF THE MGDF MODEL'S RESULTS WITH THE GDFC AND THE GDFD MODELS' RESULTS AND WITH THE EXPERIMENTAL DATA

region, where the GDFC and GDFD models predict higher (about 60% above the experimental burning rate) and lower (about 40% below the experimental burning rate)burning rates, respectively.

V.E.2 Particle Size Effects as Predicted by the MGDF Model

In order to test the MGDF model's ability to predict the effects of oxidant particle size (d_{ox}) on the burning rate, an AP/LP3 propellant containing 140 μ AP particle size and 65% of AP by weight was considered. The experimental data (r vs. P) for this propellant have been shown to correlate well with Summerfield's equation in References 2 and 6. It should be noted that the propellant chosen here has the same composition as that considered in the previous section to study pressure effects, i.e., both are AP/LP3 propellants and w= 0.65 for both of them. Only the particle sizes of these propellants are different.

As explained in Chapter II, the variations in the particle size affects only the diffusion-time parameter b, and hence, the empirical constant β. Therefore, for the numerical calculations only β has been changed while keeping other constants α, C_1, C_2, etc., the same as those cited for 78 μ particle size in the previous

section (Section V.E.1).

Since the constant C_2 used for 140μ and 78μ AP particle sizes were taken to be the same, an iterative procedure was not required in this case. Thus the MGDF equations were directly solved for the burning rate at various pressures.

In Figure V-3, a comparison of the MGDF results with both the GDFC and the GDFD results and also with experimental data is made.

As seen clearly the predicted results of the MGDF model are in good agreement with the experimental data and are much closer than both the GDFC and the GDFD results. Since the propellant considered presently contains a larger particle size than the one considered in studying the effects of pressure on r, it is concluded that the MGDF model not only predicts the effects of pressure on the burning rate correctly but also the effects of oxidant particle size effects in accordance with experimental data.

V.E.3 Mixture Ratio Effects as Predicted by the MGDF Model

One of the objectives in modifying the GDFD model was to increase the too-low mixture-ratio sensitivity, $\frac{\partial \ln r}{\partial w}$, predicted by the GDFD model. To test the MGDF model in this regard, the MGDF model equations were solved for input values appropriate for an

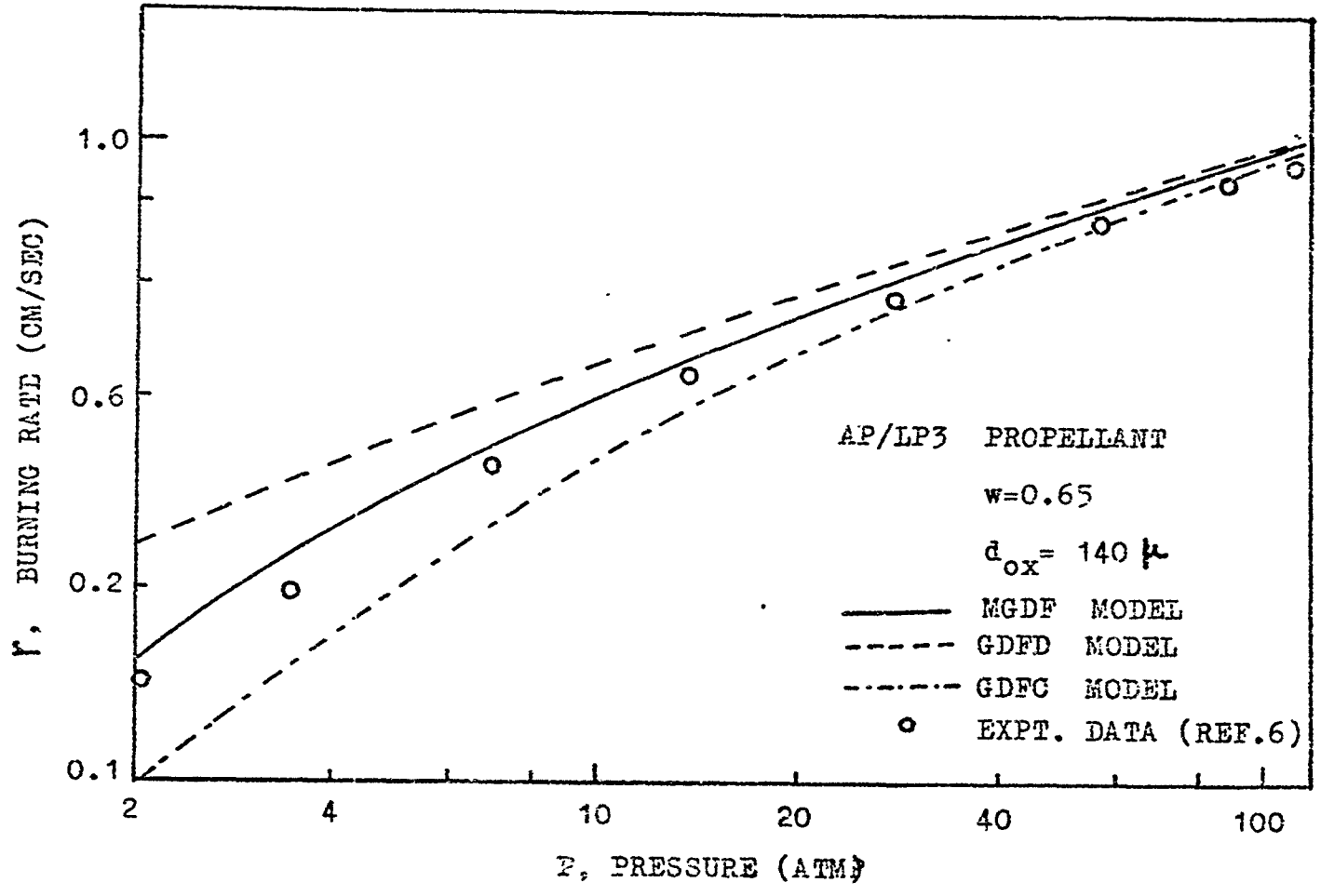

FIGURE V-3 : COMPARISON OF THE MGDF RESULTS WITH THE GDFC AND THE GDFD MODELS' RESULTS AND WITH THE EXPERIMENTAL DATA (LARGER OXIDANT PARTICLE SIZE)

AP/P13 propellant with $d_{ox} = 16\ \mu$ (1). The empirical constants needed for the numerical calculations, viz., A_s, α, β, and C_2 were determined for $w = 0.75$ and these values were ther used for other mixture ratios (i.e., $w = 0.8$, 0.85, 0.9, and 0.95). These values are listed in Table V-1.

The MGDF-model results are plotted as r vs. w in Figure V-4 where they are compared with both the GDFD-model results and the experimental data. It is seen that the sensitivities given by the MGDF model are much higher than those given by the GDFD model. For example, the mixture-ratio sensitivity, $\frac{\partial \ln r}{\partial w}$, given by the GDFD model is about 1.5 and the sensitivity given by the MGDF model is about 5.5 for $P = 2.04$ atm. The experimental results show an average value of about 5.0 for mixture ratio sensitivity at the same pressure.

Comparison of the MGDF-model results with experimental data could not be made beyond $w = 0.8$, because experimental data are not available at present. Hence, only a qualitative comparison can be made between the MGDF model predictions and existing analog data with regard to the trends of r vs. w. The MGDF model predicts maximum burning rates at different mixture ratios depending on the pressure. Such a behaviour of the burning rate has been observed in the studies involving analogs of propellants.

FLAME TEMPERATURES

T_2 = 2450 ^{o}K (w = 0.75)

T_2 = 2800 ^{o}K (w = 0.80)

T_2 = 3030 ^{o}K (w = 0.85)

T_2 = 2960 ^{o}K (w = 0.90)

T_2 = 2500 ^{o}K (w = 0.95)

EMPIRICAL CONSTANTS

α = 6.136×10^{-5}

β = 0.2659

C_1 = 1.8×10^{-12}

C_2 = 5.0×10^{-18}

TABLE V-1 - LISTING OF INPUT VALUES USED IN THE MGDF-MODEL CALCULATIONS

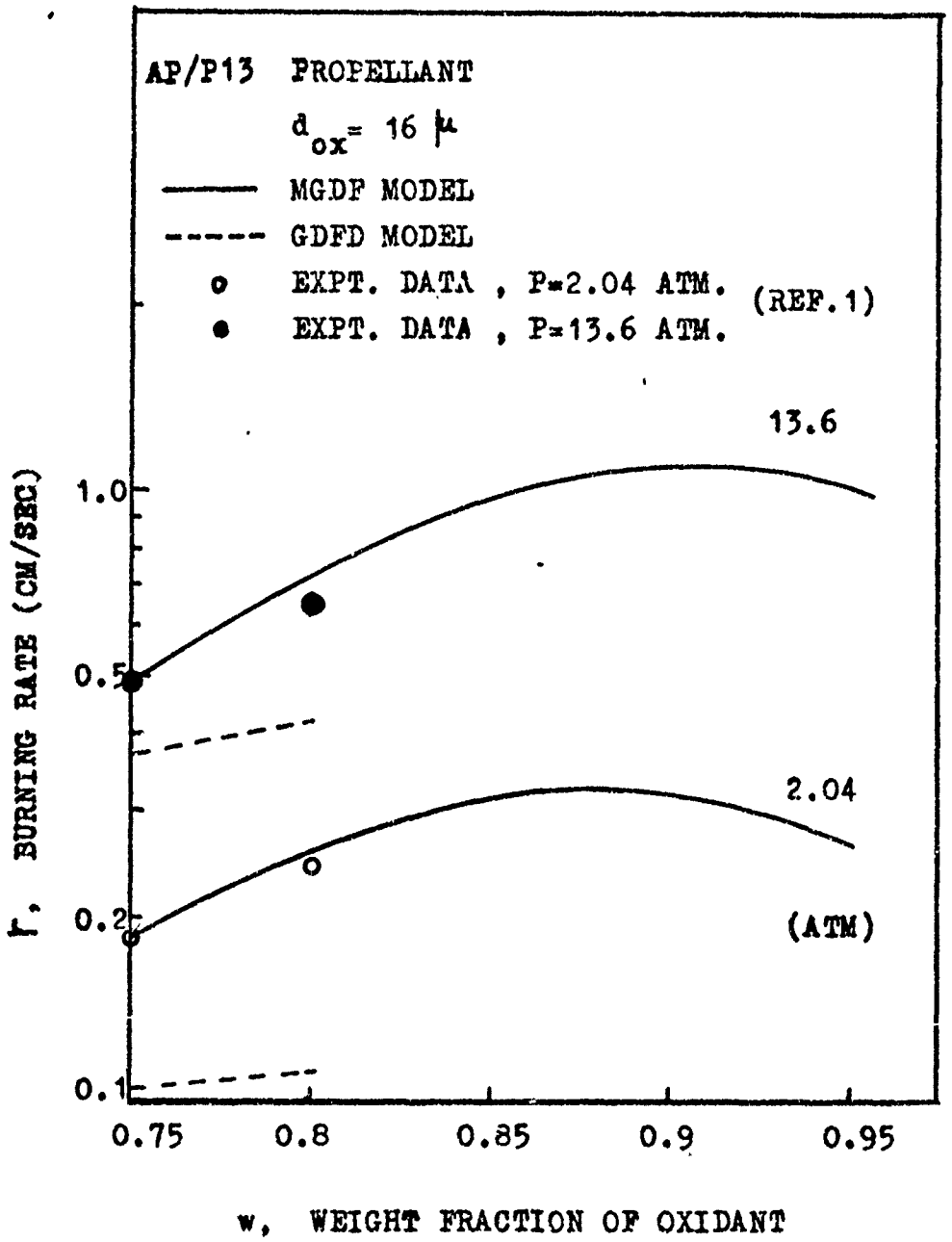

FIGURE V-4 : MIXTURE-RATIO INFLUENCES AS PREDICTED BY THE MGDF MODEL

V.E.4 Initial Temperature Effects as Predicted by the MGDF Model

Finally, the MGDF model has been tested for initial-propellant temperature influences on the burning rate. The propellant considered for numerical calculations was an AP/LP3 propellant with $d_{ox} = 140\mu$ and $w = 0.65$. Initial temperatures were varied between $300^{o}K$ and $200^{o}K$. The results of the numerical calculations are plotted in Figure V-5.

The MGDF model predicts that the burning rate increases as the initial temperature is increased over a wide range of pressure. This prediction is in qualitative agreement with the experimental data. The initial temperature sensitivity, $\frac{\partial \ln r}{\partial T_o}$, given by the MGDF model is about $0.08\%/^{o}C$, whereas the experimental results available for a different propellant (AP/PBAA) (7) is about $0.2\%/^{o}C$. The lower initial temperature sensitivity given by the MGDF model may be due to the fact different propellants were considered in the experimental and theoretical investigations. Hence, no definite conclusions can be made about the merits or demerits of the MGDF model based on this test.

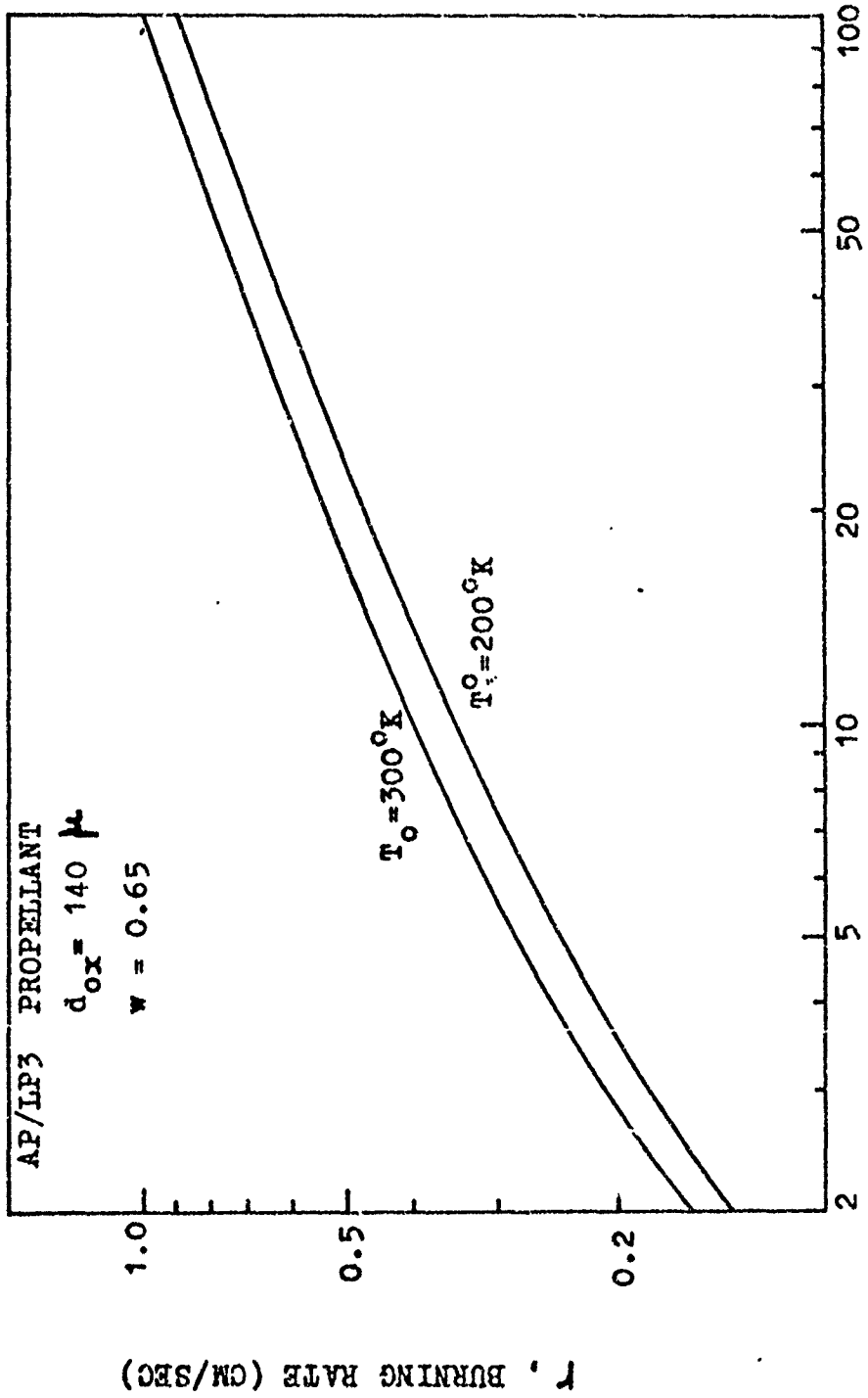

FIGURE V-5 INFLUENCES OF THE INITIAL TEMPERATURE AS PREDICTED BY THE MODF MODEL

V.F CONCLUSIONS

On the basis of the above tests made on the MGDF model, the following conclusions are drawn :

(i) The MGDF model predicts reasonable burning rate variations with pressure in the range of 1 to 100 atm. The MGDF gives results which are much closer to experimental data than those of the GDF'' and GDFD models.

(ii) The oxidant particle size effects predicted by the MGDF model are also in agreement with experimental data and in closer agreement than those of the GDFC and GDFD results.

(iii) The mixture-ratio sensitivities predicted by the MGDF model are essentially the same as those given by experimental data and are much higher than those predicted by the GDFD model.

(iv) The predicted dependence of the burning rate on the initial propellant temperature is qualitatively in agreement with experimental data..

CHAPTER VI - MAJOR CONCLUSIONS AND SUGGESTIONS FOR FUTURE RESEARCH

VI. A MAJOR CONCLUSIONS

The present experimental and theoretical investigations with a loose-granule burner and the theoretical investigations with a premixed, laminar flame model indicate that the gasification of the surface of a composite solid propellant is probably driven by multiple heat sources (flames) in the gas phase. The influence of mixture-ratio on the burning rate cannot be explained using simplified mechanistic models which consider only one flame in the gas phase.

One of the important reactions in the gas phase has been shown, in this study, to be a reaction between fuel vapors intermixing into the AP flame and AP products in the area surrounding each AP particle. Although this mechanism was proposed long ago by Chaiken and Anderson (14), its importance has not been established until this investigation.

A modified granular diffusion flame model, formulated by including the above mentioned mechanism in the GDFD model, gives results which agree with experimental results more closely than do results from the GDFD model. The MGDF model has been comprehensively tested against experimental data and is claimed

to be the most valid model in that it is based on reasonable mechanistic grounds and it is capable of predicting the influences of important variables on the burning rate as indicated by experimental results.

VI.B SUGGESTIONS FOR FUTURE RESEARCH

There is a need for further more comprehensive data for composite solid propellants, especially for mixture-ratio (w) variations. Hence, it is suggested that future experimental investigations be planned to obtain comprehensive data at least for those which obey Summerfield's equation.

The simplified assumption made in the MGDF model with regard to the change in the first-stage flame kinetics (ζ_1) (i.e. T_{av} was used in Equation V-13 instead of T_1^*) should be removed by replacing T_{av} by T_1^* and an iterative procedure be used to solve MGDF equations.

The model should be tested for propellants containing fuels other than LP3 and P13.

Since the MGDF model cannot predict either platau or mesa burning behaviour of propellants, it is suggested that further modifications should be made to enable the model to predict these experimentally observed burning rate behaviours.

REFERENCES

1. Summerfield, M., Sutherland, G.S., Webb. M., Taback, H.J., and Hall, K.P., "Burning Mechanism of Ammonium Perchlorate Propellants," Solid Propellant Rocket Research, Progress in Astronautics and Rocketry Series, Vol. 1, Academic Press, New York, 1960, pp. 141-182.

2. Steinz, J.A., Stang, P.L., and Summerfield. M., "The Burning Mechanism of Ammonium Perchlorate-Based Composite Solid Propellants," Aerospace and Mechanical Sciences Report. No. 830, Department of Aerospace and Mechanical Sciences, Princeton University, N.J., 1969.

3. Williams, F.A., Barrere, M., and Huang, N.C., "Fundamental Aspects of Solid Propellant Rockets," AGARDOGRAPH 116, CIRCA Publications, Inc., N.Y., 1969.

4. Bakhman, N.N., and Belyaev, A.F., "Combustion of Heterogeneous Condensed Systems," Institute of Chemical Physics, Moscow Academy of Sciences, U.S.S.R., Nanka Publications, 1967; also, RPE Translation No. 19 (Editor. G.S. Pearson), Nov. 1967.

5. Von Elbe, G., King, M.K., McHale, E.T., Macek, A., Friedman, R., and Levy, J.N., "Chemical-Kinetics and Physical Processes in Composite Solid Propellant Combustion," Atlantic Research Corp., Report No. 66307, Jan. 1967.

6. Bastress, E.K., "Modification of the Burning Rates of Ammonium Perchlorate Solid Propellants by Particle Size Controls," Ph.D. Thesis, Department of Aeronautical Engineering, Princeton University, N.J., Jan. 1961.

7. Caveney, L., Private Communication, 1972.

8. Rumbel, K.E., "Poly (Vinylchloride) plastisol Propellants : Propellants Manufacture, Hazards, and Testing," Advances in Chemistry Series, 1969, pp. 36-66.

9. Adams, G.D., Newman, B.H., and Robins, A.B., "The Combustion of Propellants Based upon Ammonium Perchlorate," Eighth Symposium (International) on Combustion, The Williams and Wilkins Co., Baltimore, 1962, oo. 693-705.

10. McAlevy, R.F., Lee, S.Y., Cole, R.B., Lastrina, F.A., and Samurin, N.A., "Investigations of the AP Composite Solid-Propellant Deflagration Mechanism by Means of

Experimental Analog Techniques," AIAA Journal., Vol. 6, No. 7, 1968, pp. 1243-1251.

11. Fenn, J.B., "A Phalanx Flame Model for the Combustion of Composite Solid Propellants," Combustion and Flame, Vol. 12, No. 3, 1968, pp. 201-216.

12. Culick, F.E.C., and Dehority, G.L., "An Elementary Calculation for the Burning Rate of Composite Solid Propellants," Combustion Science and Technology, Vol. 1, 1969.

13. Wenograd, J., "Study of the Kinetics and Energetics of Propellant Decomposition Reactions and Applications to Steady State Combustion Mechanism," Proceedings of the Third ICRPG Combustion Conference, CPIA Publication No. 138, Vol. 1, Feb. 1967, pp. 89-94.

14. Chaiken, R.F., and Anderson, W.H., "The Role of Binder in Composite Propellant Combustion," Progress in Astronautics and Rocketry Series, Vol. 1, Academic Press, N.Y., 1960, pp. 227-249.

15. Nachbar, W., "A Theoretical Study of the Burning of a Solid Propellant Sandwich," Solid Propellant and Rocket Research,

Progress in Aeronautics and Rocketry Series, Vol. 1, Academic Press, N. Y., 1960, pp. 207-226.

16. Hertzberg, M., "The Combustion of Pure and Composite Propellants. The Expansion and Application of Laminar Flame Theory to Heterogeneous Solid Propellants," Oxidation and Combustion Reviews, Vol. 5, No. 1, Oct. 1971.

17. Hermance, C.E., "A Model of Composite Propellant Combustion Including Surface Heterogeneity and Heat Generation," AIAA Journal, Vol. 4, No. 9, 1966, pp. 1620-1637.

18. Hermance, C.E., "A Detailed Model of the Combustion of Composite Solid Propellants," Proceedings of the 2nd ICRPG/AIAA Solid Propulsion Conference, CPIA Publication, June 1967, pp. 89-103.

19. Beckstead, M.W., Derr, R.L., and Price, C.E., "A Model of Composite Solid Propellant Combustion Based on Multiple Flames," Lockheed Propulsion Co., Report. No. TR-69-190, 1970.

20. Beckstead, M.W., Derr, R.L., and Price, C.E., "A Model of Composite Solid Propellant Combustion Based on Multiple

Flames," AIAA Journal, Vol. 8, No. 12, 1970, pp. 2200-2207.

21. Williams, F.A., "Combustion Theory," Addison Wesley, 1965.

22. Zelenzik, F.J., and Gordon, S., "A General IBM 704 or 7090 Computer Program for Equilibrium Compositions, Rocket Performance, and Chapman-Jouguet Detenations," NASA TN D-1454, 1966.

23. Beckstead, M.W., Private Communication, March 1971.

24. Derr, R.L., and Osborn, J.R., "An Experimental Investigation of the Gaseous Phase Reaction Zone in a Composite Solid Propellant," Report. No. TM 67-6, Jet Propulsion Center, Purdue University, Sept. 1967.

APPENDIX A - FLAME-TEMPERATURE MEASUREMENTS

A modified Na-D line reversal technique has been used to measure the flame temperature of the loose-granule burner. The method was used previously by Sutherland (1) and Derr (24) for similar purposes. The theory and the derivation of equations have been reported in the cited references. Hence, in the following sections, only the fabrication of loose-granule burners suitable for temperature measurement is described along with the instrumentation and error evaluation used.

This method depends on measurment of the radiation intensity from a flame in a finite spectral region, i. e., that of the Na-D lines (0. 5890-0. 5896 μ). Flame temperatures were calculated from variations produced by intermittently transmitting light from a tungsten lamp through the flame. Using Wien's law and Kirchoff's law, the flame temperature can be expressed as a function of 1. brightness temperature of the tungsten lamp, 2. intensity of the tungsten lamp, 3. intensity of the flame and 4. intensity of the lamp after being absorbed by the flame.

The following equation expresses this relationship :

$$\frac{1}{T_F} = \frac{1}{T_{Br,L}} + \frac{\lambda}{C_2} \ln \frac{D_1 - D_2}{D_3} \qquad \ldots \text{ A-1}$$

where T_F is the flame temperature, $T_{Br,\lambda}$ is the brightness temperature of the tungsten lamp, λ is the mean Na-D lines wave length, c_2 is the physical constant in Wien's law and D_1, D_2, and D_3 are the deflections produced by radiation from the lamp, radiation from the lamp after being absorbed by the flame, and the radiation from the flame, respectively.

A.1 FABRICATION OF LOOSE-GRANULE BURNERS

Because the method used is an optical method, it requires that the position of the flame under investigation be visible to a measuring apparatus. Loose-granule burners fabricated in lead-foil containers have been found to be suitable for this purpose, since the lead melted and exposed the flame zone for temperature measurements. The thickness of the lead foil used was 0.015".

A.2 DESCRIPTION OF INSTRUMENTATION

A schematic arrangement of the instrumentation is shown in Figure A-1. The apparatus producing and measuring radiation intensities consisted of a tungsten-filament lamp, mechanical choppers, an interference filter, a photomultiplier, and an oscillographic recorder.

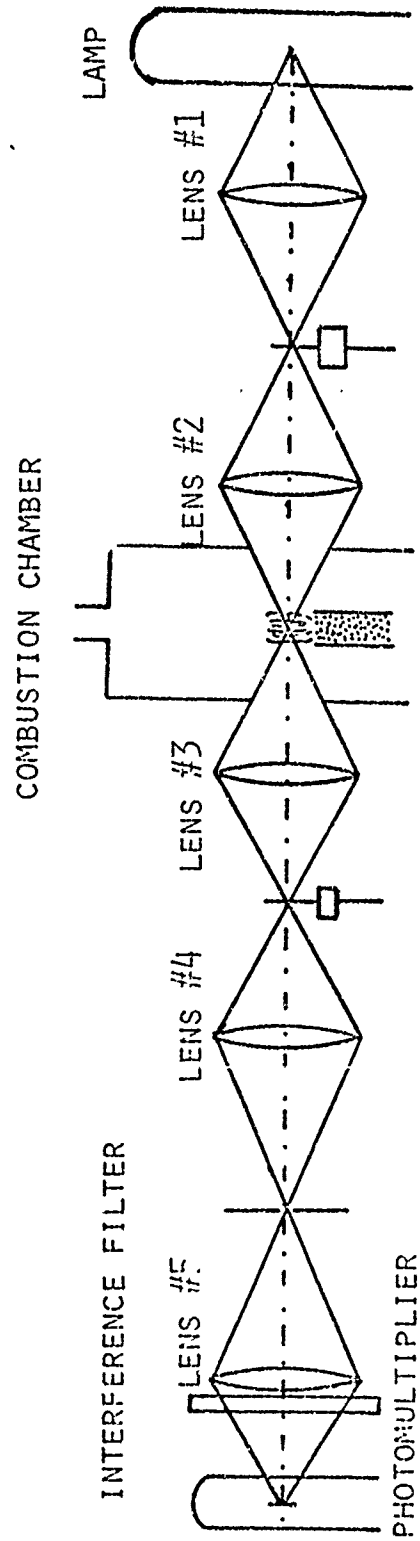

FIGURE A-1 SCHEMATIC OF TEMPERATURE MEASURING APPARATUS

The filament of the tungsten lamp was focused by the lens 1 on a hole in the chopper 1. The lens 2 focused the light on the flame and lens 3 focused the image of both the flame and lamp filament on chopper 2. Finally, the radiation was passed through an interference filter and focused on a slit preceding a photomultiplier tube. The resultant signal was amplified and recorded by an oscillographic recorder.

When both the choppers obstructed the light a zero reference mark was obtained; when the holes in both the choppers were open a signal (D_2) proportional to the intensity of the lamp radiation after absorption by the flame was obtained. When fhopper 1 alone obstructed the light signal (D_3) proportional to the intensity of the flame radiation was obtained in the absence of a flame.

A.3 ERROR EVALUATION

Standard errors to be corrected for are well documented by Derr (24). All of these have been taken into account in the present investigation. One possible error which has not been considered in the previous investigations (1, 24) is that due to signal noise, which causes errors in the measurements of D_1, D_2, and D_3. Using Equation A-1, the error in T_F, viz., ΔT_F, is found in terms of

ΔD_1, ΔD_2, and ΔD_3 to be :

$$\left| \frac{\Delta T_F}{T_F^2} \right| = \frac{\lambda}{C_2} \left[\frac{\Delta (D_1 - D_2)}{(D_1 - D_2)} - \frac{\Delta D_3}{D_3} \right] \quad \ldots \text{ A-2}$$

The maximum error in T_F results when ΔD_1 is positive and ΔD_2 and ΔD_3 are negative :

$$\frac{\Delta T_F}{T_F^2} = \frac{\lambda}{C_2} \left[\frac{2 \Delta D}{(D_1 - D_2)} + \frac{\Delta D}{D_3} \right] \quad \ldots \text{ A-3}$$

where ΔD's represent the average of ΔD_1, ΔD_2, and ΔD_3.

Typical magnitudes of D_1, D_2, and D_3 were found to be 10, 8, and 3 (cm) respectively, and ΔD was observed to be of the order of 0.05 (cm). For these values, the maximum error in the flame temperature would be of the order of $30^{\circ}K$.

APPENDIX B - LISTING OF THE COMPUTER PROGRAM USED FOR THE MGDF-MODEL CALCULATIONS

```
      COMMON A,Y,EF,RH0,T2,XLI,XRI,EPS,IEND,P,HS,HI,AS,ES,
     1       FA,FB,D,FC,C,T1,R,T0WI,G,T0,EE,DF,D0X,TAV,
     2       NJ0B,HAP,CA,CB,CC
      EXTERNAL FCT
    1 READ(5,103)NJ0B
  103 FORMAT(I)
      GO TO(2,3,4,5,6,8,9),NJ0B
    2 READ(5,105)A,T2,TAP,T0,P
      READ(5,106)HF,HAP,DF,D0X
      READ(5,107)AS,ES,EE,Y
      READ(5,108)CA,CB,CC
      READ(5,109)EPS,IEND
      GO TO 1
    3 READ(5,105)A,T2,TAP,T0,P
      GO TO 1
    4 READ(5,106)HF,HAP,DF,D0X
      GO TO 1
    5 READ(5,107)AS,ES,EE,Y
      GO TO 1
    6 READ(5,108)CA,CB,CC
      GO TO 1
  105 FORMAT(5F)
  106 FORMAT(4F)
  107 FORMAT(4F)
  108 FORMAT(3F)
  109 FORMAT(2F)
    8 TAV=(T2+TAP)/2.
      HS=A*HAP+(1.-A)*HF
      RH0=1./(A/1.95+(1.-A)/DF)
      WRITE(6,110)A,T2,T0,P
  110 FORMAT(' WT,FR=',F16.4,' T2=',F10.1,' T0=',F10.1,
     1   ' P=',F10.2)
      WRITE(6,111)HF,HAP,DF,AS,ES
  111 FORMAT(' HF=',F10.2,' HAP=',F10.2,' DF=',F10.2,
     1 ' AS=',F10.2,' ES=',F10.1)
```

```
      WRITE(6,112)EE,Y,D0X
  112 F0RMAT(' EE=',F20.10,' Y=',F20.10,' D0X=',F20.10)
      AB=CA*RH0*TAV**2.75*EXP(22000./(1.986*TAV))/(1.95*
     1 P**2.*D0X**2.)
      AF=AB/(1.+AB)
      AC=CA
      AD=CB
      WRITE(6,113)AC,AD,AB
  113 F0RMAT(' CA=',E20.10,' CB=',E20.10,' M=',E20.10)
      WRITE(6,114)AF
  114 F0RMAT(' WT FR FUEL=', F40.10)                              #
      T0NE=1384.687+32252.12*AF-235047.4*AF**2.+702179*
     1 AF**3.
      WRITE (6,115)T0NE
  115 F0RMAT(' T0NE=',F20.5)
      HI1=0.3*(T0NE-T0)+HAP
      HI=-A*HI1
      WRITE(6,116)HI
  116 F0RMAT(' HI=',F20.5)
      T0WI=CB*TAV*EXP(22000./(1.986*TAV))/P
      WRITE(6,117)T0WI
  117 F0RMAT(' T0WI=',E30.10)
      E=EE
      EF=E*T2*EXP(20000./(2.*1.986*T2))/P
      G0 T0 1
    9 READ(5,12)XLI,XRI
   12 F0RMAT(2F)
      CALL RTMI (X,F,FCT,XLI,XRI,EPS,IEND,IER)
      IF(IER.NE.0)G0 T0 101
      WRITE(6,50)R
   50 F0RMAT(/////E16.8)
      T0W2=P*30.*(EF+G)**2./(82.05*T2)
      EL2=82.05*RH0*R*T2*T0W2/(30.*P)
      EL1=82.05*RH0*R*T1*T0WI/(30.*P)
      QT=C
      QT1=R*RH0*0T
      QII=.0002*(T2-T1)/(EL2*RH0*R)
      QI=QT-QII
      QI1=R*RH0*0I
      QIIF=QII*R*RH0
      T0W1=T0WI
      WRITE(6,21)T0W1,T0W2,EL1,EL2
   21 F0RMAT(////E16.8,E16.8,E16.8,E16.8)
      WRITE(6,20)QT,QT1
   20 F0RMAT(' 0T=',E20.6,' QTF=',E20.6)
```

see note on page 125

```
      WRITE(6,22)QI,QI1
 22   FØRMAT(' QI=',E20.6,' QIF=',E20.6)
      WRITE(6,23)QII,QIIF
 23   FØRMAT(' QII=',E10.4,' QIIF=',E10.4)
      ET=P/CC
      EV=P**.6666666
      WRITE(6,300)ET,EV
300   FØRMAT(' P/R=',F10.5,' P2/3=',F10.5)
      GØ TØ 1
101   WRITE(6,10 )IER
100   FØRMAT(' ERRØR CØDE=',I3)
      GØ TØ 9
      END
      FUNCTIØN FCT(X)
      CØMMØN A,Y,EF,RH0,T2,XLI,XRI,EPS,IEND,P,HS,HI,AS,ES,
     1       FA,FB,D,FC,C,T1,R,TØWI,G,TØ,EE,DF,DØX,TAV,
     2       NJØB,HAP,CA,CB,CC
      R=AS*EXP(-ES/(1.986*X))
      C2=0
      C=.3*(X-TØ)+HS
      D=.0002*(T2-X)
      G=(Y*T2**.83333)/(X**.875*P**.3333333)
      WRITE(6,2)X,R
  2   FØRMAT(//' TS=',F12.4,' R=',E16.6)
      FA=R**2.
      FB=1.-(FA*TØWI*82.05*RH0**2*C)/(P*0.0002*30.)
      FC=-.3*TØ+HS+HI*C2
      FCT=FA-.0002*(T2-X/FB)/((EF+G)**2.*RH0**2.
     1*(.3*X/FB+FC))
      RR=SQRT(FA-FCT)
      T1=X/FB
      WRITE(6,5)T1,RR
  5   FØRMAT(' T1=',F12.4,' RR=',E16.8)
      CC=R
      RETURN
      END
```

Note : T_1^* (TONE) given in this program is for AP/P13 propellant (valid in $0.9 < w < 1.0$)

T_1^* (TONE) for AP/LP3 propellant is given by

TONE = 1398.21+13891.07 * AF - 33482.12*AF**2.0